ELUCIDATING THE ROLE OF SMAD7 IN PANCREATIC CANCER THROUGH IN VIVO STUDIES

Sudha Satish Savant

Submitted to the faculty of the University Graduate School
in partial fulfillment of the requirements
for the degree
Doctor of Philosophy
in the Department of Biochemistry and Molecular Biology,
Indiana University

September 2017

Accepted by the Graduate Faculty, Indiana University, in partial fulfillment of the requirements for the degree of Doctor of Philosophy.

Murray Korc, MD, Chair

Ronald C. Wek, PhD

Doctoral Committee

Lawrence A. Quilliam, PhD

June16, 2017

Jing Wu Xie, PhD

Dedication

I dedicate this dissertation to my parents, Monica and Satish Savant, and to my husband, Rajesh Sardar, as without their unconditional love and support this would have not been possible.

Acknowledgments

I want to thank my advisor, Murray Korc, and my committee, Ronald Wek, Lawrence A. Quilliam and Jing Wu Xie for their guidance and support during my graduate studies. I would like to thank all the past and current members of the Korc lab for their feedback and scientific discussions in the lab.

I would like to thank all the faculty, staff and students of the Biochemistry and Molecular Biology Department and of the Simon Cancer center for their support throughout my graduate studies. Additionally, I would like to thank the Graduate division, especially Randy Brutkiewicz, Tara Hobson-Prater and Brandy Wood for their support throughout graduate school and for providing opportunities and nurturing my professional career.

I am grateful to Barry Muhoberac, Melissa Fishel, Lakshmi Prabhu, Eshaani Mitra and my parents for their suggestions and support with this thesis.

I would like to thank my brother, family and friends for their continued support and love throughout the graduate journey.

Sudha Satish Savant

Elucidating the role of Smad7 in pancreatic cancer through *in vivo* studies

Pancreatic ductal adenocarcinoma (PDAC) is the fourth leading cause of death with a mere 9% survival rate. PDACs harbor *KRAS* (92-95%) and *CDKN2A* (90%) mutations, overexpress tyrosine kinase receptors, their ligands, and transforming growth factor-β (TGF-β) isoforms. Canonical TGF-β signaling is mediated via Smad2, Smad3 and Smad4, whereas inhibitory Smad6 and Smad7 attenuate TGF-β signaling. Smad7 is overexpressed in PDAC and blocks TGF-β-mediated growth inhibition *in vitro*. However, the exact role of Smad7 in PDAC is not known. We have established a genetically engineered mouse model of PDAC in which conditional expression of *Smad7* and oncogenic $Kras^{G12D}$ are driven in the pancreas by *Pdx1-Cre*. These *LSL-*$Kras^{G12D}$*;SMAD7;Pdx1-Cre*(KS7C) mice exhibit accelerated progression of pancreatic intraepithelial neoplasia (PanIN) to PDAC by comparison with *LSL-*$Kras^{G12D}$*;Pdx1-Cre* (*KC*) mice harboring the $Kras^{G12D}$ mutation alone, whereas in the absence of oncogenic Kras, pancreatic histology remains normal in spite of a 9- fold increase in *Smad7* mRNA levels. KS7C pancreata exhibit increased PanIN and pancreatic cancer cell proliferation, and these changes are recapitulated in a tetracycline (tet) inducible mouse model of Smad7 (KtetS7C). In both models, pre-neoplastic lesions and PDACs exhibited increased levels of anterior gradient 2 (AGR2), hyper-phosphorylated retinoblastoma protein (p-pRb) and p-Smad2, but low levels of p-Smad3 and p21. Smad7 overexpression in human pancreatic cancer cells (hPCCs) results in downregulated p21 and upregulated AGR2 mRNA and protein levels, and decreased binding of Smad3/4 complex to the *AGR2* promoter. Smad3 silencing in hPCCS also resulted in downregulated *p21* mRNA and upregulated *AGR2* mRNA levels. These findings indicate that Smad7 blocks TGF-β pathways, in part, by preferentially decreasing Smad3

phosphorylation and enhancing AGR2 expression in PDAC, and suggest that targeting Smad7 may constitute a novel therapeutic approach in PDAC.

Murray Korc, MD, Chair

Contents

List of Tables

List of Figures

Abbreviations

3D 3-dimensional. 28, 48, 49, 64, 66, 101

α - SMA alpha smooth muscle actin. 16, 27, 47-48, 64-65

ADM acinar-to-ductal metaplasia. 13, 20, 40-46, 63, 92, 96, 99

AGR2 (gene: *AGR2*) anterior gradient 2. v, vi, ix, xiii-xiv, 29, 33, 83-85, 90-95, 101-102, 104-105, 108-110, 116, 137

ANOVA analysis of variance. 24

BCA Bicinchoninic Acid. 22-23

CAF cancer associated fibroblast. 2

CDKN1A cyclin-dependent kinase inhibitor 1A. ix, xiii, 80, 85-87, 102-104, 108

CDKN2A cyclin-dependent kinase inhibitor 2A. v, 2

cDNA complementary DNA. vii, 17, 18, 22, 25, 112, 114

CDK cyclin dependent kinase. 10,11

ChIP Chromatin Immunoprecipitation. 29, 33, 35-37, 94-95, 104

CIP kinase inhibitor protein. 10, 11

CK19 murine cytokeratin 19 (gene: Krt19). 27, 35, 41, 47-48, 64, 65

CKI cyclin kinase inhibitor. 10

CS7 COLO-357 cells overexpressing c-Myc tagged *SMAD7.*xiii, 73-75, 80-81, 83-84

CSham COLO-357 cells overexpressing pLNX backbone*.* 74-76, 95, 115

DMEM Dulbecco's Modified Eagle Medium. 24-26

DNA deoxyribonucleic acid. vii, 9-11, 17, 19, 21-22, 30, 37, 114

ECM extracellular matrix. 2-3

EGFP enhanced green fluorescent protein. 17-21, 31-32

EMT Epithelial to Mesenchymal Transition. 3, 14, 47, 64, 96, 100

ES embryonic stem. vi, 17, 38

FBS fetal bovine serum. 24-25, 27, 59-60

FC Fold Change. 29, 116, 137

GEF guanine exchange factor. 12

GEMM Genetically Engineered Mouse Model. 16, 51, 95, 99, 100, 104

*GPX2*Glutathione Peroxidase 2. xiii, 32, 83-85

GSEA Gene Set Enrichment Analysis. 29, 82, 85, 103, 104

HRP. Horse Radish Peroxidase 26

ICC Immunocytochemistry. 27, 35

Id Inhibitor of differentiation. 11

1. Introduction

1.1. Pancreatic cancer

Cancer is the disease of abnormal cell division and growth with the capacity to spread to other parts of the body. Pancreatic cancer (PC) is the cancer of the pancreas and can arise in the endocrine (account for 6% of total PC) or exocrine portion (94% of total PC) of the pancreas[1-3]. Exocrine tumors of the pancreas include acinar cell carcinoma, adenosquamous carcinoma, mucinous cystadenocarcinoma and pancreatic ductal adenocarcinoma (PDAC)[3]. PDAC is the most common form of pancreatic cancer which accounts for ~85% of total pancreatic tumors[1, 3]. In PDAC the cancer cells appear ductal like and bear ductal markers. It is the third leading cause of cancer related deaths in the United States with an over-all survival rate of 8%[4]. When presented with pancreatic cancer, less than 20% of the patients qualify for surgical resection [1, 3, 5, 6]. The dismal statistics associated with PDAC are consequences of late diagnosis of the cancer (~91% of the patients present with distant metastasis) due to lack of specific diagnostic measures and marked resistance to chemotherapy. Almost 50% of the patients diagnosed with metastatic disease have a 5-year survival of only 3% [3]. Gemcitabine had been a long standing standard of care for treating pancreatic cancer patients [2]. The slight improvement seen in the overall survival rate over the years is because of the adjunct therapy with FOLFIRINOX (a combination of fluorouracil, leucovorin, irinotecan and oxaliplatin) and nab-paclitaxel [2, 7]. However, these drugs do not prolong survival substantially and affect healthy cells adversely, thus decreasing quality of life.

In 2000, Hanahan and Weinberg, described the model of hallmarks of cancer [8] which gave a concept based on existing literature about how cancer is a multistep process and the ability of a normal cell to acquire capabilities like self-sufficiency in growth signals, insensitivity to growth, evading apoptosis, sustained angiogenesis, limitless replicative potential and ability to metastasize. Within a decade, further understanding of cancer and the microenvironment associated with it, resulted in additional cancer hallmarks like deregulation of metabolism and immune system, and tumor promoting inflammation [9]. Next generation sequencing has also revealed the presence of heterogeneity in cancers, which further adds to the complexities of cancer biology [10-12].

PDACs are characterized by desmoplasia as a consequence of the aberrant activation of pancreatic stellate cells into cancer associated fibroblasts (CAFs) that deposit

excessive amounts of extracellular matrix (ECM) components such as collagens and fibronectin [13]. In addition, the tumor microenvironment (TME) in PDAC harbors a variety of immune and inflammatory cell types that combine to suppress cancer-directed immune mechanisms [14] (Figure 1.1).Tumor progression is enhanced through autocrine and paracrine signaling cascades activated by growth factors and cytokines.

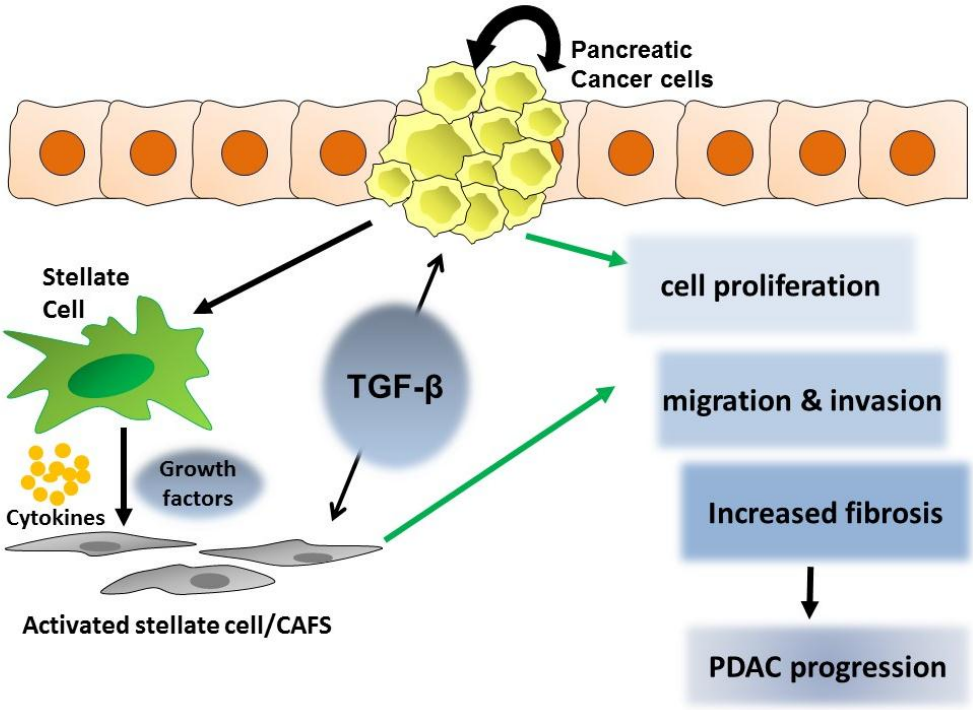

Figure 1.1 Schematic representation of PDAC desmoplasia

Schematic representation of PDAC desmoplasia, depicting pancreatic cancer cell and stellate cells which secrete cytokines and growth factors, including TGF-β. These cytokines through autocrine and paracrine signaling stimulate the stellate and cancer cells, resulting in an activated stroma rich environment, increased cancer cell proliferation, migration and invasion. Together these outcomes further contribute to PDAC progression.

PDAC is also associated with a high frequency of major driver mutations, most notably oncogenic *KRAS* (95%), *CDKN2A* (90%), *TP53* (70%) and *SMAD4 (*55%*)* as well as over-expression of tyrosine kinase receptors and ligands that bind to these receptors[11, 15-21].

Understanding the physiology and genetic makeup of pancreatic cancer cells over the last two decades has resulted in testing of a wide variety of therapeutics which target all the cancer capabilities described above [3, 7, 22, 23]. However, the complexities associated with PDAC also result in failure of most of the therapeutics at pre-clinical stages [24]. Altogether, while efforts are being made to develop better diagnostic and screening methods for PDAC, there is an urgent need for novel therapeutics to improve the current therapy and clinical outcome for PDAC[7, 25].

Transforming growth factor-β (TGF-β) isoforms belong to a large family of cytokines that bind and activate a family of serine threonine kinase receptors [26]. Previously, we have shown that all three mammalian TGF-β isoforms are over-expressed in PDAC, which correlates with decreased survival [27]. In cancer, TGF-β has been shown to play a role in tumor-promoter and tumor suppressor activity[28, 29]. TGF-β inhibits cell growth of epithelial cells [30, 31] and can also induce senescence and apoptosis and result in cell growth inhibition, thus acting as a tumor suppressor. However TGF-β can induce Epithelial to Mesenchymal Transition (EMT) of cells, (which is an important characteristic of cancer cells) angiogenesis, suppression of immune system and deposition of ECM which altogether support tumor growth [32-34].

Many reports have described the potential of targeting TGF-β in PDAC. TGF-β pathways have been targeted by (a) antisense oligonucleotides against the ligand (b) treatment with monoclonal antibodies which absorb TGF-β ligands and, (c) blocking the TβR1 receptor which prevents ligand interaction [35-37]. However, targeting TGF-β alone has not shown any promising results, probably due to; 1) mutations in the key components of the pathway; 2) the complex interaction and cross talks between the microenvironment and cancer cells and; 3) due to the large number of normal physiological functions of TGF-β and its context dependent effects[35, 38, 39]. Understanding the molecular mechanisms of the TGF-β pathway and its role in PDAC may help develop targets for attenuating specific functions of TGF-β.

1.2. Risk Factors for PDAC

There are inherited mutations associated with pancreatic cancer and 10% of pancreatic cancer patients have a familial history of the disease. The risk of being diagnosed with pancreatic cancer increases with advancing age [2, 25]. Other risk factors are mainly related to lifestyle and chronic medical conditions which include obesity, poor diet, heavy alcohol consumption and tobacco smoking. Diabetes mellitus and chronic pancreatitis (CP) are medical conditions that have also been associated with PDAC[40, 41]. CP is the inflammation of the pancreas and it may be due to hereditary factors like gene mutations or due to alcohol consumption [23, 42, 43]. The risk ratio (RR) for PDAC associated with CP is 2[44]. Studies on pancreatitis as risk factor for PDAC using mouse models will be discussed in a later section.

1.3. Pancreas

The pancreas is a retroperitoneal organ, located behind the stomach. The head of the pancreas sits in the loop of the duodenum and its neck, body and tail slope upwards and extend to the left side[45, 46] (Figure 1.2).

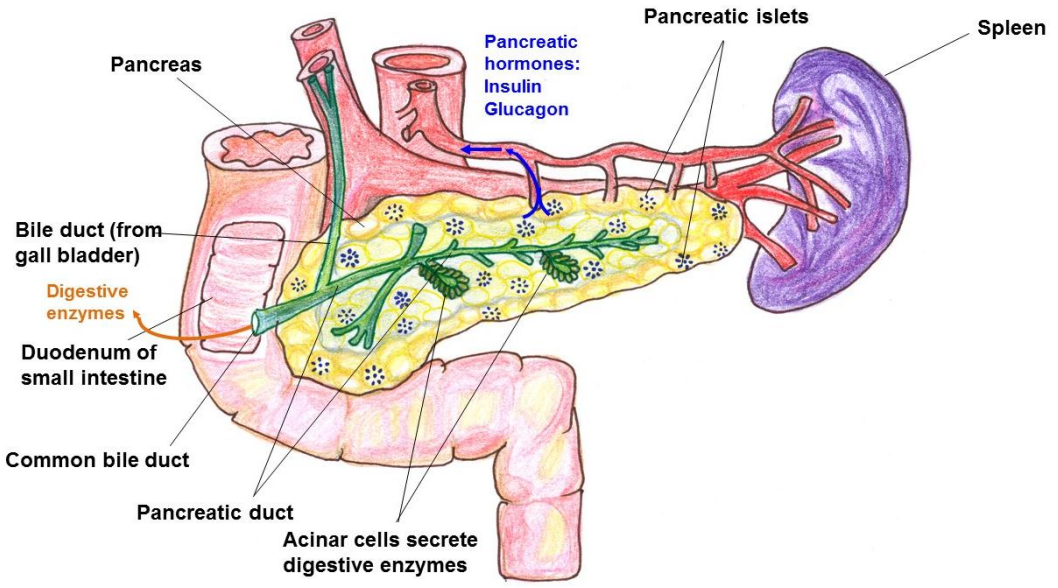

Figure 1.2 Anatomy of the Pancreas

Figure illustrates location of the pancreas in the "C" loop of the duodenum. The endocrine portion of the pancreas encompasses the pancreatic islets which secrete the pancreatic hormones insulin and glucagon,that regulate blood glucose levels. The exocrine portion is made up of the acinar cells which secrete digestive enzymes that are secreted into the small intestine via the pancreatic duct. Figure is adapted from [47].

~ 95% of the pancreas is made up of ducts and acini which synthesize and secrete enzymes that aid digestion[46-48]. The remaining portion of the pancreas is made up islets of Langerhans (~1-2%), which functions as the endocrine portion of the pancreas consisting of blood vessels, nerves, and connective tissue. The islets secrete hormones such as, insulin, glucagon, somatostatin and pancreatic polypeptide which regulate blood glucose levels, and exert other metabolic effects[47, 48].

1.4. Exocrine Pancreas

The exocrine pancreas is a compound gland made up of lobules and intralocular ducts which drain into the main pancreatic duct. A lobule is a collection of multiple acini or the secretory units along with interlobular ducts. Each secretory unit is made of an acinus which secretes zymogen granules into an intercalated duct. An acinus is a collection of 15-100 polarized acinar cells which are the units synthesizing the enzymes and releasing them into the intercalated ducts that are lined with centroacinar cells[47, 48] (Figure 1.3).

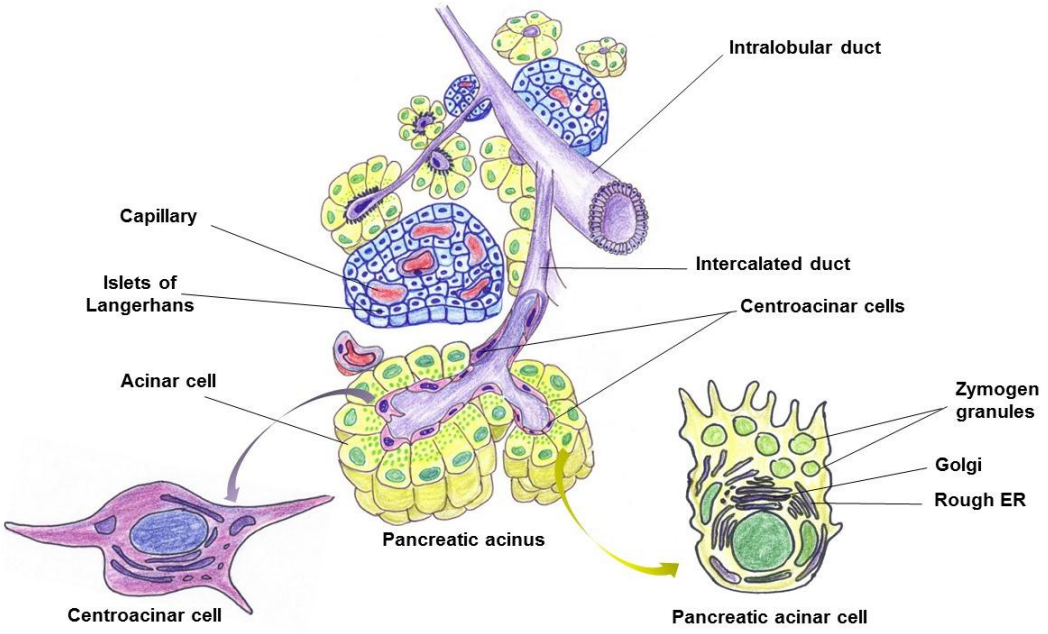

Figure 1.3 Cellular organization of the exocrine pancreas

Figure illustrates the organization of the exocrine pancreas which is a collection of the pancreatic acinar and centroacinar cells and intercalated ducts. The pancreatic acinar cell is made up with zymogen granules which produce and secrete enzymes including amylase that aid in digestion. Figure is adapted from [49]

1.5. TGF- β signaling

Transforming Growth Factor Beta (TGF-β) is a cytokine that relays signals to regulate cellular processes like; proliferation, differentiation, apoptosis and to maintain homeostasis [50-53]. There are 3 isoforms of the TGF-β ligand; TGF-β1, TGF-β2 and TGF-β3. These ligands are associated with latent TGF-β binding protein (LTBP)[54]. Of the three, TGFβ1 binds to the receptor with highest affinity. Upon activation, the TGF-β ligand dissociates from the LTB protein, and binds to the type II TGF-β receptor (TβRII). TβRII is a trans-membrane receptor with a serine/threonine protein kinase domain. When the TGF-β ligand binds to TβRII, it recruits TβRI and phosphorylates the hydroxyl (OH) group of serine and threonine residues on it[55]. The receptors form an activated heterodimeric complex and are internalized by endosomes. Within the endosomes, the Smad anchor for receptor activation (SARA) protein helps TβRI recruit the Smads to the complex[55, 56].

Receptor-regulated Smads (R-Smads) are key transcription factors, downstream of the TGF-β receptor signaling cascade. TβRI specifically recruits Smad2 and Smad3 to the complex and phosphorylates them on serine residues present on their C-terminus. The phosphorylation event changes their conformation and increases their affinity for the Co-Smad4[57]. The heterodimeric complexes of the R-Smads and Smad4 then are translocated to the nucleus where they act as transcriptional regulators of genes that regulate cell differentiation, migration, growth, apoptosis and extracellular matrix (ECM) deposition[58](Figure 1.4).

TGF-β increases deposition of fibronectin, laminin and collagen[59, 60]. Simultaneously it also downregulates expression of ECM proteases and upregulates upregulation of the ECM protease inhibitors like Plasminogen Activator (PAI-1) thereby increasing ECM deposition[60]. TGF-β inhibits cell growth in epithelial cells while it increases proliferation of cells that are mesenchymal in origin [61]. The role of TGF-β's growth inhibitory actions on epithelial cells with respect to cell cycle will be discussed in later section.

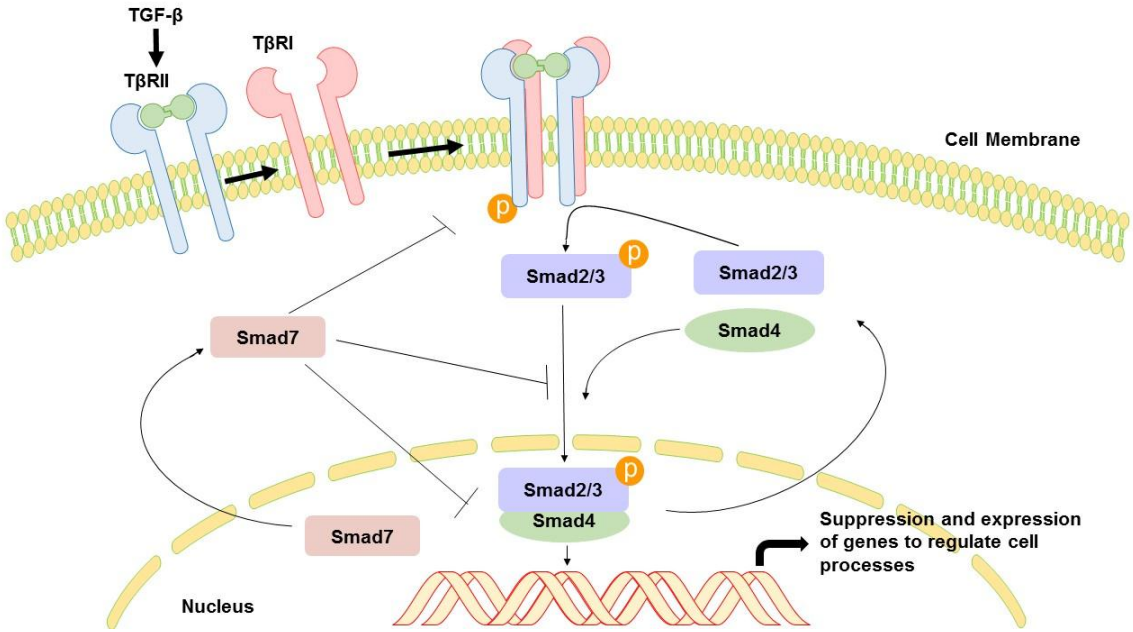

Figure 1.4 Schematic representation of Canonical TGF-β signaling

TGF-β ligand binds to TβRII, which then hetero dimerizes with TβRI, resulting in activation of downstream signaling. The phosphorylated receptor complex then recruits the receptor Smads, Smad2 and Smad3, and phosphorylates them. These then interact with Smad4, a Co-Smad, and are translocated to the nucleus, where they bind to promoter regions of target genes, along with transcriptional co –activators and repressors to upregulate or inhibit genes, respectively, that regulate cell processes like proliferation, migration and angiogenesis. Figure adapted from [26]

1.6. Smad7

Smad7 is an inhibitory Smad and a potent inhibitor of the TGF- β pathway which was first discovered in endothelial cells [62]. The SMAD7 gene is located on Chromosome 18 in humans and its expression is regulated primarily by Smad2/3 along with a variety of transcriptional activators [63, 64]. Smad7 is a ~46 kDa protein and has a conserved Mad homology-2 (MH2) domain in its C-terminal that helps it to bind to DNA [65, 66]. Its N-terminal has minimum homology to the MH1 domains of the receptor or co-Smads. The N-terminus of Smad7 allows it to exert its inhibitory effects on TβRI by physically interacting with the MH2 domain[67].Smad7 also has a short proline rich linker that allows it to interact with other proteins that contain WW domains, a short 40 amino acids long protein module [68-70](Figure 1.5).

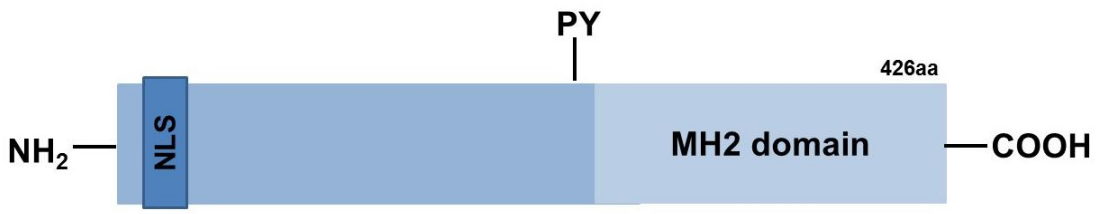

Figure 1.5 Schematics of structure of Smad7

Smad7 is made up of 426 aa residues in length represented with key regions highlighted. Smad7 contains a conserved MH2 domain similar to other Smads and has a nuclear localization sequence (NLS) at its N terminus. The linker region of Smad7 contains the PY motif, made up of proline rich residues which allow it to interact with and bind to other proteins with WW domains.

Smad7 is primarily located in the nucleus and upon activation of the TGF-β signaling cascade, it gets translocated to the cytoplasm where it inhibits the pathway by key mechanistic features, which include the following: [71](a) Smad7 has been shown to recruit phosphatases to the TβRs to dephosphorylate them [72, 73]. (b)It can also bind to TβRI and inhibit the recruitment of the R-Smads to the activated receptor complex and inhibit their phosphorylation [74, 75]. (c) Previous studies have shown Smad7 to recruit

ubiquitin ligases such as Nedd4L and Smurf1/2 to the TβRI, Smad2 and Smad4 to promote their degradation [76-78]. (d) NuclearSmad7 has been shown to interact with HDAC-1 to modulate gene expression[79].

1.7. Cell Cycle

Cell cycle or cell division is an important cell process that results in duplication of the DNA, followed by division of the cell into two daughter cells. When the cell cycle gets hijacked, a normal cell is able to avert growth inhibitory signals, impede apoptosis and undergo uncontrollable growth, resulting in cancer. The cell cycle is divided into 4 stages: Gap1 (G1), Synthesis (S), Gap2 (G2) and Mitosis (M). G1, S and G2, together are known as interphase where the cell grows and replicates its DNA. Mitosis is the phase of cell cycle, where the cell divides to form two daughter cells. Cyclins and cyclin dependent kinases (CDK) are important proteins required for the cell to go through interphase and reach the mitosis stage. The cyclin-CDK complex phosphorylates target substrates to activate or inactivate them, resulting in transcription of genes important for cell cycle progression[80, 81]. The retinoblastoma protein (pRb) is an important tumor suppressor[82], which is also a substrate for the cyclin-CDK complex[83]. pRb, when unphosphorylated, is active and remains bound to the transcription factor E2F[84], preventing it's transactivation. pRb gets phosphorylated (p-pRb) by the CyclinD-CDK4/6 complex in the G1 phase[85]resulting in the rapid phosphorylation of pRb at other sites by other Cyclin-CDK complexes which are phase specific, that result in the hyper phosphorylation of pRb. Cyclin E-CDK2 complexes are activated during late G1 and early S phase, Cyclin A-CDK2 complexes during early S to mid G2 and Cyclin A/B-CDK1 complexes during late G2 to M phases (Figure 1.6). Synthesis and degradation of each of these complexes are phase specific and tightly regulated. The pRb when completely phosphorylated, becomes inactive and dissociates from its complex with E2F allowing the latter to bind to the DNA to synthesize proteins important for cell cycle progression[86-88]. The cyclins, CDKs, DNA replication and repair proteins are some of the known targets for E2F[89]. While the cyclin – CDK complexes drive the progression of the cell cycle; they are regulated by the cell cycle inhibitors (CKI's)[90, 91]. The proteins that serve as CKIs belong to two family of proteins – the Inhibitor of CDK4 (INK4) and the kinase inhibitor protein (KIP/CIP) family[92]. The proteins of the INK4 family, which includes p16, p15, p18 and p19, are expressed in the early G1 and inhibit CDK4/6 activity specifically [93-96]. The CIP/KIP family comprises of p21, p27 and p57

[97-101]. These proteins inhibit all the cyclin-CDK complexes, specifically in late G1 and S phases to inhibit them and result in cell cycle arrest.

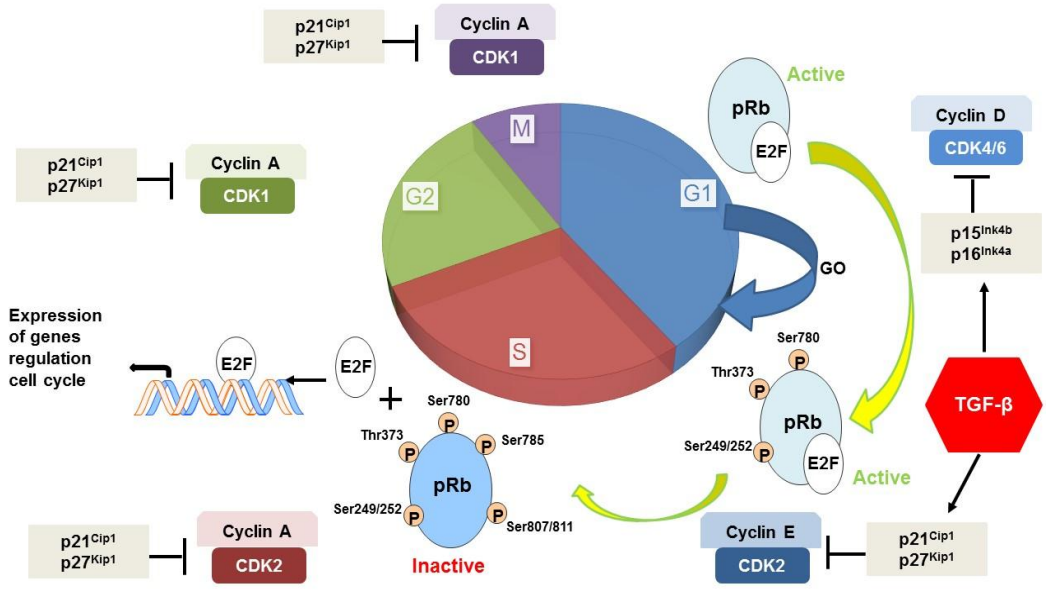

Figure1.6 Schematic representation of cell cycle

The cell cycle is divided into four phases and is governed by the synthesis of cyclins and their binding to the cyclin-dependent kinases (CDKs). The early Gap 1 or G1 phase involves Cyclin D and CDK4/6 complex. Cyclin E –CDK2 complex control transition of G1 to S phase. Cyclin A-CDK2 then drive progression through S and into G2 phase, which is followed by activation of Cyclin A-CDK1 through G2 phase and mitosis. These complexes phosphorylate pRb at specific residues, resulting in its confirmation change, which results in its dissociation from the E2F transcription factor. The unbound E2F then binds to the DNA to regulate transcription of genes required for the cell cycle, including cyclins. The activity of the CDKs is regulated by the INK4 and KIP/CIP family members which comprises of p15, p16, p21 and p27. TGF-β upregulates expression of p15,p21 and p27, thus inhibiting G1 phase and resulting in cell cycle arrest.

TGF-β is a growth inhibitory cytokine for epithelial cells. TGF-β can either induce p15, p21 and p27 or downregulate expression of c-Myc and Inhibitor of differentiation (Id) -1 and 3; which then results in inhibition of cyclin D1, cyclin A and cyclin E [102-105]. Altogether, the inhibition of the cyclins induces cell cycle arrest by blocking progression of late G1 into S phase.

1.8. *KRAS* mutations in PDAC

Kras is a small GTPase that is encoded by the *KRAS* gene. Guanidine nucleotide exchange factors (GEFs) facilitate activation of the Kras protein by aiding the exchange of GDP with GTP [106]. GTPase-activating proteins (GAPs) facilitate hydrolysis of GTP bound to Kras, which results in its activation [107]. *KRAS* is mutated in 92 to 95% of PDAC patients [11, 108]. Mice expressing oncogenic *Kras* alone (KC), have development of pancreatic intraepithelial neoplasia (PanIN) [109]. PanIN are classified into various grades depending on their structure and degree of nuclear atypia (Figure 1.7). PanIN-1A lesions consist of cuboidal to columnar epithelial cells that produce mucin and have basal nuclei. As KC mice age, these PanIN lesions progress towards PanIN-2 and PanIN-3 lesions which are characterized by loss of cell polarity and nuclear atypia. As they continue to age, the pancreas contains excessive ductal-like lesions associated with fibrous stroma[109, 110]. Previously, studies with transgenic mouse models expressing oncogenic Kras in an inducible manner have demonstrated that *Kras* is important in PDAC initiation and maintenance [111]. Induction of pancreatitis in the presence of *Kras* mutation accelerates PDAC progression in mice [111, 112]. Conditional deletion of tumor suppressors like *Rb1, p53, SMAD4* and *INK4A* have been shown to have no effects in PDAC initiation unless supplemented with oncogenic *Kras[113-117]*. Thus, Kras is an important oncogenic driver of PDAC and hence, it is important to study effects of other genes in the presence of Kras mutation to understand their role in PDAC. The KC model will be used as a control is our studies, and effects of Smad7 will be analyzed in the presence of oncogenic Kras.

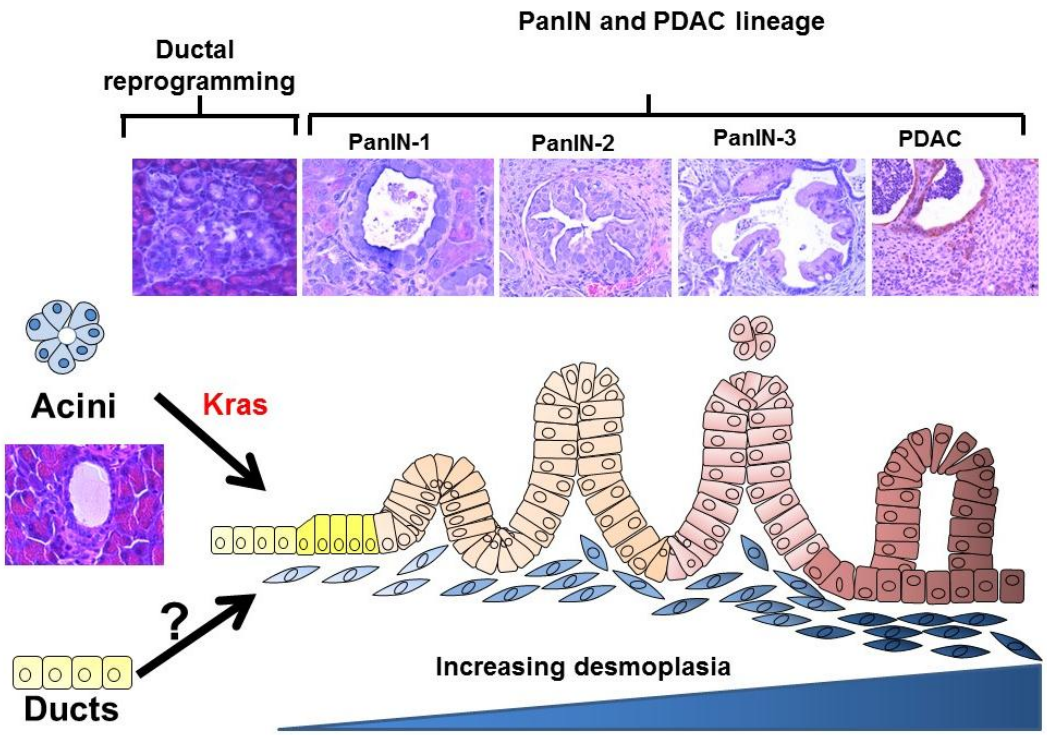

Figure 1.7 Initiation and progression of PDAC

Expression of oncogenic *Kras* in acinar cells of the pancreas results in Acinar to Ductal reprogramming (ADM). The ADM lesions then progressively develop into pancreatic intraepithelial neoplasia -1 (PanIN-1) where the cuboidal cells become columnar but with nuclei basal in position. Age, environmental insults, loss of tumor suppressor genes or mutations in pro-cancerous genes can result in progression of PanIN-1 to PanIN-2 and PanIN-3 lesions which are characterized by excessive mucin production, loss of cell polarity, atypical nuclei, and increasing desmoplasia. PanIN-3 progresses into PDAC with uncontrolled cell proliferation and invasion into the surrounding stroma. Adapted from [110].

1.9. Need for better understanding Smad7 in Pancreatic Cancer

In PDAC, there is aberrant signaling of TGF-β [26, 118] and it has been shown in mouse models that targeting TGF-β in PDAC results in decreased tumor growth [119]. However, Smad7, an inhibitor of the TGF-β pathway, is also over-expressed in PDAC, [120, 121]and its overexpression in hPCCs blocks TGF-β mediated growth inhibition that culminates into increased tumor growth[121-123]. Smad7 also interacts with p38 MAPK, resulting in the inactivation of GSK-3β and accumulation of adenomatous polyposis coli (APC) protein, which binds to the microtubule system and contributes to TGF-β-mediated cell migration [79, 124, 125]. The overexpression of Smad7 has been shown to be associated with poor survival in patients with endometrial, esophageal, colorectal, gastric, breast, skin and liver cancers[126]. Contrary to these findings, Smad7 has been shown to block TGF-β-mediated EMT and migration in HCC (liver cell lines) and lower levels of Smad7 correlate with longer survival in patients with liver cancer[127]. In prostate cancer cell lines, Smad7 has been shown to promote migratory responses in PC-3U cells [124] on one hand, while in another study using the same cells it has been shown to play an important role in apoptosis [128].

In pancreatic cancer, specifically, Wang *et al* demonstrated that low Smad7 levels correlated with lymph node metastasis and poor prognosis in pancreatic cancer patients [129]. Previously the Korc lab has demonstrated that Smad7 blocks TGF-β mediated growth inhibition by keeping pRb hyper-phosphorylated and functionally inactivating it without blocking activation of p-Smad2 levels[123]. We also demonstrated that Smad7 allows TGF-β to modulate the expression of genes such as PAI-1 and thioredoxin which enhance tumor growth [121, 122]. Xenograft models with COLO-357 cell lines overexpressing Smad7 demonstrate increased tumorigenicity. Findings from the Korc lab suggest a tumor enhancing function for Smad7, while clinical study suggests otherwise (Figure 1.8). Therefore, it is unclear if targeting Smad7 would be beneficial in PDAC.

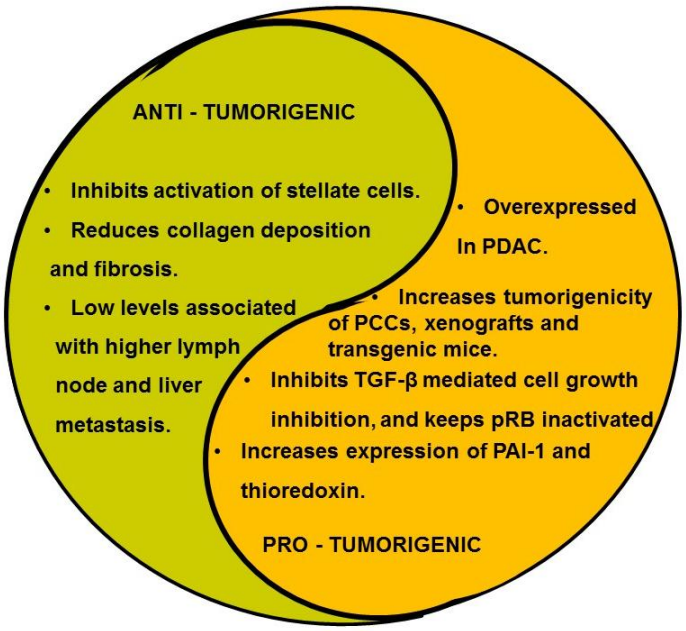

Figure 1.8 Yin and Yang model for dual role of Smad7 expression in PDAC

Smad7 plays a dual role in PDAC. On one hand Smad7 is overexpressed in hPDAC and its overexpression blocks TGF-β mediated cell growth inhibition, increases tumorigenicity inactivates p-Rb and increases expression of PAI-1 and thioredoxin. On the other hand low levels of Smad7 in hPDAC are associated with increased metastasis to the lymph nodes and liver. Overexpression of Smad7 in mouse model of chronic pancreatitis reduced activation of stellate cells, collagen deposition and fibrosis.

To better understand the role of Smad7 in context of pancreatic cancer, we have now developed a transgenic mouse model with conditional expression of Smad7 in the pancreas. In this thesis I intend to accomplish the following specific aims.

Primarily, I will focus on observational outcomes of overexpression of Smad7 (Smad7 OE) in the pancreas of mice and its effects in the presence of oncogenic *Kras*. This will elucidate the role of Smad7 in PDAC progression. Based on the previous studies in the lab [121-123] and by others [130] we expect Smad7 to accelerate PDAC progression. The goal is to determine the effects on canonical signaling pathways in the mouse tissues and see if the TGF-β pathway is attenuated by Smad7.

Secondly, my goal is to understand the mechanisms by which Smad7 inactivates pRb without attenuating p-Smad2 levels in COLO-357 cells. The effects of Smad7 on transcription of TGF-β mediated genes and its effects on p-pRb suggest alternative roles for Smad7, e.g. protein-protein interactions and or transcriptional co-activator or repressor effects without affecting TGF-β canonical signaling. Thus the goal is to unravel the mechanisms by which Smad7 modulates TGF-β to regulate gene expression.

1.10 Pancreatitis, TGF-β and Smad7

Chronic Pancreatitis (CP) is an important risk factor for PDAC [44]. Previous studies have shown that CP combined with genetic mutations in mouse models or with increased exposure to high fat diet, alcohol and tobacco smoke can lead to PDAC[131, 132].TGF-β1, -2 and -3 expression is increased in humans with acute pancreatitis [133] and after induction of acute pancreatitis in rats [134]. When wild-type mice are subjected to acute pancreatitis, it results in damage to acinar cells, increased inflammatory response, infiltration of lymphocytic infiltrates and increase in serum amylase and lipase [135]. Simultaneously when transgenic mice expressing heterozygous expression of dominant negative TβRII were subjected to acute pancreatitis, it blocked caerulein induced tissue damage and attenuated infiltration of neutrophils and macrophages [136]. When the dominant negative TβRII transgenic mice were subjected to chronic pancreatitis, they exhibited decreased fibrosis when compared to wild type mice [136, 137]. Smad7 overexpressing transgenic mice also displayed decreased collagen and alpha smooth muscle actin (α-SMA) [138, 139] when compared with wild type mice. Anti-inflammatory treatment in mice induced with chronic pancreatitis and expressing oncogenic Kras, resulted in prevention of PanIN progression to PDAC[131, 140]. Induction of acute pancreatitis in the presence of oncogenic Kras results in accelerated PanIN progression to PDAC [111, 112] Thus we hypothesized that overexpression of Smad7 will protect against caerulein-induced acceleration of PanIN progression in the KC genetically engineered mouse models (GEMM). In this thesis, we will compare and contrast the KC and KS7C mice subjected to caerulein-induced acute pancreatitis.

2. Materials and Methods

2.1 *LSL-SMAD7* Transgene Generation

The *pBTG* (plasmid #15037, depositing investigator D. Melton) and *pRosa26PAM1* (plasmid #15036, depositing investigator D. Melton) vectors were obtained from Addgene. These vectors are modifications of vectors originally created by F. Constantini (Srinivas et al. [141] and P. Soriano [142], respectively. The *pBTG* vector has a multiple cloning region upstream of IRES-eGFP. A previously cloned *HA-SMAD7* cDNA was cloned into *pBTG* using the NheI/SalI restriction sites. After screening the resulting clones for successful integration, the entire *HA-SMAD7-pIRES-eGFP* portion was cloned into *pRosa26PAM1* using the PacI/AscI restriction sites. There was appreciable recombination observed with amplification of the final product. The final full-length (>15Kb) plasmid was linearized using PacI, gel-purified and submitted to the Dartmouth Transgenic Mouse Facility for Embryonic Stem (ES) cell electroporation and selection.

2.2 ES Cell Electroporation, Selection, Injection and Screening

All ES cell electroporation and the selection was performed by the Dartmouth Transgenic Mouse Facility. Following transduction, ES cell pools were selected for neomycin resistance and cloned into parallel 96-well plates. The genomic DNA was isolated from >250 clones using proteinase K digestion, phenol/chloroform extraction and ethanol precipitation. Successful integration events in ES clone genomic DNA were first screened *en masse* using PCR analysis to detect 5' and 3' portions of the *LSL-SMAD7* transgene. At least 3 sets of primers were used at each end. For clones that amplified both ends of the transgene, a more rigorous PCR analysis was performed. The forward primer hybridized to an area within the *Rosa26* locus upstream from where the 5' arm was homologous and the reverse primer amplified from within the transgene, close to the LSL region (refer Table 2.1, Primer 1 and 2).The PCR reaction included 10X MGB reaction buffer (0.6M Tris pH8.8, 0.167M $(NH_4)_2SO_4$, 0.0066M $MgCl_2$ and 0.5% gelatin), 10µM dNTP, Dimethyl sulfoxide (DMSO), primers, beta-mercaptoethanol (β-Me) and Qiagen HotStar Taq polymerase. The successful product from this PCR was 1.5Kb. ES cell clones that had positive signals from all three screening PCRs were then screened using standard Southern blot analysis. Briefly, ten micrograms of genomic DNA from each ES clone was run on a 1% agarose gel and transferred overnight to a Hybond-XL (GE Healthcare, US) membrane by alkaline capillary transfer. The membrane was then dried and prehybridized with FBI buffer (1.5X SSPE, 10%

Polyethylene glycol (PEG) 8000 and 7% Sodium Dodecyl Sulfate (SDS)) at 65°C for at least 1 hour prior to overnight hybridization. To screen the 5' integration event, the *rosa-5'* probe was digested from the *pROSA26-5'* plasmid (a gracious gift from P. Soriano), ^{32}P-dCTP labeled and hybridized overnight at 65°C. To screen the 3' integration event, the *eGFP* probe was ^{32}P-dCTP labeled and hybridized overnight at 60°C. Following hybridization, the membranes were washed extensivelyas follows: 2XSSC briefly, 2x20 minutes with 2XSSC, 0.1%SDS at 65°C, 20 minutes with 0.5XSSC, 0.1%SDS at 65°C, 20 minutes with 0.25XSSC, 0.1%SDS at 65°C, and a final 20 minutes with 0.1XSSC, 0.1%SDS before exposing to film for 48 to 96 hours at -80°C. Targeted clones were expanded for blastocyst injection.

2.3 Generation of SMAD7 overexpressing transgenic mice

A lox-stop-lox (*LSL*) *SMAD7* transgene was created using the Soriano Rosa26 gene trap strategy [141, 142]. The transgene includes selection components for screening ES cell recombinants; neomycin (NeoR) and Diphteria toxin A (DT-A), a HA-tagged human *SMAD7* cDNA, and an IRES driving *eGFP* (Figure 2.1A). Using these materials, the transgene was inserted in a manner that allows expression to be driven by the endogenous *ROSA26* promoter. Integration of the transgene was 85% in ES cell clones screened (Figure 2.1B) with the correct position and orientation within the *Rosa26* locus (Figure 2.1C, 2.1D). As can be seen, clones #68, 69 and 71 had proper integration of the entire transgene, while #72 had a partial recombination event and was not at the correct position (Figure 2.1E). Clones #68 and 69 were used for blastocyst injection and subsequent *Rosa-LSL-SMAD7* mouse generation.

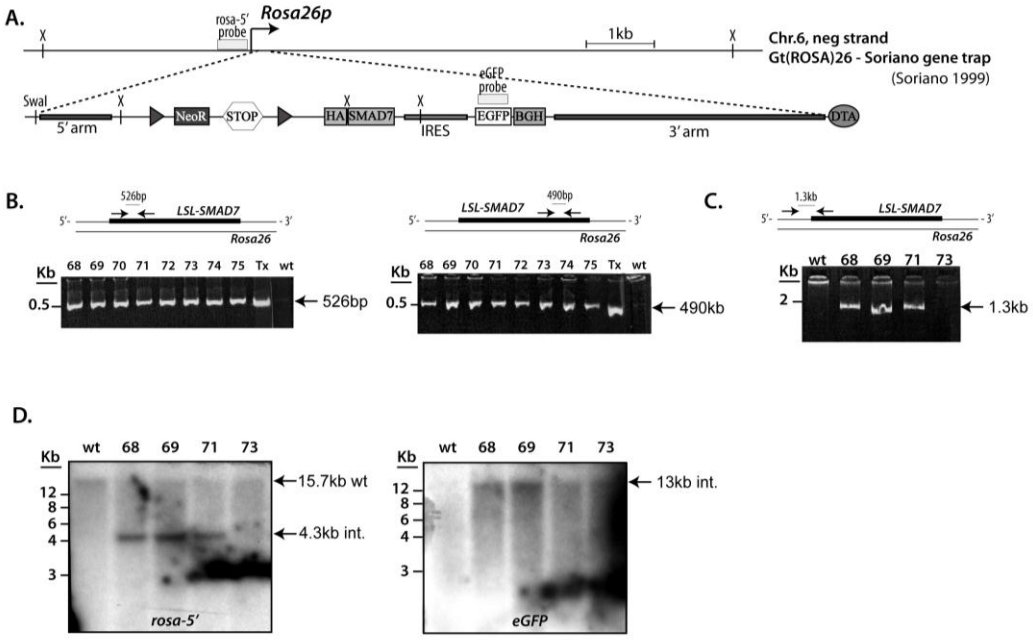

Figure 2.1 Generation a of *SMAD7* overexpressing transgenic mice

This figure describes the generation and validation of the *Rosa-LSL-SMAD7* (S7) mice. **(A)** The S7 transgene was designed using Soriano Rosa26 gene trap constructs [142]. Within the transgene, a lox-STOP-lox (LSL) is upstream of HA-tagged human *SMAD7*, followed by an IRES driving expression of *eGFP*. EcoRI restriction sites are designated by an "X". **(B)** The left (5'; 526bp product) and right (3'; 490bp product) panels are PCR analysis detecting for incorporation of different ends of the transgene in ES cell clones after two rounds of selection. There was high integration of the transgene, as evidenced by a positive PCR signal in >90% of the clones screened. Tx: purified transgene, wt: wild-type ES cell genomic DNA. **(C)** MGB PCR analysis detecting the correct insertion of the *LSL-SMAD7* transgene into the Rosa26 locus. The primers were designed in that the forward primer hybridized to the endogenous Rosa26 sequence and the reverse primer hybridized close to the LSL, after the 5' arm. The target amplification was 1.3Kb and was detected in ~85% of the positive ES cell clones. **(D)** Southern blot analysis using the *rosa-5'* probe to screen the 5' integration event (left) or the *eGFP* probe to screen the 3' integration event (right). With an EcoRI digest and *rosa-5'* probe (left), the correct integration should yield a 4.3Kb band while wild-type should be 15.7Kb. The blot was stripped and re-probed with *eGFP* probe (right), which with an EcoRI digest should yield a 13Kb band only if integrated.

2.4 Mouse Maintenance and Genotyping

Blastocyst injections and chimeric breeding were carried out using the C57bl6/J strain by the Dartmouth Transgenic Mouse Facility. The mice were humanely handled, and experiments were approved by the Institutional Animal Care and Use Committee at Dartmouth and by Laboratory Animal Resource Centre (LARC) at Indiana School of Medicine. Genotyping of the F1 progeny was achieved using an established screening protocol for the *eGFP* sequence by Jackson Labs (refer Table 2.1, Primer 3 and 4). The successful F1 progeny was used to maintain heterozygous breeding of Rosa-LSL-SMAD7 mice. Sections 2.1, 2.2, 2.3 and 2.4 were designed and performed by Dr. Alixanna Norris when she was a post-doctoral fellow in Dr. Korc's laboratory at Dartmouth.

2.5 Generation of KS7C, KtetS7C and KR$^{+/-}$S7C mouse models

Genetically Engineered Mice Conditional *Rb*$^{-/-}$, *Pdx1-Cre* mice, and *LSL-Kras*^{G12D} mice were obtained from the Mouse Models of Human Cancer Consortium at National Cancer Institute (NCI) (strain numbers 01XC1, 01XL5,and 01XJ6, respectively). The *tetO-Smad7and Rosa26rtTA-EGFP (R26rtTA-EGFP)* mice were previously described [143] and were a generous gift from Dr. Simon Conway at Indiana University School of Medicine.

KS7C mice: The triple mutant *LSL-SMAD7*; *Pdx1-Cre*; *LSL-Kras*^{G12D} mice (KS7C), and various littermate controls (KC or S7C) were on a mixed FVB; 129; C57Bl/6J genetic background. These mice were also backcrossed six generations into C57Bl/6Jand KC and KS7C mice were assessed at 3 months and 6 months of age.

KR$^{+/-}$S7C mice: The quadruple mutant *Rb*$^{-/-}$*,LSL-SMAD7*; *Pdx1-Cre*; *LSL-Kras*^{G12D} mice (KR$^{+/-}$S7C), and various littermate controls (KR$^{+/-}$C or KC) were on a mixed FVB; 129; C57Bl/6 genetic background.

KtetS7C: The quadruple mutant *tetO-Smad7and Rosa26rtTA-EGFP*; *Pdx1-Cre*; *LSL-Kras*^{G12D} mice (KtetS7C) were maintained on a mixed genetic background. Pregnant mice were administered green dyed doxycycline food pellets at concentration of 200mg/kg (BioServ) for induction of Smad7 *in utero*, or mice were administered green

dyed doxycycline food pellets at ages of 1, 2 and 3 months of age, up to 6 months. The control mice were provided with regular diet (Figure 2.2).

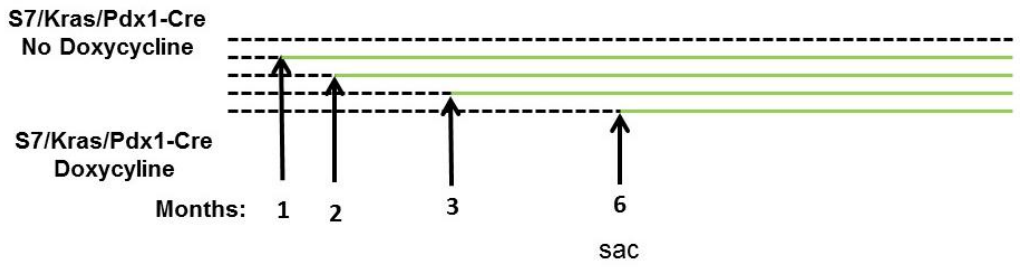

Figure 2.2 Schematic for regime of doxycycline food for KtetS7 mice

KtetS7 mice were fed with Doxycycline food at 1 month, 2 month and 3 month of age to induce expression of *Smad7* at different time points. Mice fed with regular food (no overexpression of *Smad7*) were used as controls.

2.6 DNA extraction from tail

Tail snips were collected from 2 week old mice and digested with 150 µL tail lysis buffer at 95ºC for 50 minutes in thermocycler. The tails were cooled and neutralized with 1M Tris HCl, pH 8.2.

2.7 Genotyping

LSL-Kras^{G12D}

The protocol provided on NCI mouse repository was used to amplify mutant ***LSL-Kras^{G12D}*** allele.

Pdx1-Cre, LSL-SMAD7,tetO-Smad7

Refer to Table 2.2 for PCR set up and Table 2.3 for cycling conditions.

LSL-Rb$^{-/-}$

The protocol provided on NCI mouse repository was used to amplify ***LSL-Rb$^{-/-}$***allele with slight modifications. There was no DMSO used and the final concentration of $MgCl_2$ used was 1.25mM compared to 2mM in final reaction. For the PCR conditions, the annealing time was reduced to 1 minute instead of 2 minutes.

Rosa26rtTA-EGFP

Protocol as described under JaxLab stock#005670.

2.8 RNA isolation from murine pancreatic tissues and cell lysates and conversion to cDNA

RNA was isolated from frozen pancreatic tissue of mice using the low-temperature guanidine isothiocyanate method as described previously [144, 145]. RNA was isolated from cell lysates using Trizol – Chloroform method [146]. The RNA was then analyzed for quantity and contamination on Nano drop (Thermo Scientific). Equal amount of RNA (50ng-2000ng) for each sample was diluted with water to make up the volume of 9 µL. It was then converted to cDNA using a high capacity RNA to cDNA kit from Applied Biosystems (Carlsbard, CA).

2.9 DNA extraction from cells

DNA was isolated from human pancreatic cancer cells (hPCCs) using the spin column protocol with DNeasy kit from Qiagen.

2.10 Gene expression analysis

Expression of *Hs_SMAD7, Rn_SMAD7, Hs_p21*, *Hs_AGR-2 and Mm_AGR-2* (Hs- human, Rn – Rat and Mm- mouse) was determined using pre-validated primer and probe sets (Assays on Demand, Applied Biosystems,Carlsbard, CA). Expression of *MUC1, MUC13* was analyzed using SYBR green method. 2X power SYBR Green enzyme mix (Applied Biosystems) 2X Fast Taqman PCR mix (Applied Biosystems, Carlsbard, CA) were used to prepare a 20 µL reaction with primer and an equal amount of cDNA. qPCR was performed with an ABI ViiA™ 7 sequence detection system (Applied Biosystems, Carlsbard, CA). Each sample was assayed in triplicates and Rps6, β-actin or 18S were used as endogenous controls for normalization in tissues, mPCCs and hPCCs respectively. Gene expression was calculated relative to control using the 2-ΔΔCt method. Data are plotted as means +/- SEM.

2.11 Protein isolation and quantification

Protein was isolated from cells by using complete lysis buffer (RIPA buffer with 1X protease inhibitor cocktail (tablets from Roche, Mannheim, Germany), 10mM Sodium orthovandate, 10mM β-Glycerophosphate and phenylmethylsulfonyl flouride (PMSF)).

The protein in each sample was quantified by Bicinchoninic Acid Assay (BCA) using the Pierce BCA Protein Assay Kit from Thermo Fisher Scientific (Rockford, IL).

2.12 Immunoblotting and quantification of bands

Equal amounts of protein (20µg), as measured by BCA, were run on 10, 12 or 15% Sodium dodecyl sulfate – polyacrylamide gel electrophoresis (SDS-PAGE), transferred to 0.45 or 0.22 µM PVDF membrane, blocked with 5% BSA or 5% skimmed milk (according to antibody data sheet) in TBS-0.05%/Tween-20 and immunoblotted with the indicated primary antibodies overnight at 4°C. After three washes in TBS-0.05%/Tween-20, Horse Radish Peroxidase (HRP) conjugated secondary antibodies (1:5000) were applied for one hour at room temperature. This was followed by three washes, and protein bands were detected using enhanced chemiluminescence (ECL) western blot detection reagent (Thermo Fisher Scientific) on X-Ray or Bio-Rad gel documentation system using Image lab software. Antibodies against β-actin or α-tubulin were used to assess loading of lanes. Quantification of band areas in each immunoblot was performed with ImageJ software (http://imagej.nih.gov/ij/), using blots from three independent experiments for each set of data. Quantification was presented as mean ± SEM. Target protein band intensity was normalized to indicated housekeeping protein. For phosphoprotein analysis, normalized signal of each phosphoprotein was expressed relative to the normalized total amount of that protein.

2.13 Histology, Immunohistochemistry (IHC), and Immunofluorescence (IF)

Mice were sacrificed at various time points – 1.5, 3, 6, 9 or 12 months for the KS7C mice, 3 months and 6 months for the KtetS7C mice and at 3 months or at morbidity for the $KR^{+/-}$S7C mice. The tissues from each mouse were collected and fixed in 10% formalin overnight, processed using an automated tissue processor (STP 420, Thermo Scientific, Waltham, MA) and embedded in paraffin. Sections (5µm thick) were prepared using the HM355s microtome (Thermo Scientific, Waldorff, Germany). H&E staining was performed for one section for each mouse using a standard protocol [147]. For IHC or IF, the tissues were deparaffinized, rehydrated and then subjected to antigen retrieval with antigen unmasking solution (Vector Labs, Burlingame, CA) or Tris EDTA (pH9).Tissues were incubated overnight with primary antibody as per data sheet (refer Table 2.4). For IHC detection, biotinylated secondary antibodies and a NOVA RED detection kit (Vector Labs) were used. For IF, fluorescent secondary antibodies were used. Nuclei were

visualized with 4, 6-Diamidino-2-phenylindole (DAPI).Masson's Trichrome (American MasterTech, Lodi, CA) was performed according to manufacturer's recommendations. Alcian blue staining was performed according to a standard protocol from IHC world [147].

2.14 IF quantification

Images were acquired using an Olympus BX60 microscope and a QImaging EXi Blue camera. For quantification, images were acquired from 5 different fields at 20X magnification and overall intensity was determined using Cell Profiler software and mean values were plotted with +/- SEM from 6 mice in each group[39].

2.15 Statistics

One-way ANOVA with Dunnett's post hoc tests and student*t*tests were used where applicable to test the significance of differences using Sigma Plot 12.0 Software (Systat Software, Inc, Chicago, IL). Survival curves and Kaplan-Meyer survival analyses were also generated and analyzed using Sigma Plot. A p-value < 0.05 was considered statistically significant in all tests.

2.16 Cell culture

The human PCC lines (COLO-357 and IUSCPCC-1) were grown in Dulbecco's Modified Eagle Medium(DMEM) (Lonza, Allendale, NJ) supplemented with 7% fetal bovine serum (FBS) (Tissue Culture Biologicals, Los Alamitos, CA), 100U/ml penicillin and 100mg/ml streptomycin (Hyclone, GE Lifesciences, Logan, Utah). BPXPC-3 and ASPC-1 were grown in Rosewell park memorial institute medium(RPMI) media (Hyclone) supplemented with 5% FBS, 100U/ml penicillin and 100mg/ml streptomycin. For the tetracycline inducible Smad7 cell lines similar media was used, but regular FBS was replaced with tetracycline free (TF) FBS (Clontech, Mountain View, CA). The mouse cell lines (KC, $KR^{+/-}$S7C and KS7C) were grown in RPMI supplemented with 5% FBS and antibiotics. The KtetS7C cell line was grown in RPMI supplemented with 5% TF FBS and antibiotics. The serum free (SF) media used in the experiments was DMEM or RPMI containing 0.5% FBS, 5 mg/ml Apo-transferrin, 5 ng/ml sodium selenite and antibiotics. For induction of Smad7 in hPCCs and KtetS7C cells, the cells were treated with TF media supplemented with 2µg/mL Doxycycline (Sigma Aldrich, St. Louis, MO). Human COLO-357 overexpressing SMAD7 PCCs were as described previously [123]. The

IUSCC-PC-1 cell line was established from a patient-derived orthotopic xenograft in an athymic mouse [148]. IUSCC-PC-1 cells were authenticated, and confirmed to be human and free of pathogens and other cell types by IDEXX Bioresearch (St. Louis, MO). PCCs were cultured in DMEM with 1% antibiotic (100 units/ml penicillin; 100 mg/ml streptomycin) and 7% FBS.0.5nM TGF-β1 was used for all cell culture experiments.

2.17 Tetracycline inducible SMAD7 overexpressing hPCCs

Adding c-Myc tag to SMAD7 cDNA: Primers FP_S7a and RP_S7myc (Refer primer table for sequence) and clone S7XL6 from Origene (Rockville, MD) was used as a template to amplify c-Myc tagged SMAD7 cDNA. Gateway cloning of SMAD7-cMyc cDNA: Next, the att B1 and attB2 sites were added to the SMAD7-c-Myc cDNA using primers FP_attB1 and RP_attB2. This product was gel purified and used as template for cloning into the donor vector (pDONR^{TM}221, Invirogen) using BP Clonase enzyme (Invitrogen) to prepare the S7-c-Myc P221 entry vector. The plasmid was transformed into NEB® 5-alpha Competent E. coli (High Efficiency) competent cells (New England BioLabs, Ipswich, MA). Miniprep for plasmid isolation was carried out using Qiagen kit for 8 of these colonies and the plasmids were screened for presence of SMAD7 by PCR using the primers FP_S7a and RP_S7myc. LR Clonase enzyme was then used to catalyze *in vitro* homologous recombination between the entry S7-c-Myc P221 entry plasmid and the gateway destination lentiviral vector, PLIX-402 (a gift from David Root, Addgene plasmid # 413394). The reaction was then transformed into NEB competent cells and once again 8 colonies were picked and their plasmids were screened for SMAD7-c-Myc insertion by sequencing using LNCX-FP and PLIX_seqRP. The plasmids were sequenced for the transactivator rtTA (**r**everse **t**etracycline-controlled **t**rans**a**ctivator) and the Tet Responsive Element (TRE) with PLIX_SQ_FP1 & RP1 and PLIX_SQ_FP2 and RP2 respectively. The sequence for SMAD7-c-Myc, rtTA and TRE match 100% when blasted against the known sequence plasmid from colony #7. A maxi – prep using Qaigen kit was performed for colony # 7 and this was further used for transfecting hPCCs.

The SMAD7-c-Myc PLIX-402 lentiviral plasmid was then transfected into 293T cells, along with packaging plasmids PAX-2 and pMD2.G, using lipofectamine to generate viral particles. The media from the transfected 293T was collected 48, 72 and 96 hours post transfection and used to transduce hPCCs. A similar transfection was carried out using the PLIX-402 without the SMAD7-c-Myc gene to generate Sham hPCCs as controls. 4-6

µg of puromycin was used to select the hPCCs with the SMAD7-c-Myc gene. The hPCCs used for transduction were ASPC-1, BXPC-3, COLO-357 and IUSCC-PC1. Validation of SMAD7 mRNA and protein was carried out for ASPC-1, BXPC-3 and COLO-357 cell lines.

2.18 Constitutive overexpression of SMAD7 in hPCCs

c-Myc tagged SMAD7 in pLNCX vector has been previously described[123]. Phoenix cells were transfected with the retroviral c-Myc SMAD7 construct using lipofectamine. The media from the transfected Phoenix cells was collected 48, 72 and 96 hours post transfection and used to transduce IUSCC-PC1cell line. COLO-357 cells transduced with this plasmid have been previously described [123]. Validation of SMAD7 mRNA by q-PCR and proteins by western blotting was carried out for both the cell lines.

2.19 Knockdown of SMAD3 in COLO-357

pGIPZ lentiviral vector containing SMAD3 targeting shRNA was transfected into 293T cells along with packaging plasmids PAX-2 and pMD2.G using lipofectamine to generate virus particles. The viral supernatant from the transfected cells was used to transduce COLO-357 cells. Simultaneously Sham COLO-357 (control) were generated using only the pGIPZ backbone. The cells were selected with 4 µg of puromycin and then sorted by flow cytometery for green fluorescent protein (GFP). Knockdown of Smad3 was validated by analyzing mRNA and protein levels.

2.20 SMAD3 CRISPR of hPCCs

Guide Oligo sequences targeting Exon 6 of SMAD3 were designed using Blenching software. The sequences of which are:

G1-FP: P-5'CACCGTACGAGCTGAACCAGCGCGT3';

G2-FP: P-5' CACCGCCGGCTCGCAGTAGGTAAC3'. Each guide sequence was then annealed with a reverse compliment sequence, G1-RP: P- 5' aaacACGCGCTGGTTCAGCTCGTAC3' and G2-RP: P-5'aaacGTTACCTACTGCGAGCCGGC 3'. The annealed guide1 and guide2 were then cloned into plasmids pSpCas9n (BB)-2A-Puro (PX462) V2.0 (a gift from Feng Zhang [Addgene plasmid # 62987]) and pSpCas9n (BB)-2A-GFP (PX461) V2.0 (a gift from Feng Zhang [Addgene plasmid # 48140]) respectively using standard protocol [149]. The plasmids containing the guides were then co-transfected into COLO-357 and IUSCC-

PC-1 cells. Simultaneously plasmids with scrambled guide sequences from Santa Cruz Biotechnology (SC-43728) were also transfected into COLO-357 and IUSCC-PC-1 to create sham cells. 48 hours post transfection, the cells were sorted for GFP and then plated in 7% DMEM with 4µg/mL puromycin. The cells were then allowed to recover, and plated as single cells by serial dilution method into 96-well plates. Single cell clones for each cell lines were then isolated and validated for Smad3 knockout by protein and mRNA expression. The portion flanking Exon6 was amplified by PCR using the primers S3-Exon FP and S3- Exon RP and sent for sequencing to analyze the mutations.

2.21 Isolation of mouse cells from tumor

A small piece of the tumor was washed with Hank's Balanced Salt Solution (HBSS) from Lonza containing 1% antibiotic-antimycotic (Gibco, Carlsbad, CA) two times. The tissues were then cut into small pieces using sterile scalpels. These pieces were then transferred into a conical tube with 5mL of collagenase IV, (Worthington, Lakewood, NJ) 2mg/mL in HBSS and incubated for 1 hour at 37°C. After 1 hour, 5mL of HBSS was added to the collagenase and it was filtered through a 70 µM sieve. The cells were then centrifuged at 1000rpm for 4 minutes, re-suspended in RPMI media with 20% FBS and 1% antibiotics. The cells were plated in a 60mm dish and PCCs were cultured. They were then slowly weaned to media with 5% RPMI[113]. The cells were routinely checked for Mycoplasma and then were authenticated, and confirmed to be murine and free of pathogens and other cell types by IDEXX Bioresearch (St. Louis, MO).

2.22 Immunocytochemistry (ICC)

5000 cells per well were seeded onto chamber glass slides coated with chemically modified CC^2 growth surface (Lab-Tek, Thermo Scientific) and incubated at 37°C and 5% CO_2 in growth media until ~80 % confluence was achieved. Then the cells were fixed in 10% formalin for 15 minutes at room temperature followed by three quick washes in Phosphate buffered saline pH 7.4 (PBS). The cells were permeabilized and blocked by incubating with 0.15% Triton X-100, 1% BSA in 5% normal goat serum (blocking solution) for 30 minutes. The cells were then incubated with cytokeratin 19 (CK19) (1:200 dilution) or/and Alpha smooth muscle actin (α-SMA) (1:100) in blocking buffer for an hour. Dylight 488 conjugated goat anti-rat secondary antibody (1:400) was used to probe for CK19 and Dylight 555 conjugated goat anti-mouse secondary antibody (1:400) was used to probe for α-SMA. The coverslips were mounted using Prolong Gold

Antifade mounting medium containing DAPI (Thermo Fisher Scientific) for nuclear staining. The cells were imaged using an Olympus BX60 microscope and a QImaging EXi Blue camera or Leica DMI3000 inverted microscope outfitted with a DFC300 FX camera.

2.23 Cell proliferation assays

3-(4, 5-dimethylthiazol-2-yl)-2, 5-diphenyltetrazolium (MTT) from Sigma Aldrich was used to determine cell proliferation [150]. Each of the mouse cell lines - KC, $KR^{+/-}$S7C, KtetS7C, and KS7C were seeded (5000/well) in 6 wells of a 96-well plates. Proliferation was assessed at 48 hours after incubating them with 12.5µL of MTT solution (1mg/mL) for 3-4 hours. Viable cells convert MTT to an insoluble formazan product. This was solubilized by adding acidified isopropanol to cells which resulted in a purple solution. The absorbance of the solution was measure by U.V spectrophotometer at 560nm. The value of absorbance is directly proportional to number of viable cells. The mean value for absorbance of control-treated cells was normalized to 100%, and changes in proliferation were calculated as percent control in three independent experiments. Data are shown as means +/- SEM.

2.24 3-Dimentionsional (3D) tissue culture

Mouse cells were grown in 3D culture as previously described [151]. Briefly, each well of a 96-well plate was coated with 1% soft agar with media, followed by seeding2000 mouse cells per well with 3% Matrigel (BD Biosciences). Four days post-plating and every three days thereafter the Matrigel was replenished with fresh media with or without 500 pM TGF-β1. Images were acquired with a Leica DMI3000 inverted microscope outfitted with a DFC300 FX camera before each treatment. On the 14^{th} day, colony growth was quantified using the MTT. Cells were stained with 20µL MTT and then scanned. Colony density and area were determined using ImageProPlus, version 7.0. The total density and area of KC cells (control) was normalized to 100%, and changes in growth for KS7C, $KR^{+/-}$S7C and KtetS7C were calculated as a percentage of control.

2.25 Orthotopic injections

KS7C and $KR^{+/-}$S7C (200,000 cells) were suspended in 30µL of PBS and injected directly into the mouse pancreas of 8 weeks old, male NOD scid gamma (NSG) mice by the Indiana University Simon Cancer Center *In vivo* Therapeutics Core. The mice were monitored for tumor formation each week for 3-6 weeks. Animals were sacrificed when moribund. Tumor, spleen, liver, kidney and lungs were collected for parfin embedding. Cell lines were isolated from the tumors and metastatic lesions.

2.26 Induction of Acute Pancreatitis

The mice to be injected were fasted overnight. KC and KS7C mice were injected every hour with caerulein or with vehicle (0.05M NH_4OH) alone for upto 7 hours [112, 134]. The procedure was repeated 48 hours later. Caerulein (Sigma, St. Louis MO) was diluted in 6% dextran 70, 0.9% NaCl and injected at a dose of 50µg/kg of body weight. Six KS7C mice were injected with caerulein in parallel with six KC mice. A second group of KC and KS7C mice received injections of carrier buffer only. All animals were fasted for 12 hours before the experiment.

2.27 Chromatin Immunoprecicpitation (ChIP) Assays

Sham or Smad7 overexpressing COLO-357 and IUSCC-PC1 cells were plated in 15-cm dishes, cross-linked with formaldehyde and glycine and then collected. ChIP assays were performed with c-Myc, Smad3 and 4 or control IgG antibodies using the Simple ChIP Enzymatic Chromatin IP kit (Cell Signaling, Danvers, MA) as per manufacturer's instructions. The *AGR2*promoter (See Table 2.1 for sequence) was amplified by q-PCR and the percent input was calculated based on C_T values.

2.28 Gene Set Enrichment Analysis (GSEA)

A Smad3 gene signature was generated using public microarray expression data of A549 cells treated with TGF-β or SiS3 (specific inhibitor of p-Smad3) and TGF-β for 24 hours[152]. GSE-26858 expression files were downloaded from GEO-database, and differential gene expression analysis was performed using R (version 3.2) and the limma package (version 3.4, Bioconductor)[153, 154]. Genes that were significantly differentially expressed between TGF-β versus TGF-β plus SIS3 (FC =>2 or <=2, p <

0.05) (Supplementary Table 6.1) were then used to generated a Smad3 signature. To determine whether the generated Smad3 signature was enriched in pancreatic cancer patients, Gene Set Enrichment Analysis (GSEA) was performed comparing expression of adjacent normal human pancreas tissue and corresponding tumors. GSE-62452 expression data of adjacent normal and pancreatic cancer human samples were downloaded from the GEO-Database [155, 156]. Data were prepared from the downloaded microarray expressionset, and a GSEA was performed against the generated Smad3 signature using the GSEA desktop application (Gsea2-2.2.3, Broad Institute) according to GSEA guidelines [157].

2.29 Composition of buffers used

A. RIPA buffer for cell lysis for protein extraction:

50mM Tris-HCl, pH 7.4; 1% NP-40; 0.25% Na-Deoxycholate; 150mM NaCl; 1mM EDTA; 1mM NaF

B. 5X Running Buffer

0.96M Glycine; 125mM Tris

C. 10X TBS

1.36M NaCl; 200mM Tris, pH 7.6

D. Stripping Buffer

2% SDS; 62.5mM Tris, pH 6.8. 350µL β-Mercaptoethanol (BME) was added to 50mL just before use.

E. Transfer Buffer

25mM Tris; 192nM Glycine; 20% Methanol

F. Upper Buffer for SDS-PAGE Gel

0.5M Tris; 0.4% SDS, pH 6.8

G. Lower Buffer for SDS-PAGE Gel

1.5M Tris; 0.4% SDS, pH 8.8

H. 6X Protein loading dye

1g SDS, 7mL upper buffer, 3mL Glycerol, 600µL BME, 0.6% bromophenol blue

H. DNA lysis buffer for genotyping

50mM NaOH, 2mM EDTA

2.30 Primers used (Table 2.1)

Name	**Experiment**	**Direction**	**Sequence**
	LSL-SMAD7 integration in ES	Forward	5’ GGCGGACTGGCGGGACTA 3’
	LSL-SMAD7 integration in ES	Reverse	5’ GGGACAGGATAAGTATGACATCATCAAGG 3’
EGFP mut _FP	*LSL-SMAD7*genotyping	Forward	5’ AAGTTCATCTGCACCACCG 3’
EGFP mut _RP	*LSL-SMAD7*genotyping	Reverse	5' TCCTTGAAGAAGATGGTGCG 3'
K005	*LSL-Kras^{G12D}* genotyping	Forward	5' AGCTAGCCACCATGGCTTGAGTAAGTCT 3'
K006	*LSL-Kras^{G12D}* genotyping	Reverse	5' CCTTTACAAGCGCACGCAGACTGTAGA 3'
Cre1	*Pdx1-Cre* genotyping	Forward	5' TGATGAGGTTCGCAAGAACC 3'
Cre2	*Pdx1-Cre* genotyping	Reverse	5' CCATGAGTGAACGAACCTGG 3'
R007	*Rb-1* genotyping	Forward	5' GGCGTGTGCCATGAATG 3'
R008	*Rb-1* genotyping	Reverse	5' AACTCAAGGGACCTG 3'
Tet_S7FP	*tetO-Smad7*genotyping	Forward	5’ ATCCACGCTGTTTTGACCTC 3’
Tet_S7RP	*tetO-*	Reverse	5’ GAGCGCAGATCGTTTGGT 3’

	*Smad7*genotyping		
GrtA P1	*Rosa26rtTA-EGFP WT* genotyping	Forward	5'CTGGCTTCTGAGGACCG3'
GrtA P2	*Rosa26rtTA-EGFP WT* genotyping	Reverse	5'CAGGACAACGCCCACACA3'
GrtA P3	*Rosa26rtTA-EGFP mut* genotyping	Forward	5'AGGGCGAGGAGCTGTTCA3'
GrtA P4	*Rosa26rtTA-EGFP mut* genotyping	Reverse	5'TGAAGTCGATGCCCTTCAG3'
Mm_Muc1 FP	*Mm_Muc1* expression	Forward	5’ ACATCTTTCCAACCCAGGAC 3’
Mm_Muc1 RP	*Mm_Muc1* expression	Reverse	5’ GAGACTGCTACTGCCATTACC 3’
Mm_βAct FP	*Mm_βAct* expression	Forward	5' GGCTGTATTCCCCTCCATCG 3'
Mm_βAct RP	*Mm_βAct* expression	Reverse	5'CCAGTTGGTAACAATGCCATGT 3'
Hs_MUC1 FP	*Hs_MUC1* expression	Forward	5’ AGTACCCCACCTACCACAC 3’
Hs_MUC1 RP	*Hs_MUC1* expression	Reverse	5’ CCCTACAAGTTGGCAGAAGTG 3’
Hs_MUC13 FP	*Hs_MUC13* expression	Forward	5’ CAGTATCAGAAACATTTGACCCAG 3’
Hs_MUC13 RP	*Hs_MUC13* expression	Reverse	5’ GGTGACAGAGATGTGCTTACAG 3’
Hs_GPX2 FP	*Hs_GPX2* expression	Forward	5’ GCTTCCCTTGCAACCAATTTG 3’
Hs_GPX2 RP	*Hs_GPX2* expression	Reverse	5’ TTCTGCCCATTCACCTCAC 3’

Hs_18S FP	*Hs_18S* expression	Forward	5' GTAACCCGTTGAACCCCATTC 3'
Hs_18S RP	*Hs_18S* expression	Reverse	5' CCATCCAATCGGTAGTAGCG 3'
FP_S7a	Adding c-Myc Tag to Smad7	Forward	5' CATGTTCAGGACCAAACGATCT 3'
RP_S7Myc	Adding c-Myc Tag to Smad7	Reverse	5' CAGATCCTCTTCTGAGATGAGTTTTTGTTCG TACCGGCTGTTGAAGATGAC 3'
FP_attB1	Adding att sites to c-Myc-SMAD7	Forward	5' GGGGACAAGTTTGTACAAAAAAGCAGGCTG CATGTTCAGGACCAAACGATCTG 3'
RP_attB1	Adding att sites to c-Myc-SMAD7	Reverse	5' GGGGACCACTTTGTACAAGAAAGCTGGGT CCTACAGATCCTCTTCTGAGATGAGTTTTTG 3'
LNCX-FP	sequencing for GOI in PLIX402 plasmid	Forward	5' AGCTCGTTTAGTGAACCGTCAGATC 3'
PLIX_seq RP	sequencing for GOI in PLIX402 plasmid	Reverse	5' CCGGATCCTTAGTGGTGGTG 3'
PLIX_SQ_FP1	sequencing the rtTA sequence in PLIX402	Forward	5’ GTGGTGATGTTGAAGAAAACCCTGG 3’
PLIX_SQ_RP1	sequencing the rtTA sequence in PLIX402	Reverse	5’ AAGCAGCGTATCCACATAGCG 3’
PLIX_SQ_FP2	sequencing the TRE sequence in PLIX402	Forward	5’ AGGCAAAGAGAAGAGTGGTGCA 3’
PLIX_SQ_RP2	sequencing the TRE sequence in PLIX402	Reverse	5’ CGTGTGATTCCAAATCTGTTCC 3’
AGR2_chip FP4	*AGR2* promoter for	Forward	5’ GTCCCAACTCTGCCCTAAAC 3’

	ChIP		
AGR2_chip RP4	*AGR2* promoter for ChIP	Reverse	5’ AACTAGCAGGCCCTTAGATAGA 3’
S3-Exon 6 FP	sequencing Exon 6 of Smad3 in CRISPR cells	Forward	5' CTCCAGACACCTGAGCATCTTG 3'
S3-Exon 6 RP	sequencing Exon 6 of Smad3 in CRISPR cells	Reverse	5' CCTTCAGAGGCTGTGTGTTCAG 3'

2.31 PCR reactions (Table 2.2)

Sr. No.	**Substance**	**Final conc *LSL-SMAD7***	**Final conc *Pdx-1 Cre***	**Finalconc *tetO-Smad7***	**Cloning of Smad7**
1	Buffer	1X	1X	1X	1X
2	dNTPs	0.375mM	0.25mM	0.25mM	0.25mM
3	MgCl2	1.5mM	1.5mM	1.5mM	1.5mM
4	FP	0.6µM	0.5µM	0.5µM	0.5µM
5	RP	0.6µM	0.5µM	0.5µM	0.5µM
6	Taq	0.025U/µL	0.025U/µL	0.025U/µL	0.025U/µL

2.32 PCR cycling conditions (Table 2.3)

Step #	**Step**	**Final conc *LSL-SMAD7***	**Final conc *Pdx-1 Cre***	**Finalconc *tetO-Smad7***	**Cloning of Smad7**
1	Hot start	95 ºC 15 minutes	95 ºC 15 minutes	95 ºC 15 minutes	95 ºC 15 minutes
2	Denaturing	95 ºC	95 ºC	95 ºC	95 ºC

		30 seconds	30 seconds	30 seconds	30 seconds
3	Annealing	55 ºC 45 seconds	58 ºC 30 seconds	60 ºC 1 minute	55/56 ºC 45 seconds
4	Extension	72 ºC 1 minute	72 ºC 30 seconds	72 ºC 1 minute	72 ºC 1 minute
5	# of cycles steps 2-4	34	35	34	35
6	Extension	72 ºC 10 minutes	72 ºC 2 minutes	72 ºC 2 minutes	72 ºC 10 minutes
7	Hold/End	10 ºC - ∞	10 ºC - ∞	10 ºC - ∞	10 ºC - ∞

2.33 List of antibodies used (Table 2.4)

Antibody	Vendor	Dilution	Application
CK19	DSHB	1:10/1:200	IHC/ICC
α - SMA	Sigma	1:100	ICC
p-Histone H3 (S10)	Cell Signaling	1:200	IHC
Phospho RB(S807/S811)	Cell Signaling	1:400 /1:1000	IF/ IB
Ki67	Novocastra	1:200	IF
Phospho Smad2	Millipore	1:200	IF
Phospho Smad3	Abcam	1:200	IF
Insulin	Abcam	1:800	IF
Amylase	Abcam	1:400	IHC

Glucagon	Abcam	1:400	IF
c-Myc	Millipore	1:1000/1 µg	IB/IP/ChIP
Smad7	Abcam	1:1000	IB
PP-1c	Santacruz	1:500	IB/IP
β-actin	Cell Signaling	1:50,000	IB
γ-tubulin	Sigma	1:1200	IB
Total Smad3	Cell Signaling	1:1000	IB
Total Smad2	Cell Signaling	1:1000	IB
Total Smad3	Cell Signaling	1:50	ChIP
Total Smad4	Cell Signaling	1:100	ChIP
Total pRB	Pharminogen	1:1000	IB
AGR-2	Abcam	1:1000/1:1000	IHC/IB
p21	Santacruz (F-5)	1:50/1:200	IF/IB

3. Results

Transforming growth factor beta (TGF-β) signaling is awry in PDAC and all of its three mammalian isoforms are overexpressed [27, 118]. The canonical signaling pathway involves phosphorylation of Smad2 and Smad3 which then bind with Smad4. These Smad complexes then translocate from the cytoplasm of the cells to the nucleus to modulate gene transcription that in turn regulate cellular processes such as proliferation, differentiation, migration, deposition of extra cellular matrix, and apoptosis. Inhibitory Smad6 and Smad7proteins serve as negative feedback regulators for the TGF-β pathways and are over-expressed in patients with PDAC [120, 121, 158].

The Korc lab has previously shown that overexpression of Smad7 (Smad7 OE) in COLO-357 cells inactivates pRb or keeps it hyper-phosphorylated by blocking TGF-β-mediated de-phosphorylation of pRb[123]. Consequently, there is a loss of TGF-β-mediated growth inhibition in spite of the ability of TGF-β to phosphorylate Smad2 and to up-regulate p21, an important inhibitor of cell cycle progression. PAI-1 expression increases with Smad7 overexpression in COLO-357 cells and TGF-β and confers an ability to the PCCs to form large tumors in nude mice[121, 122]. However, another study has reported that in PDAC patients, low levels of Smad7 correlate with poor prognosis and lymph node metastasis [129]. These findings appear to contradict each other and suggest a dual role for Smad7 in PDAC. Therefore we generated a transgenic mouse model to unravel the role of Smad7 and its effects on the canonical TGF-β pathway in pancreatic cancer. We first examined the effects of Smad7 overexpression in the context of *Kras* mutation in PDAC. A tetracycline inducible Smad7 mouse model was used to induce Smad7 expression at different ages to determine if it played a role in initiation or progression of PDAC or both. Mouse tissue, human PCCs, and primary cell lines from mouse tumors were used to confirm previous findings and address the impact of Smad7 on pRb phosphorylation and p21 levels. Effects on phosphorylation of Smad2 and Smad3 were analyzed by IF of mouse tissues and by western blotting using lysates prepared from cells treated with TGF-β. In addition, ChIP assays were performed to see if Smad7 bound directly to DNA that regulate expression of TGF-β-mediated genes that were altered by overexpression of Smad7.

3.1 Validation of *SMAD7* overexpression in mice genetically modified with *Rosa-LSL-SMAD7and Pdx1-Cre (S7C)* transgene

To overexpress *SMAD7,* the mice harboring the *LSL-SMAD7* transgene on the Rosa26 locus were crossed with those encoding the *Pdx1-Cre* gene (S7C). The Cre recombinase is expressed from the *Pdx-1* promoter, which is transcriptionally active in the ES cells of the foregut endoderm around 8.5 days [159, 160] and contributes to formation of the early pancreatic bud cells. At 9.5 days, along with P48 transcription factor, Pdx-1 then gives rise to pancreatic progenitor cells. Thus, the Cre recombinase is expressed in all pancreatic progenitor cells and removes the lox stop lox cassette from the *Rosa-LSL-SMAD7* transgene, which allows for expression of the *SMAD7* specifically in the pancreas (Figure 3.1-A).

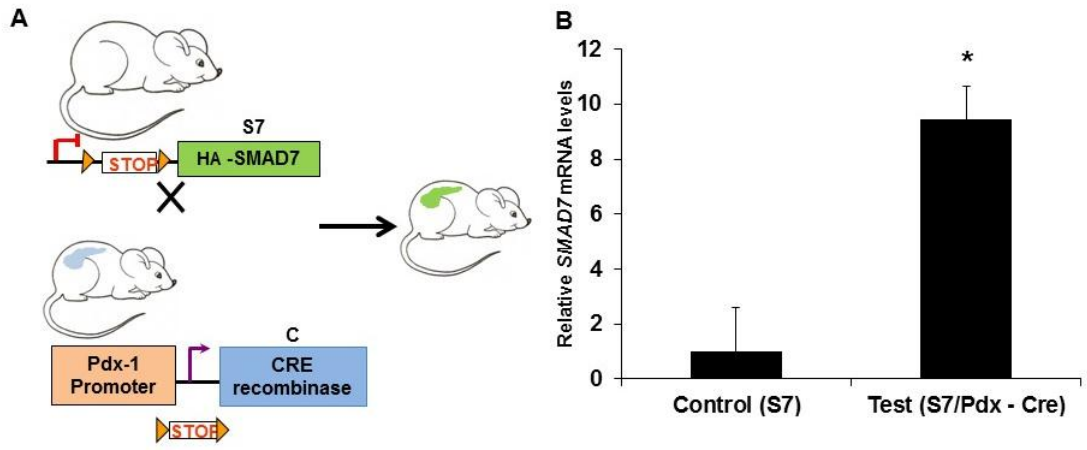

Figure 3.1 Validation of *SMAD7* overexpression in mice with *Rosa-LSL-SMAD7* and *Pdx1-Cre* transgene

(A) Schematic figure showing *LSL-SMAD7 (S7)* transgenic mouse, when crossed with mice harboring *Pdx1-Cre (C).* The Cre (blue) is expressed in the pancreatic progenitor cells (blue) which results in removal of the stop cassette preceding the *SMAD7* transgene, thus resulting in expression ofSMAD7 in the pancreas of the mice (S7C mice). **(B)** *SMAD7* mRNA levels measured by q-PCR are significantly elevated in the S7C (test) mice compared to the ones with S7 (control) alone. Data are the means ± SEM from 4 individual mice done in triplicates for each group. *p value <0.05 was considered significant.

Levels of *SMAD7* mRNA were determined by qPCR in the pancreata of four S7C mice and 4 mice with only the *SMAD7* transgene (WT). Compared to WT mice, the S7C mice had a 9-fold increase in *SMAD7* expression (Figure 3.1-B). To determine if *SMAD7*overexpression affected pancreas development or its function, tissues from two 3 month, two 6 month, and two 12 month old S7C mice were stained with H&E and IF or IHC for expression of insulin, glucagon and amylase. The pancreata of all the mice showed normal histology and normal expression and distribution of insulin and glucagon in the islets, and amylase in the acinar cells (Figure 3.2). Taken together, these results suggest that pancreas development, morphology and physiology are not compromised by Smad7 overexpression.

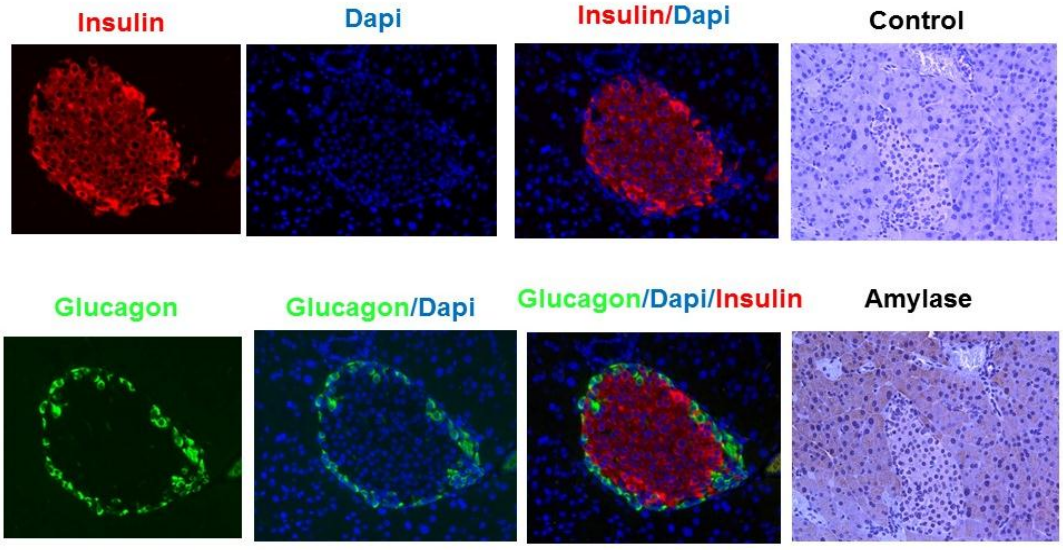

Figure 3.2 Overexpression of *SMAD7* alone does not affect pancreas development or physiology

Representative IF images (from 6 different mice) of 5 µm sections from a 12 month-old S7C mouse revealed co-expression of Insulin (red) and glucagon (green) in islets. Amylase expression in acinar cells was demonstrated by IHC.

3.2 *SMAD7* overexpression accelerates PanIN progression when combined with oncogenic *Kras mutation*

Approximately 92-95% of pancreatic cancers harbor *Kras* mutations, which is the main oncogenic driver gene for PDAC[161].The *Kras* mutation leads to the formation of PanIN lesions by 8 weeks of age in mice that progress to PDAC by 9-11 months[160]. Since expression of oncogenes or deletion of tumor suppressors cooperates with the *Kras* mutation, we next introduced $Kras^{G12D}$ into the mice in combination with *SMAD7* and the*Pdx1-Cre* gene (KS7C) (Figure 3.3 A). Mice encoding the $Kras^{G12D}$ and *Pdx1-Cre* (KC) transgenes were used as controls. 12-14 mice per group were used for survival analysis and 3-6 mice per group were sacrificed at 3, 6, 9 and 12 months of age to assess PDAC progression. All the mice with KS7C genotype displayed acinar to ductal metaplasia (ADMs) at 8 weeks of age, and 3 of 6 mice developed PDAC by 3 months of age. These mice exhibited significantly lower survival compared to KC mice (Figure 3.3 B).

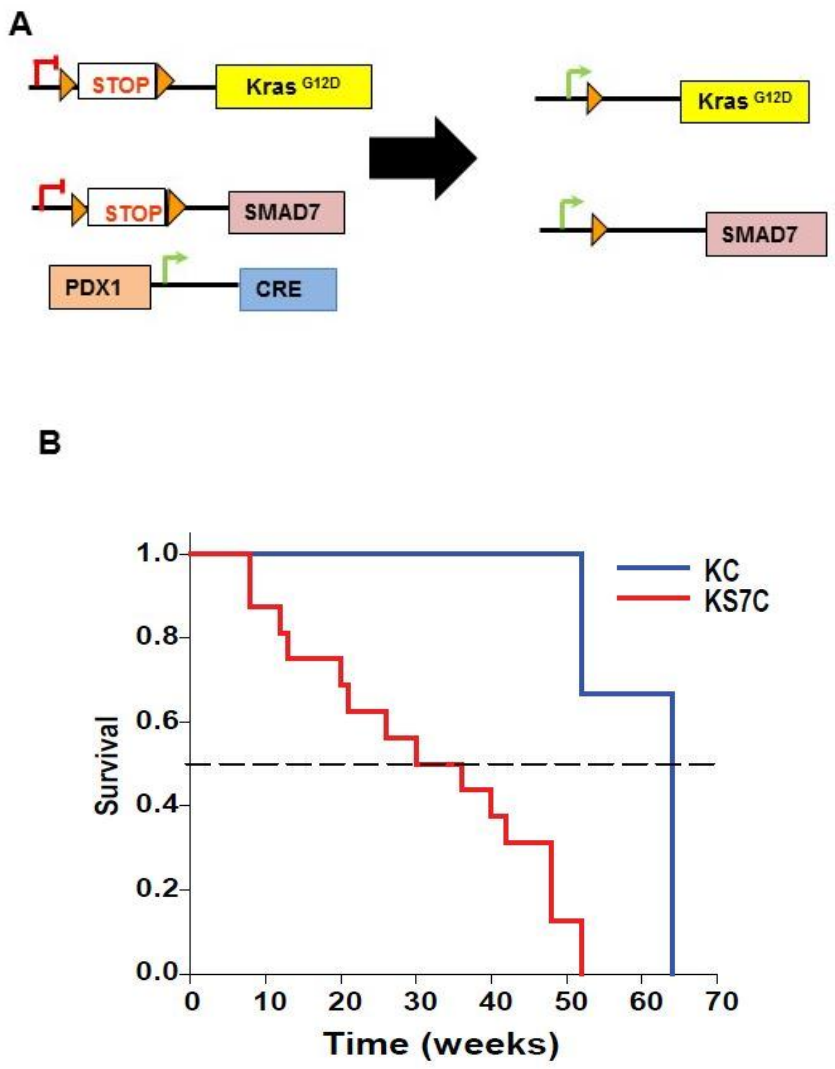

Figure 3.3 The KS7C mouse model that express oncogenic Kras in presence of Smad7 OE

(A) Schematic representation of generation of the KS7C mouse model. **(B)** Mice harboring both the oncogenic *Kras*^{G12D} and *SMAD7* transgene (KS7C) exhibit significantly lower survival (p value < 0.001) compared to KC mice (N=12 for KC, N=14 for KS7C).

Histopathological analysis and IHC staining with CK19 revealed that KS7C mice had an increased number of abnormal lesions compared to age matched KC mice. Figure 3.4 is a representative section of pancreas from KC and KS7C mice, which shows mostly normal acinar cells with foci of ADMs and PanIN1 (top panel) for a KC mouse. Age

matched KS7C mouse section (bottom panel) showed cystic lesions with PanIN3 *insitu* carcinoma.

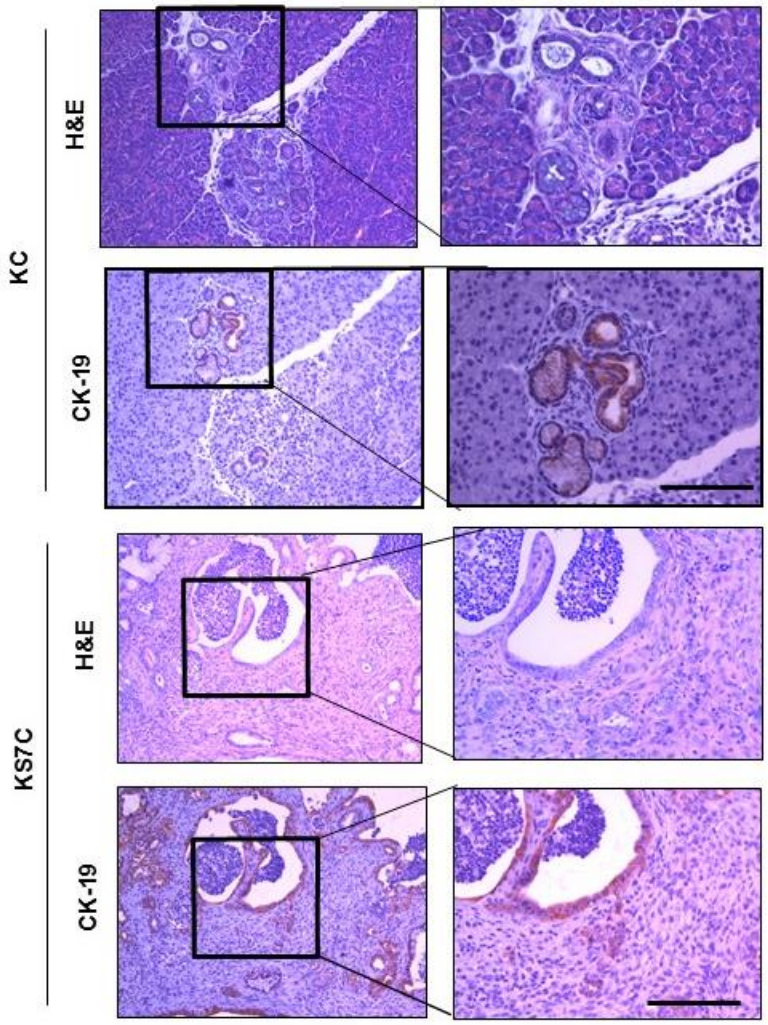

Figure 3.4 Smad7 overexpression combined with oncogenic *Kras* accelerates progression of PanIN

Representative images from 6 month old KC and KS7C mice showing that KC mice have some normal tissue and a foci of ADMs and low-grade PanIN. By contrast, KS7C mouse pancreata revealed high-grade PanIN and invasion of epithelial cells into the surrounding stroma as seen marked by CK19 positive cells. Scale bars represent 100μM. Magnified inset shown in the right column.

Next, images of 5 random fields for 6 KC and 6 KS7C mice were taken and the number of ADMS, PanINs and PDAC lesions per field were counted. The KS7C mice displayed higher number of ADMs, PanIN1A, B and 2 compared to the KC mice at 3 and 6 months of age. (Figure 3.5 A). The incidence of PDAC was also significantly increased in KS7C mice when compared to the KC mice (Figure 3.5 B). These results indicate that Smad7 OE increases ADM formation and accelerates PanIN to PDAC progression.

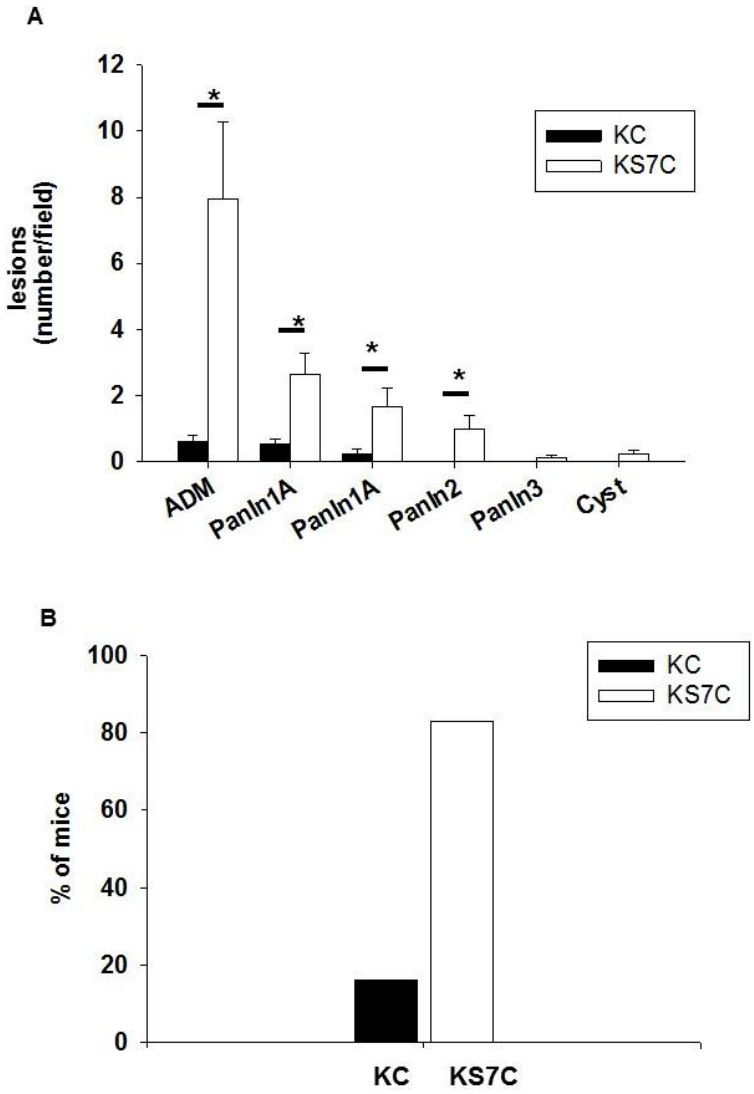

Figure 3.5 Smad7 overexpression increases PanIN formation and incidence of PDAC

(A) Bar graph represents the number of ADM and PanIN lesions observed per field for 3-6 month old KC mice (black) and KS7C mice (white). **(B)** Bar graph represents the percent of KC mice that develop PDAC at 12 months of age with (white) or without (black) Smad7 overexpression. * p value < 0.05 was considered significant.

3.3 Tetracycline inducible *Smad7* mouse model

To further test the findings of the autochthonous *SMAD7* mouse model and to address the question of whether *Kras* mutation in combination with*SMAD7* overexpression at different stages after *Kras* mutation accelerates PDAC, tetracycline inducible SMAD7 mice [143] were crossed with the KC mice, generating KtetS7C animals. *Smad7* expression was measured in the pancreas by q-PCR and was 14-fold higher in the pancreata of mice that received doxycycline in their food when compared to those that were fed regular diet (Figure 3.6 A). To confirm that the Tet-on promoter was not leaky and doxycycline alone did not change the expression *Smad7,* we compared levels of *Smad7* in mice with the *tet-Smad7* transgene in presence (test) or absence of the *Pdx-1 Cre* transgene. Both groups of mice received doxycycline in their food. The mice with the *Pdx-1 Cre* transgene displayed an 18-fold increase in *Smad7* mRNA levels compared to mice without the gene (Figure 3.6 B).

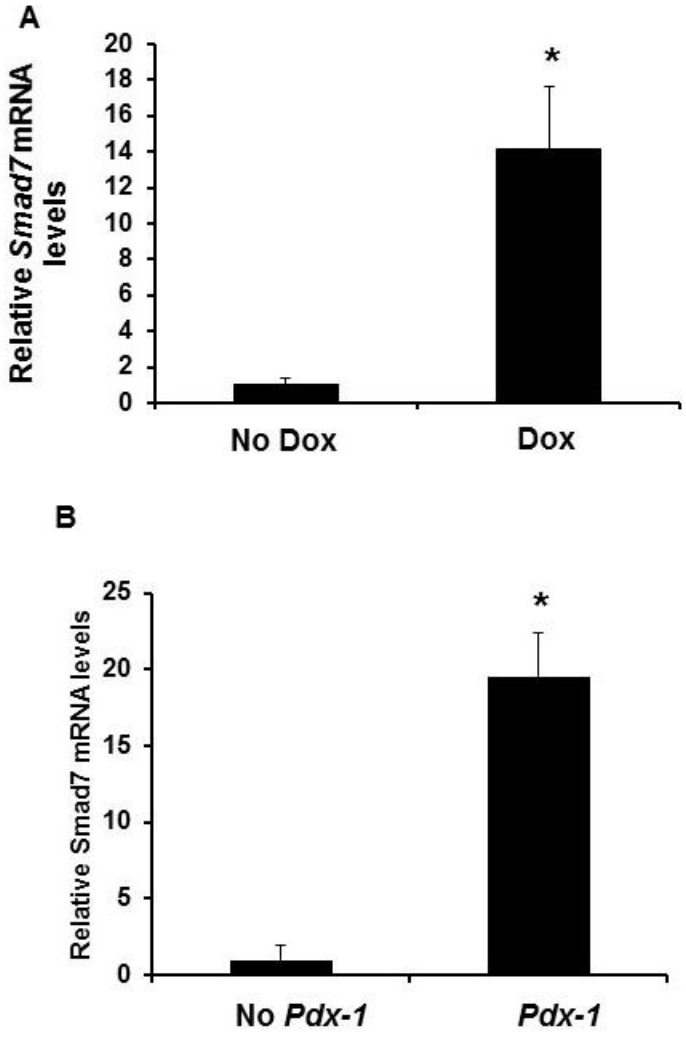

Figure 3.6 Validation of *Smad7* expression in Tet inducible Smad7 mouse model

(A) *Smad7* mRNA levels were measured by q-PCR and showed significant increases in the KtetS7C (test) mice fed with doxycycline compared to those without doxycycline (control). **(B)** *Smad7* mRNA levels measured by q-PCR are significantly elevated in the KtetS7C (test) mice fed with doxycycline compared to those without Pdx-1 Cre (control). Data are represented as mean ± SEM from 6 individual mice (A) and 4 individual mice (B), done in triplicates for each group. * p value < 0.05 was considered significant.

The KtetS7C mice were provided with doxycycline in their food at various time points (1 month, 2 months and 3 months of age to induce *Smad7* expression. All mice were sacrificed at 6 months of age. The KtetS7C mice on doxycycline displayed accelerated progression of ADMs to PanIN lesions (Figure 3.7 A) and had higher incidence of PDAC (Figure 3.7 B) when compared to mice that did not receive doxycycline. The mice induced with doxycycline at 1, 2 and 3 month of age all had more aggressive disease compared to mice with no doxycycline. However, no overall significant differences were observed between the various times of induction.

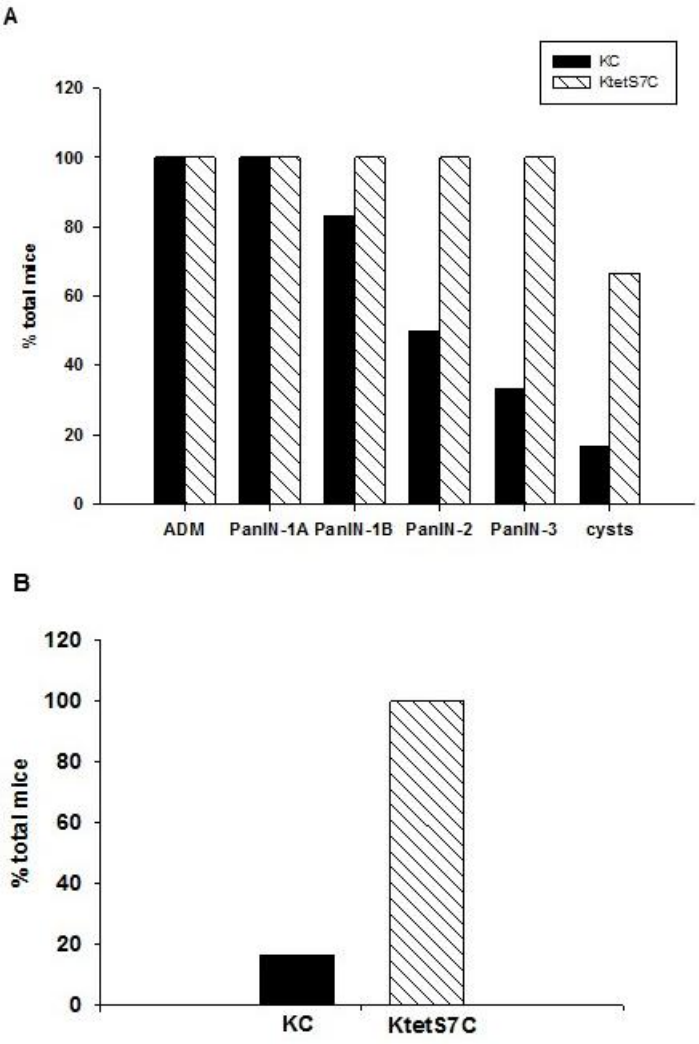

Figure 3.7 Smad7 overexpression accelerates PDAC progression

(A) Bar graph represents the percentage of mice exhibiting ADM and PanIN lesions for 6 month old KtetS7C mice provided with doxycycline feed at 1 month (patterned bar) to induce *Smad7* and KtetS7C mice provided with regular feed, without doxycycline (black bars). **(B)** Bar graph represents the percent of KtetS7C mice that developed PDAC at 6 months of age fed doxycycline (patterned) or with regular feed (black).

3.4 KS7C and KtetS7C cell lines

To further address the molecular mechanism underlying Smad7 overexpression in PDAC development, primary cancer cell lines were established from the tumors derived from the KS7C and the KtetS7C mice as described in Chapter 2. Cells were stained with CK19, a marker for epithelial cells and α-SMA, a marker for mesenchymal cells. Both cell lines stained positive for CK-19 and α-SMA (Figure 3.8 A). These findings indicate that the cell lines are of epithelial origin, but the positive α-SMA staining suggests that they may have undergone EMT. Next, the levels of *Smad7* expression were validated by qPCR in both the cell lines compared to the cell line derived from a KC mouse. The cell line derived from the KtetS7C mouse model was grown and maintained in TF media. To induce Smad7 expression, the cells were treated with 2 µg/mL of doxycycline in TF media. Levels of *Smad7* were compared among the KC cell line, the KtetS7C cell line in TF media, and KtetS7C treated with doxycycline (Figure 3.8 B). By comparison, there was no difference in the levels of*Smad7*between the KC and the KtetS7C cells grown in TF media, indicating that the tetracycline promoter is tightly regulated for expression of *Smad7* in these cells. There was a 110-fold increase in *Smad7*mRNA levels upon doxycycline treatment of the KtetS7C cells. The KS7C cell line exhibited a 30-fold increase in *SMAD7* levels as judged by qPCR when compared to the cell line derived from a KC mouse (Figure 3.8 C).

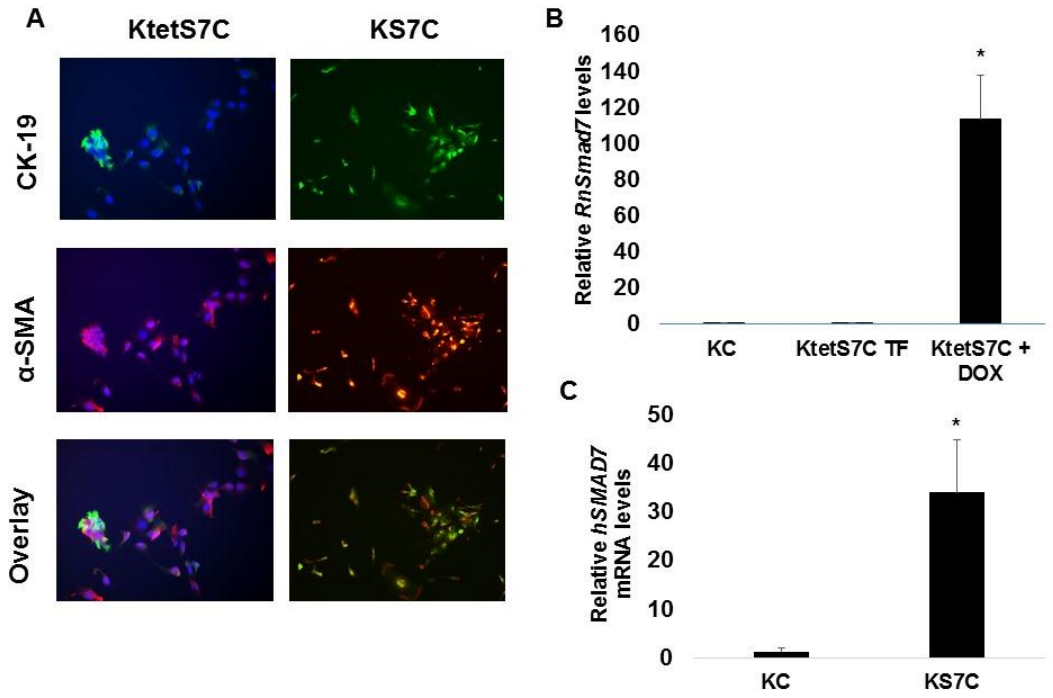

Figure 3.8 **Validation of** KS7C and KtetS7C cell lines

(A) Cells derived from tumors stain positive for CK19 and α-SMA, indicating that they are epithelial in origin; however there are suggestions of the cells transitioning into a mesenchymal type. **(B-C)** Bar graph showing significantly higher levels of *SMAD7*mRNA in KS7C or KtetS7C cells compared to KC cells by qPCR. Data are represented as mean ± SEM for three individual experiments for each cell line.*p value < 0.05 considered significant.

Next, all three cell lines were grown in 3D tissue culture to analyze the differences in proliferation and colony formation. Although viable, KC cell lines failed to grow large colonies in 3D. The KS7C cell lines in contrast form large, spherical colonies and covered over 3 times the area when compared to the KC cell line (Figure 3.9 A and B). The KtetS7C cells were plated in TF media with 2 µg/mL of doxycycline. These cells were viable and they formed large spherical colonies. Colony sizes were not as large as the KS7C cell lines, however still significantly larger than the KC cell line. The colonies formed by the KtetSC cell line covered 2.5 times the area of that of the colonies formed by KC cell line. Thus Smad7 overexpression increased proliferation in 3D tissue culture. These results are consistent with previously published results on COLO-357 cells overexpressing Smad7 that formed large colonies in soft agar [121].

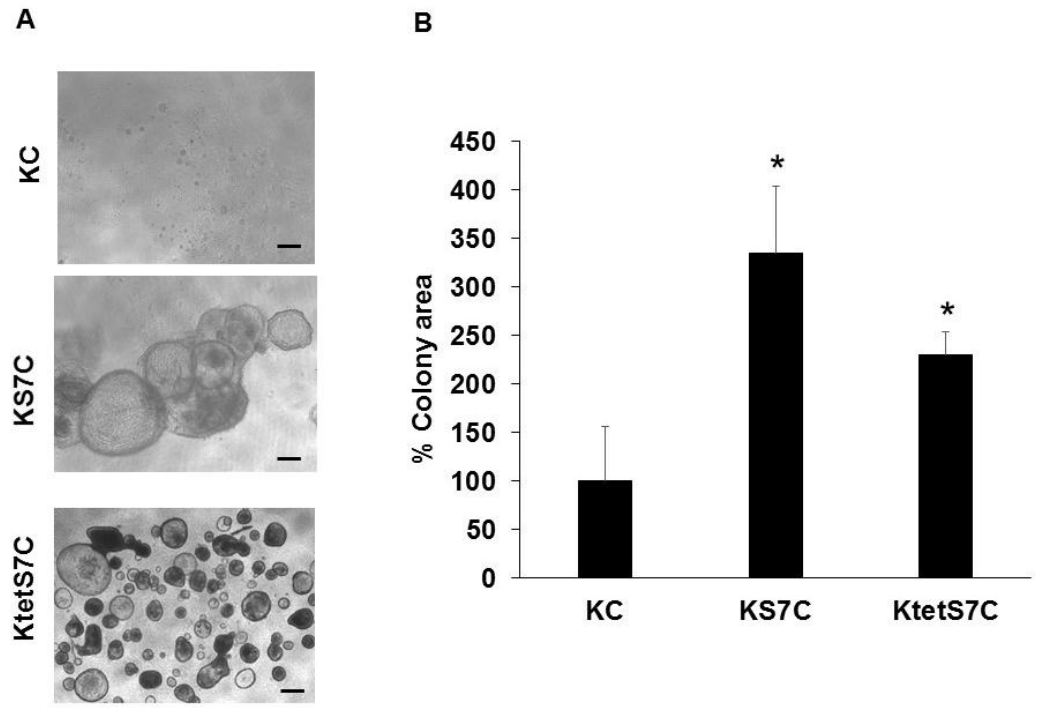

Figure 3.9 Smad7 overexpression increases proliferation

(A) Representative images from 3 independent experiments in 3D demonstrating that KS7C and KtetS7C proliferate at higher rates compared to KC and form large colonies in vitro. **(B)** Bar graph quantifying area occupied by colonies formed by the three cell lines. Results are the average of 3 independent experiments ± SEM. Scale bar represents 100 µM.*p value < 0.05 considered significant.

3.5 Orthotopic mouse model with KS7C cell line

To test the tumorigenic potential of the KS7C cell line, the cells were orthotopically injected into the pancreas of 8 weeks old, male NSG mice. These mice developed palpable tumors within 2 weeks from the day of injection. The median survival time of the injected mice was 34 days (Figure 3.10 A) and 7 of the 9 mice had ascites in their abdomen. Tumors formed from the KS7C cells were small and not densely fibrotic for each of the 9 mice (Figure 3.10 B). All mice had complete infiltration of cancer cells in their liver (Figure 3.10 B). One of the mice had intestinal seeding, and 3 of the 9 mice had metastatic nodules on their spleen. Thus the KS7C cell line is highly tumorigenic and metastatic.

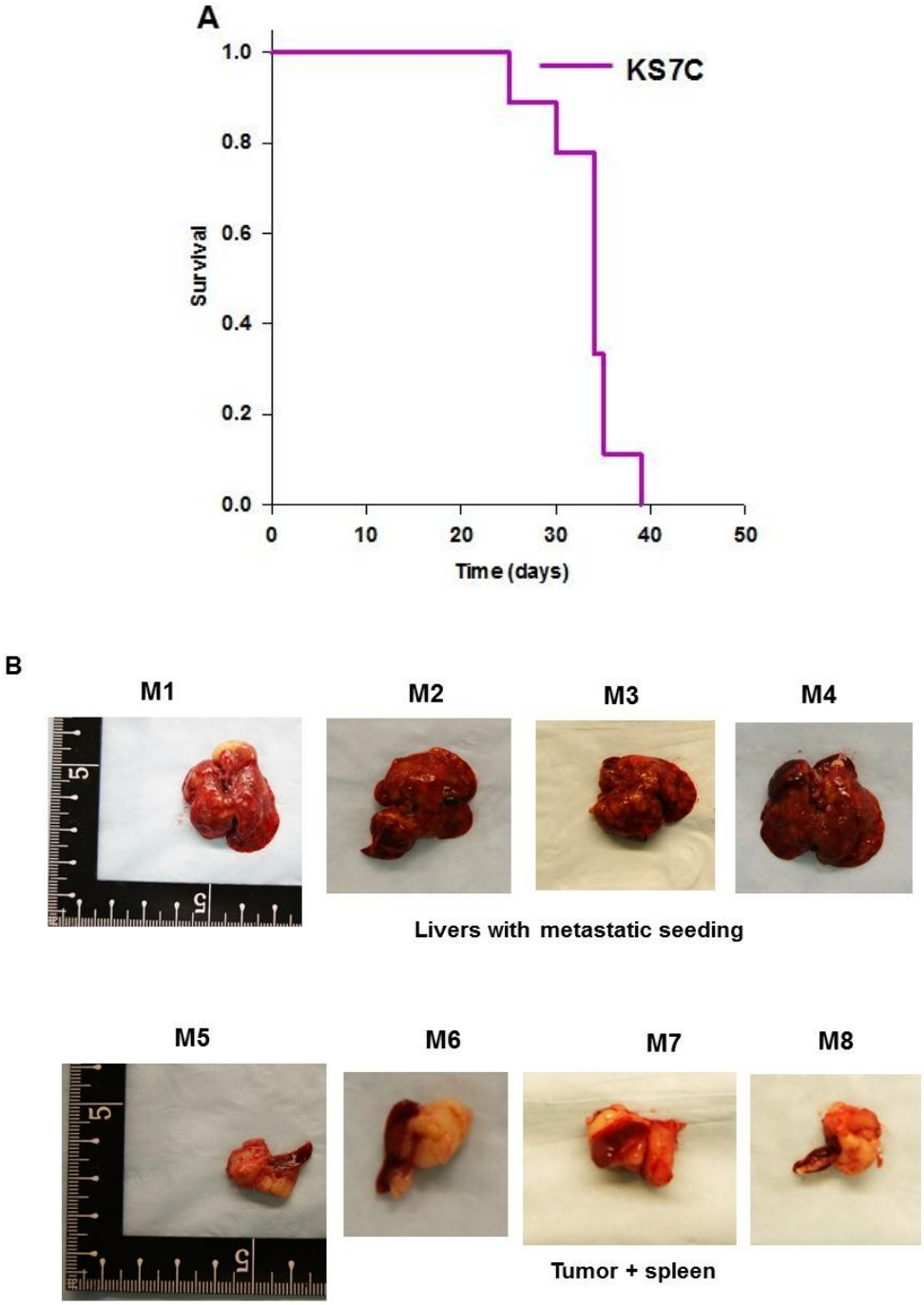

Figure 3.10 Orthotopic mouse model with KS7C cell line

(A) Kaplan-Meier curve for KS7C cell line orthotopic mice (N=9). **(B)** Represenative images from 4 different miceinjected with KS7C cell line, showing extensive metastatic seeding to the liver (M1, M2, M3, M4) and small non fibrotic tumors attached to spleen (M5, M6, M7, M8).

3.6 Smad7 promotes PDAC progression by disrupting TGF-β-mediated cell growth inhibition and inactivating functional pRb

Previously, it has been shown that in the presence of inactivated pRb or hyperphosphorylated pRb, TGF-β can exert mitogenic effects in PCCs [39]. Studies from our lab have also demonstrated that in hPDAC and in mPDAC tumors from GEMMs of PDAC with oncogenic Kras and deletion of $p16^{Ink4a}$ (KIC) and p53 (KPC), there is evidence for activated TGF-β signaling and inactivated pRb in actively proliferating cells [39]. Thus the levels of *Smad7* in the pancreas of KIC and KPC mice were examined by qPCR. The KC mice had *Smad7* levels similar to wild type (WT) mice, or mice with no transgene. However, the pancreata from the KIC and KPC mice exhibited significantly elevated*Smad7* levels compared to lesion-matched KC mice (Figure 3.11). These results suggest that enhanced expression of Smad7 in mouse tumors was not sufficient to attenuate p-Smad2 levels, however pRb remained inactivated.

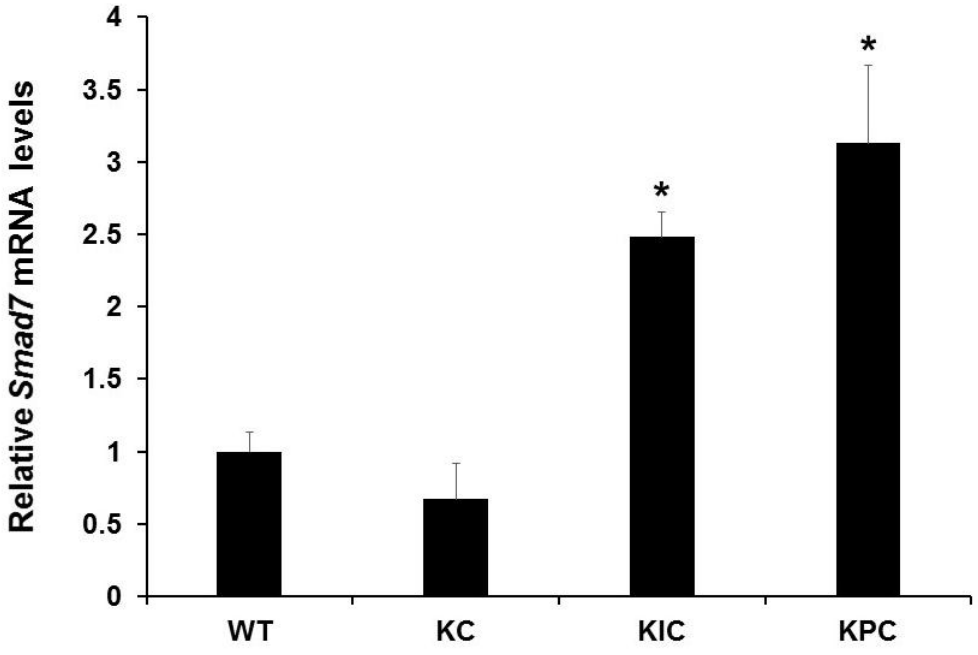

Figure 3.11 Expression of *Smad7* is enhanced in PDAC mouse models

Levels of *Smad7* mRNA in KIC and KPC mice models were significantly elevated compared to lesion-matched KC mice by q-PCR. Data are represented as mean ± SEM from 3 independent experiments.* p value < 0.05 considered significant.

Overexpression of Smad7 in COLO-357 PCCs impedes the ability of TGF-β to maintain pRb in an active, hypo-phosphorylated state even in the presence of activated p-Smad2 [122]. Therefore we next analyzed p-pRb and p-Smad2 in KS7C mice pancreatic lesions at various ages and exhibiting different grades of PanIN lesions. Serial sections from mouse tissues were co-stained with antibodies recognizing p-Smad2 and Ki67 followed by staining of serial section with those recognizing p-pRb and Ki67. Figure 3.12 and 3.13 are representative images from 3 mice (M1, M2, and M3). Co-expression of p-pRb and p-Smad2 was observed in proliferating cells of PanIN and cystic lesions of KS7C mice. KC mice tissues (control) were also stained for pRB and p-Smad2. KC mice pancreata exhibited abundant p-Smad2, however their PanIN lesions showed low positivity for p-pRb (Figure 3.14). Previously the Korc lab has published similar observations which

showed that PanIN lesions in KC mice pancreata exhibited abundant p-Smad2 with very few Ki67 and p-pRb positive cells [39].

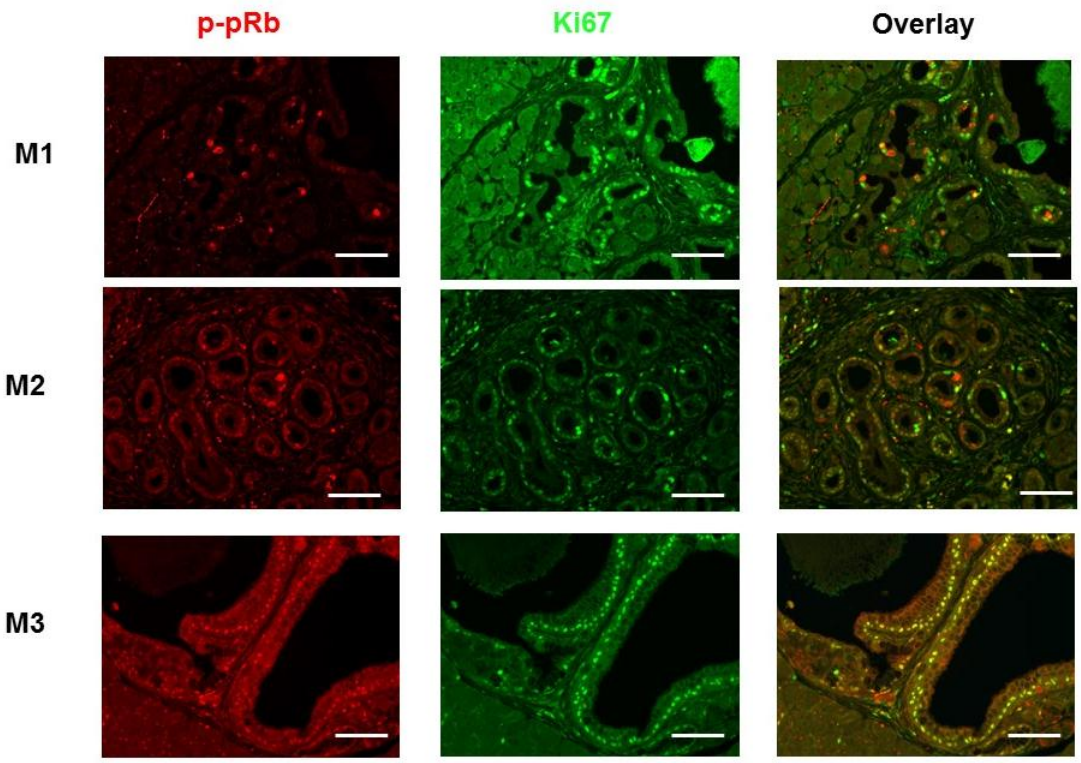

Figure 3.12 Co-localization of p-pRb and Ki67 in pancreatic tissue of KS7C mice

Double IF of 5µm serial sections from 3 different KS7C mouse tissues using antibodies that recognize Ki-67 (green) and p-pRb (red). Results show that p-pRb co-express with Ki-67 (yellow) in lesions of these mice. Scale bars represent 100µM.

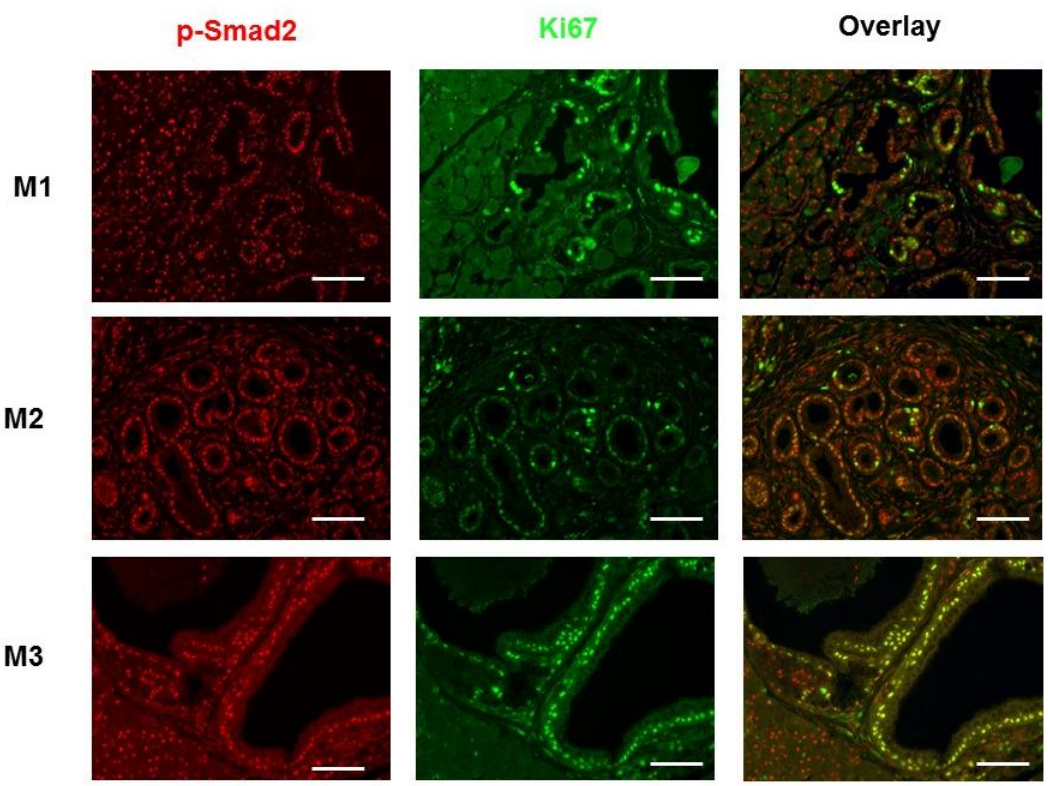

Figure 3.13 Co-localization of p-Smad2 and Ki67 in pancreatic tissue of KS7C mice

Double IF on 5µm serial sections from 3 different KS7C mouse tissues using antibodies that recognize Ki-67 (green) and p-Smad2 (red). Results show that p-Smad2 co-express with Ki-67 (yellow) in lesions of these mice. Scale bars represent 100µM.

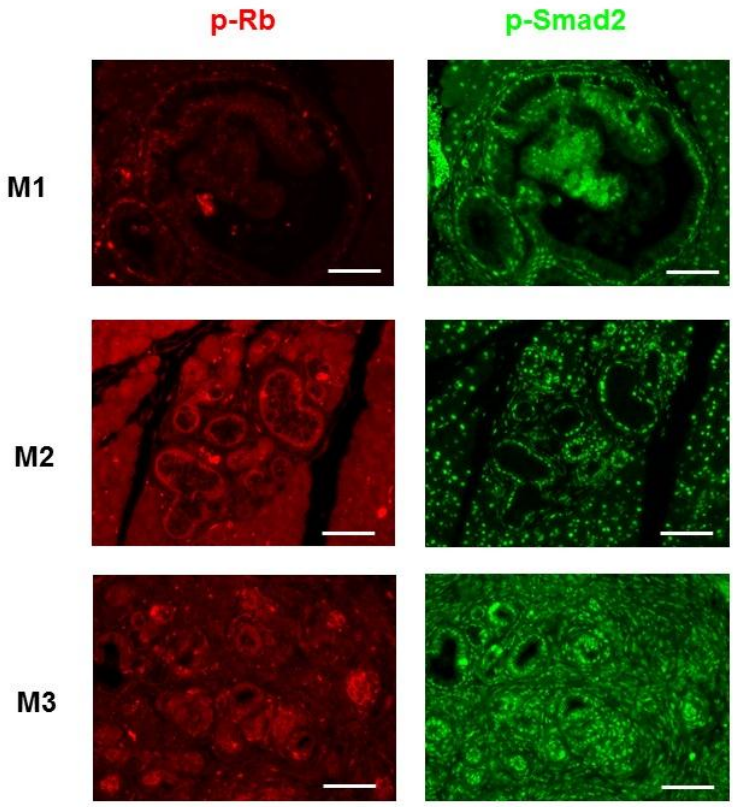

Figure 3.14 Co-localization of p-pRb and p-Smad2 in KC mice

IF on 5µm serial sections from 3 different KC mouse tissues using antibodies that recognize p-pRb (red) and p-Smad2 (green). Results showed that p-Smad2 is abundant in KC mice pancreata with very few positive p-pRb in lesions of these mice. Scale bars represent 100µM.

The cells that stained positive for p-pRb and p-Smad2 were then quantified based on total Ki67 positive cells for individual mice (Figure 3.15 A and B). The ratios of p-pRb to Ki67 and p-Smad2 to Ki67 were found to be similar to those previously published in hPDAC tissues (~62% and 65% respectively). Thus Smad7 overexpression *in vivo* also results in pRb inactivation in the presence of activated p-Smad2 signaling.

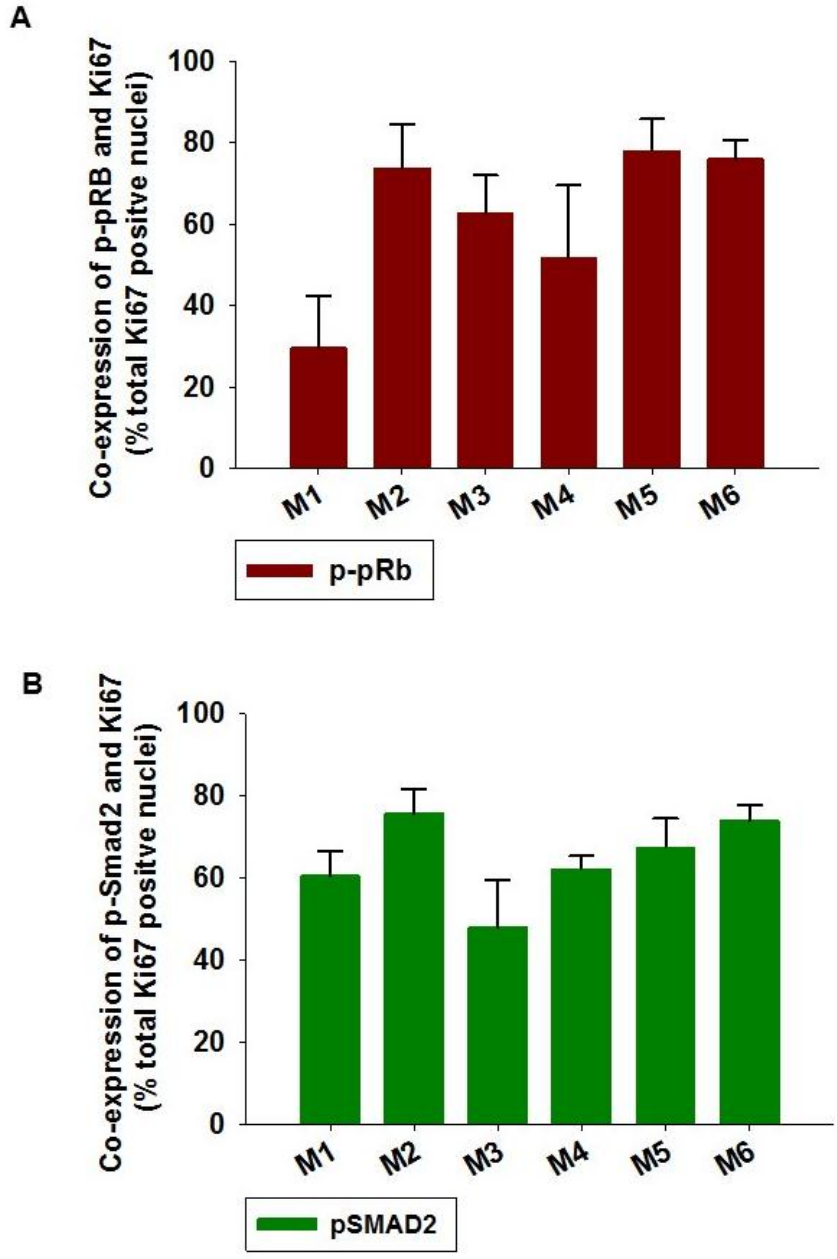

Figure 3.15 p-pRb and p-Smad2 levels are elevated in proliferating cells of KS7C PanIN lesions

Quantification of various grades of lesions in 6 different KS7C mice showed that the average percent of Ki67 positive PCCs expressing p-pRb **(A)** and p-Smad2 **(B)** is 62% and 65%, respectively. For each mouse, data are represented as mean percent ± SEM.

We next measured the levels of p21 protein in the KS7C mice. The KS7C mice tissues did not show any positivity for p21 in highly proliferative cysts (Figure 3.16 A-M1). The low grade PanIN lesions (M2) showed weak positivity in some of the cell nuclei (circled). KC mice were used as controls. The lesions of KC mice showed positivity for p21 (Figure 3.16 B), which was consistent with previously published findings [39].

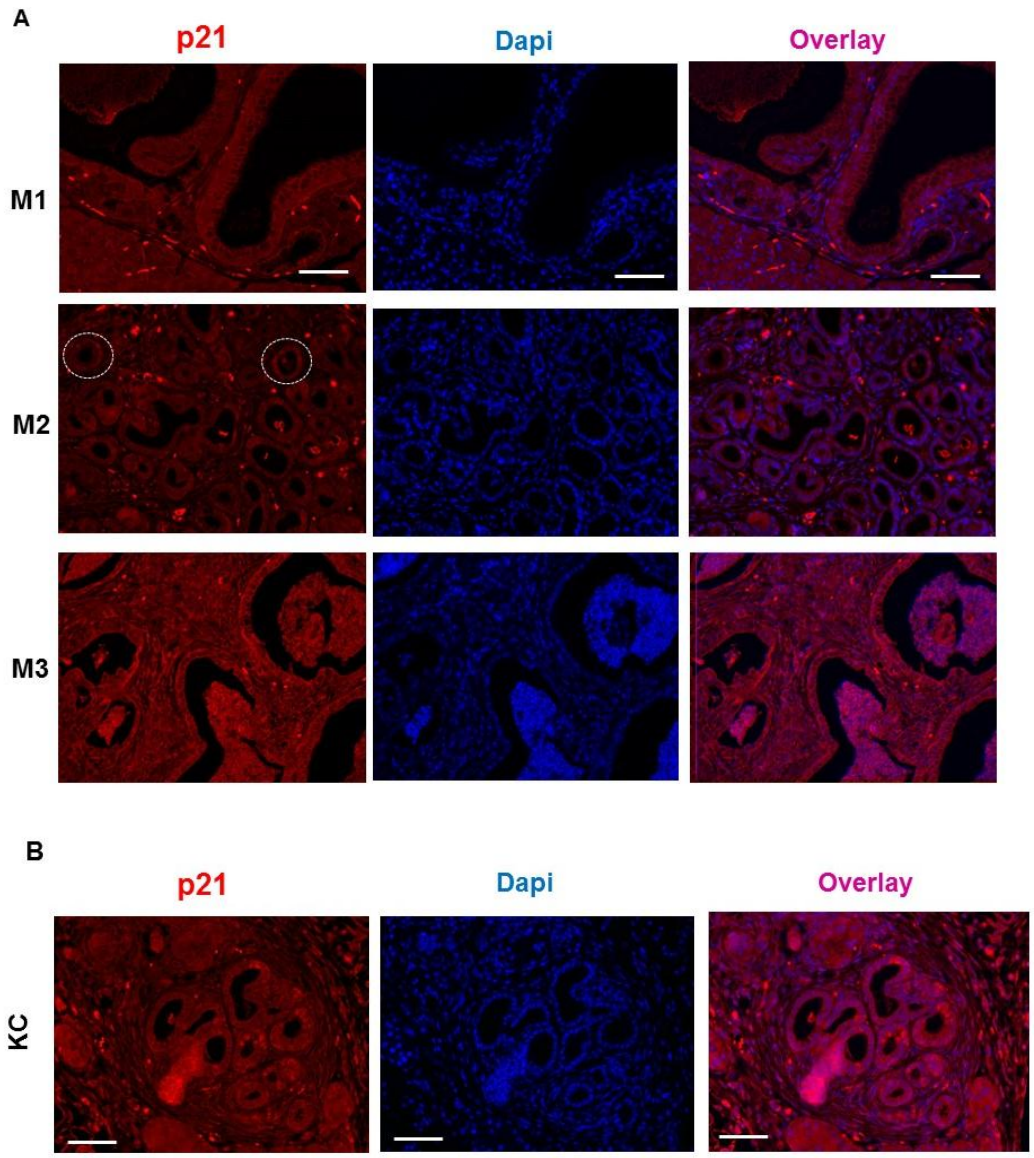

Figure 3.16 p21 levels are attenuated in KS7C mice tissues

IF on 5 µm serial sections from 3 different KS7C mouse tissues (A) for p21 (red) showed no positivity in most cells and weak positivity in some (dotted circle). Cells in PanIN lesions of KC mice (B) mice stained positive for p21. Nuclei are stained blue with DAPI. Scale bars represent 100µM.

To address whether there were differences in canonical signaling of TGF-β pathways between the KC and KS7C cell lines described in section 3.4, these cells were cultured in SF conditions and then treated with TGF-β1. The cell lines established from the KS7C

mouse model exhibited increased p-pRb when grown in SF condition compared to those derived from the KC mice (Figure 3.17 A). When these cells were treated with TGF-β1, the p-pRb levels decreased in both cell lines, however the levels of p-pRb in KS7 cells treated with TGF-β were still higher compared to KC cells in SF conditions.

The pRB antibody detects both phosphorylated and unphosphorylated pRb. To confirm that there is enhanced dephosphorylation of pRb in KC cell line and not degradation, the KC and KS7C cell lines were grown in 5% FBS and their pRb levels were measured (Figure 3.17 B). Both cell lines express equal levels of pRb. When grown in SF condition, the KC cell line underwent rapid dephosphorylation of pRb and growth arrest. However, the KS7C cell line continued to proliferate in SF conditions, and showed increased levels of p-pRb, indicating that it is a Smad7 dependent effect. We next measured p-Smad2 levels in these cells. The amount of p-Smad2increased in KC cells when they were treated with TGF-β1for 24 hours. In KS7C cells treated with TGF-β1, TGF-β1 mediated phosphorylation of Smad2 was attenuated, but not fully blocked (Figure 3.17 C). There were similar levels of total Smad2/3 proteins in both of these cell lines. These results indicate that overexpression of Smad7does not block Smad2 activation *in vivo* or *in vitro*, however elevated levels of Smad7 do lead to inactivation of pRb (Figure 3.18).

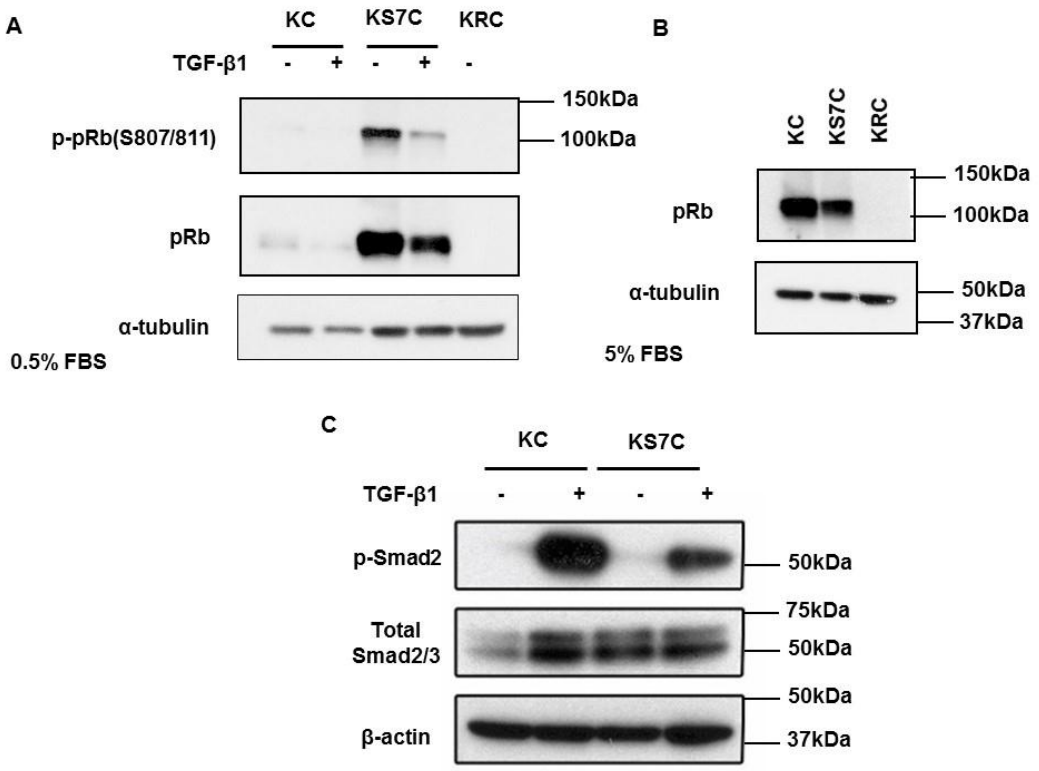

Figure 3.17 p-pRb and p-Smad2 levels in KS7C cell line

(A) The KS7C cell line grown in SF condition has more p-pRb than the KC cell line grown in SF conditions (0.5% FBS). Levels of p-pRb were reduced upon addition of 0.5nM TGF-β1 in either of these cell lines. **(B)** There were similar levels of p-Rb between these cell lines when grown in media with 5% FBS. **(C)** TGF-β1 enhanced the levels of p-Smad2 in the KC cell line. This upregulation was attenuated in the KS7C cell line. β-actin was used as loading control. Shown are representative blots from three independent experiments. The total Smad2/3 and β-actin are the same as those for Figure 3.27 as data was collected from same blot.

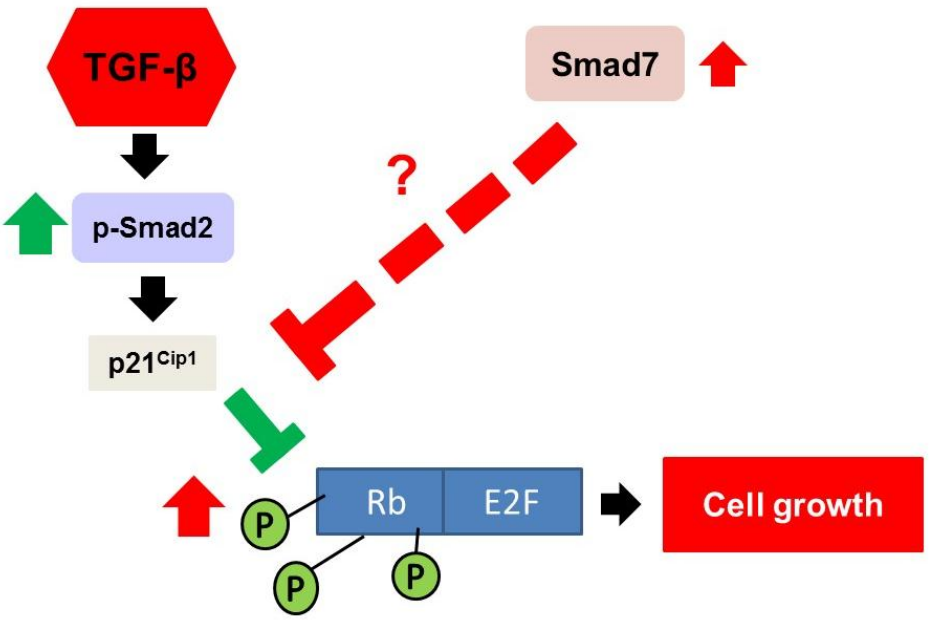

Figure 3.18 Smad7 OE allows activation of p-Smad2 by TGF-β, however it decreases p21 and keeps pRb inactivated

Smad7 OE does not block TGF-β mediated p-Smad2 (depicted by green arrows); however Smad7 OE results in downregulation of p21 levels, resulting in accumulation of p-pRb (inactive pRb) and increased thus increased cell proliferation.

3.7 PDAC progression in $KR^{+/-}S7C$ mice and $KR^{-/-}C$ mice

As described in section 3.6, Smad7 keeps pRb in a hyper-phosphorylated state *in vivo.* Therefore I next determined whether heterozygous deletion of *Rb1* combined with overexpression of *Smad7* and oncogenic *Kras* ($KR^{+/-}S7C$) would recapitulate features seen in mice with oncogenic *Kras* and homologous deletion of *Rb1* (KRC). The $KR^{+/-}C$ mice were used as controls compared with the $KR^{+/-}S7C$. The median survival for $KR^{+/-}$ S7C mice was 24 weeks which is longer than that for previously published KRC mice (~10 weeks) [114]. However, the KC and $KR^{+/-}C$ (median survival 36 weeks) mice survived for a significantly longer period when compared to the $KR^{+/-}S7C$ mice (Figure 3.19).

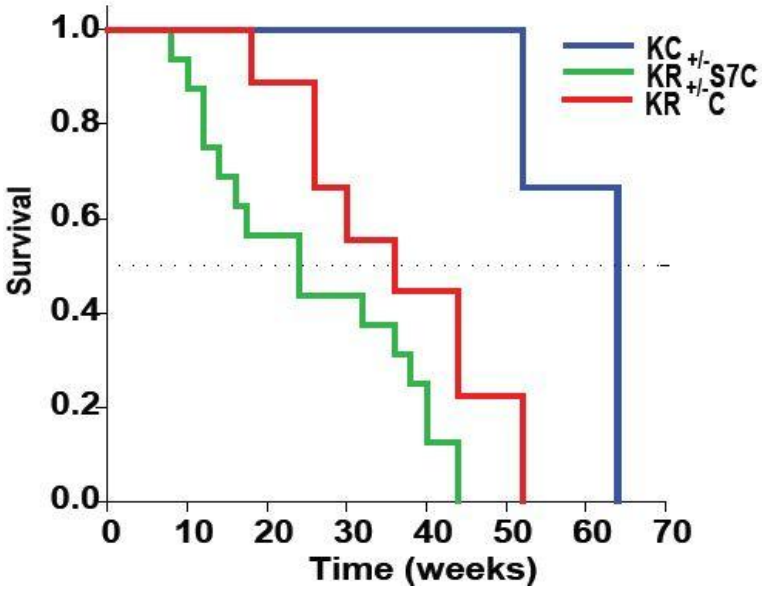

Figure 3.19 Survival of $KR^{+/-}$S7C mice

The $KR^{+/-}$S7C mice survive for significantly shorter time than the $KR^{+/-}$C (p-value 0.0385) or the KC mice (p-value <0.001). (N=12 for KC, N=15 $KR^{+/-}$S7C, and N=7 for $KR^{+/-}$C).

Gross examination of the pancreata from some of these mice showed cystic nodules and 2 of the mice (one 2 months and one 6 months old) had visible tumors.Next, we compared the grades of PanIN and presence of cysts in $KR^{+/-}$S7C mice with previously published reports of KRC mice between 2-3 months of age. The percent of mice exhibiting each of the grades of PanINs between the two mouse models was not significantly different. (Figure 3.20).The $KR^{+/-}$S7C mPDAC also displayed high levels of p-Smad2 and p-pRb (Figure 3.21) as seen in other mouse models of PDAC and in the KS7C mice. The presence of p-pRb in these mice also indicated that there was no loss of heterozygosity of *Rb1*in these lesions. Altogether, heterozygous loss of *Rb1* with *Smad7* overexpression has the same effects as loss of homozygous *Rb1.* These findings suggest that Smad7 exerts its effect on PanIN initiation and progression via inactivation of pRb.

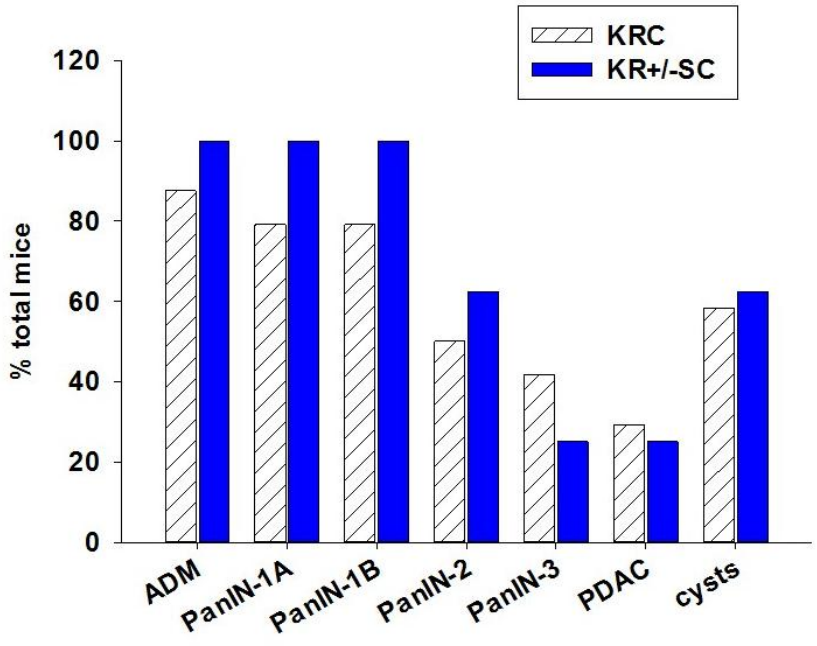

KR$^{-/-}$C Adapted from Carriere et al, 2011, Gastroenterology

Figure 3.20 PDAC progression in KR$^{+/-}$S7C mice and KR$^{-/-}$C mice

The bar graph depict the percent of mice in KR$^{+/-}$S7C (blue bars) and KR$^{-/-}$C groups (white bar with pattern, data adapted from Carriere et al, 2011, Gastroenterology) with ADMs, PanIN lesions, and PDAC progression.

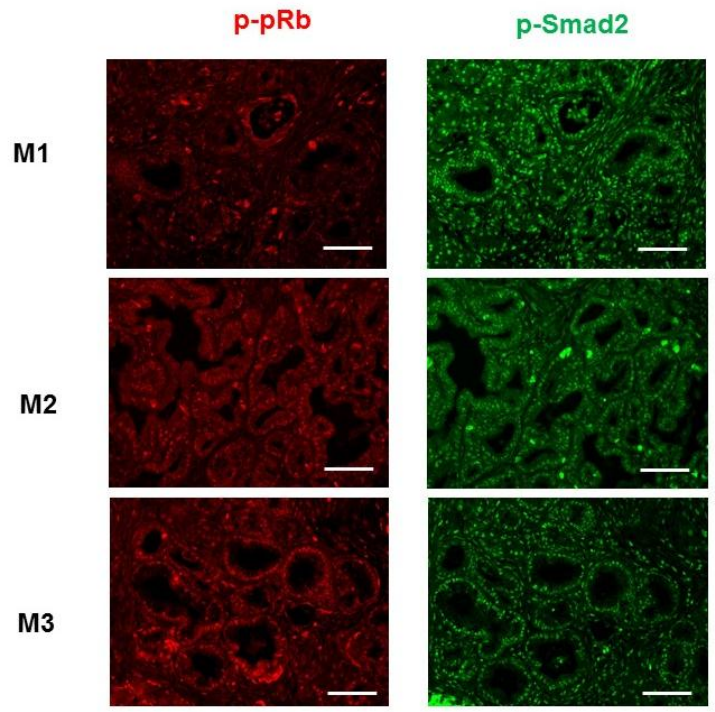

Figure 3.21 Co-localization of p-pRb and p-Smad2 in pancreatic tissue of $KR^{+/-}$S7C mice

IF of 5 µm serial sections from 3 different mice. The $KR^{+/-}$S7C mPDAC tissue showing expression of p-pRb (red), and p-Smad2 (green). Scale bars represent 100µM.

3.8 $KR^{+/-}$S7C cell lines

A primary cancer cell line from a 5.5 month $KR^{+/-}$S7C mouse tumor was established as described above. The tumor derived cells stained positive for CK19 and α-SMA (Figure 3.22 A), indicating that these cells have an epithelial origin and may be undergoing EMT. These cells exhibited a 4-fold increase in *Smad7* compared to the KC cell line (Figure 3.22 B).The $KR^{+/-}$S7C cells when grown in 3D tissue culture formed spherical colonies and showed increased colony growth formation (Figure 3.23 A) compared with the KC cells. The area covered by colonies formed by the $KR^{+/-}$S7C cells was 2.5 times more area than similarly cultured KC cells (Figure 3.23 B).

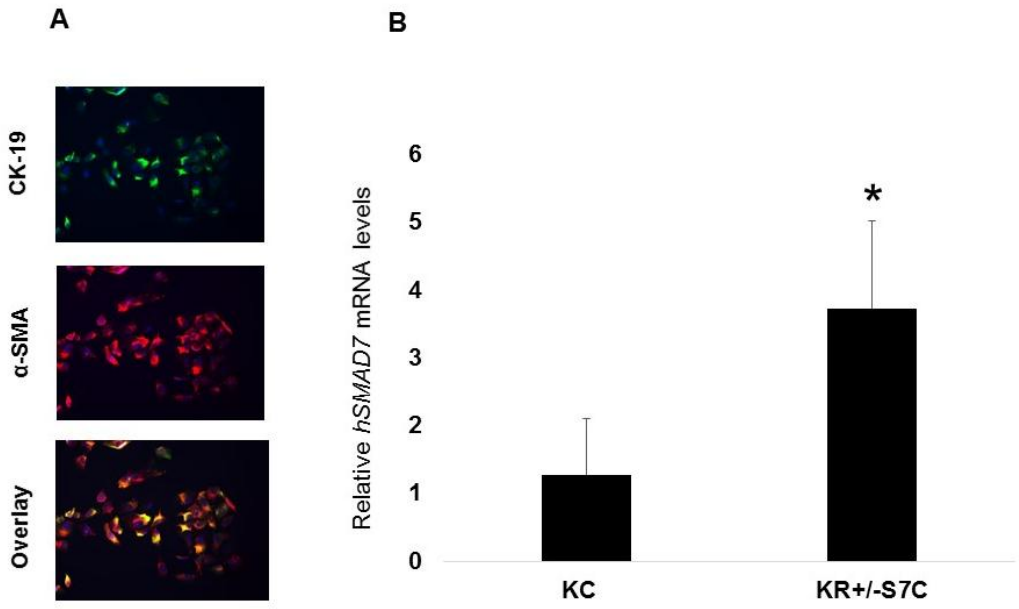

Figure 3.22 Validation of the $KR^{+/-}$S7C cell line

(A) Cells derived from tumors of $KR^{+/-}$S7C mice stain positive for CK19 and α-SMA indicating that they are epithelial in origin, however they maybe transitioning into mesenchymal type. **(B)** Bar graph showing significantly higher levels of SMAD7 in $KR^{+/-}$S7C cells compared to KC cells by qPCR. Data are represented as mean ± SEM for three individual experiments for each cell line.* p value < 0.05 considered significant.

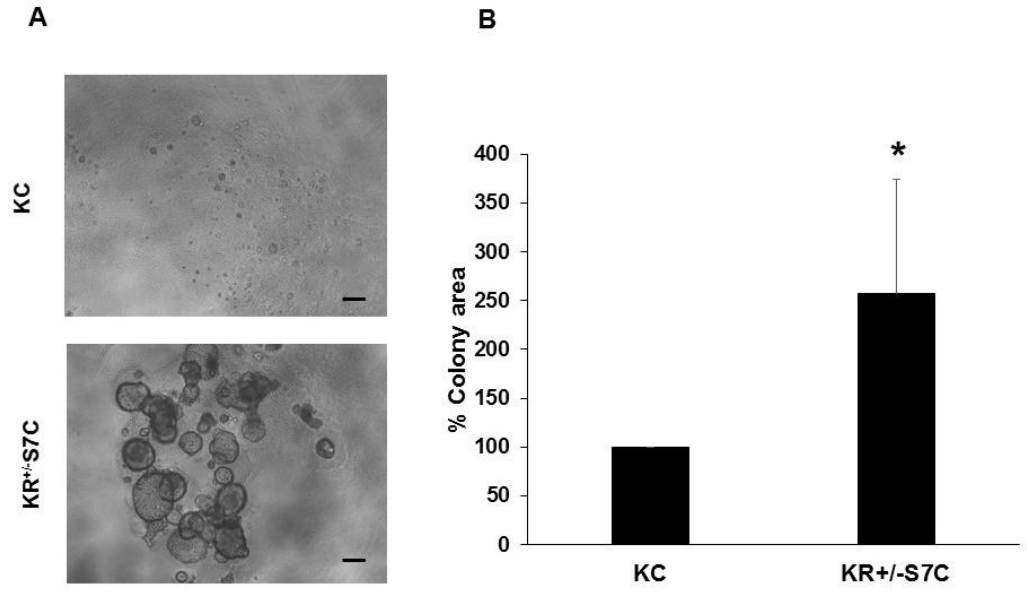

Figure 3.23 *Smad7* overexpression and *Rb1* deletion increased colony growth

(A) Representative images from 3 independent experiments in 3D demonstrating that $KR^{+/-}$S7C cells proliferate at a higher rate compared to KC and form large colonies in vitro. **(B)** Bar graph quantifying area occupied by colonies formed by the two cell lines. The area is plotted as the average of 3 independent experiments ± SEM. Scale bars represent 100µM.*p value < 0.05 considered significant.

3.9 Orthotopic mouse model with $KR^{+/-}$S7C cell line

To test the tumorigenic potential of the $KR^{+/-}$S7C cell line, the cells were orthotopically injected into the mouse pancreas of 8 weeks old, male NSG mice. The mice developed palpable tumors following 1 week from the day of injection and the median survival time was 31 days for these mice (Figure 3.24 A). Tumors formed from the $KR^{+/-}$S7C xenograft were large and very fibrotic for each of the 9 mice (Figure 3.24 B). Furthermore all mice had tumors that were locally invasive (Figure 3.24 B). No visible metastatic nodules were seen in any of the mice tissues, including spleen, liver or lungs. Thus heterozygous loss of *Rb1* and overexpression of Smad7 increased tumorigenicity of cells *in vitro* and *in vivo*.

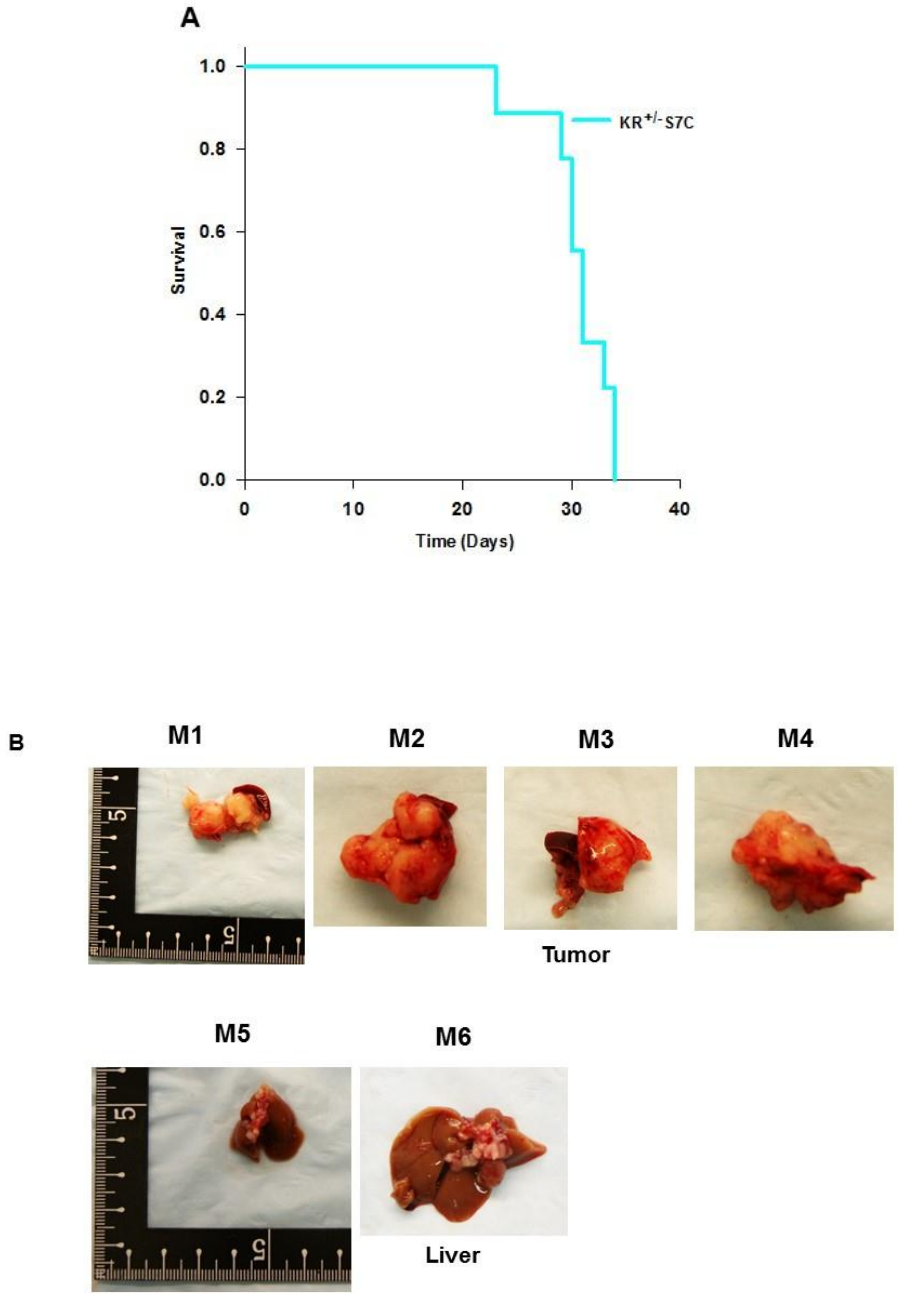

Figure 3.24 Orthotopic mouse model with $KR^{+/-}$S7C cell line

(A) Kaplan-Meier curve for $KR^{+/-}$S7C cell lines orthotopic mice (N=9). **(B)** Representative images from 4 mice (M1, M2, M3, M4) injected with $KR^{+/-}$S7C cell line, showing large protruding fibrotic tumor, attached to spleen and images from two mice (M5, M6) showing no visible metastatic lesions to the liver.

3.10 Smad7 decreases p-Smad3 *in vivo*

Previous studies by our lab and others [39, 123, 130, 162] have used p-Smad2 as an indicator for activated TGF-β. The KS7C mice exhibited increased p-Smad2 levels in the Ki67 positive cells of their lesions (Figure 3.14) as shown by IF. However, Smad2 and Smad3 are both downstream signaling molecules for canonical TGF-β signaling. Therefore the KS7C mice were then stained for p-Smad3 and there was an absence of p-Smad3 in the KS7C mice (Figure 3.25). The figure shows p-Smad3 levels in different stages of lesions from three different mice (M1, M2 and M3).

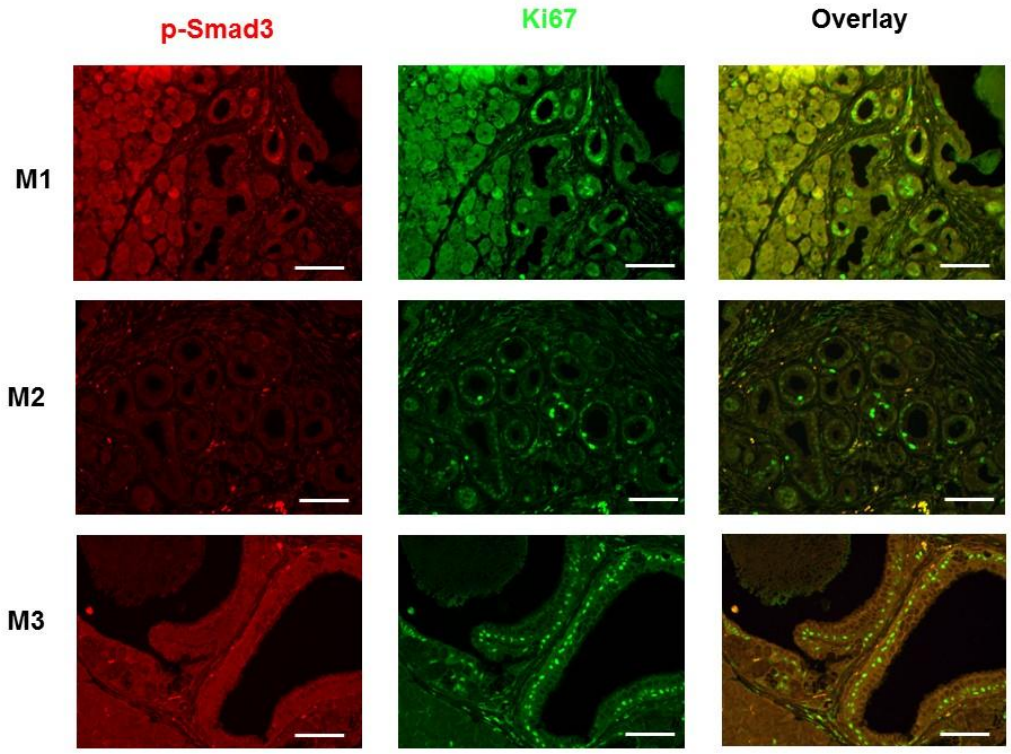

Figure 3.25 p-Smad3 levels are decreased in KS7C mice tissues

IF of 5 µm serial sections from KS7C mouse tissues for Ki-67 (green) and p-Smad3 (red). Minimal p-Smad3 was detected in the lesions of these mice.

The lesions of KC mice on the other hand stained positive for p-Smad3 as seen in figure 3.26. M1 and M2 represent sections from a 3 month and 6 month KC mouse respectively.

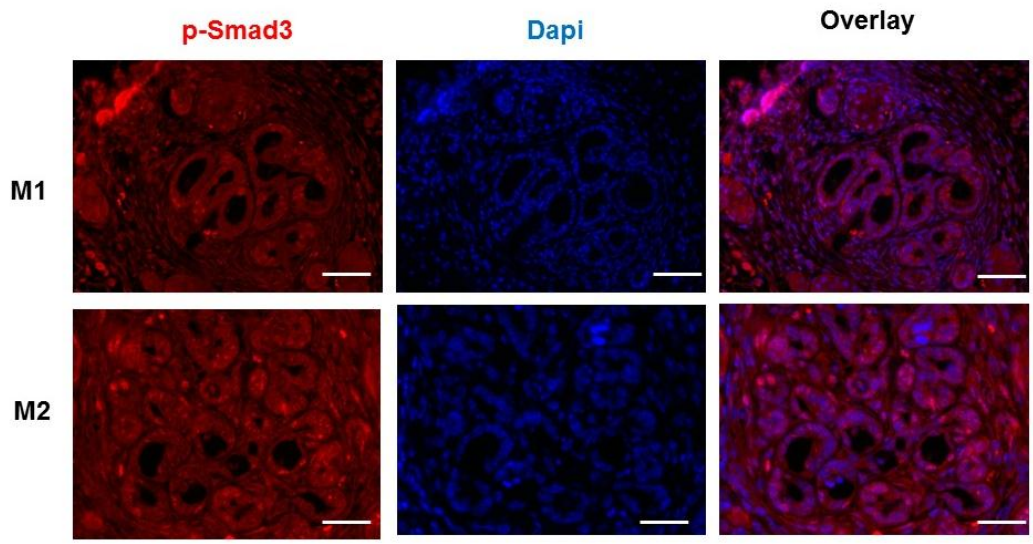

Figure 3.26 p-Smad3 staining in KC mice tissues

IF of 5 µm serial sections from two KC mouse tissues for p-Smad3 (red) showed that there was p-Smad3 positivity in the nuclei (stained blue with DAPI) in lesions of these mice. Scale bars represent 100µM.

When the KC cell line was treated with TGF-β1 for 24 hours, it showed abundant p-Smad3 levels compared to SF conditions (Figure 3.26). However phosphorylation of Smad3 was largely blocked in the KS7C cell line upon treatment with TGF-β1 (Figure 3.27). These results indicate that Smad7 allows for phosphorylation of Smad2 upon exposure to TGF-β both *in vitro* and *vivo*. However, overexpression of Smad7results in a complete attenuation of p-Smad3 levels *in vivo* and a marked attenuation of p-Smad3 levels *in vitro.*

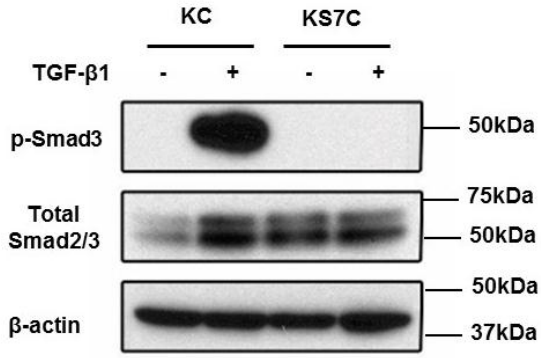

Figure 3.27 Overexpression of Smad7 attenuates induction of p-Smad3 in KS7C cells when treated with TGF-β1

p-Smad3 levels were upregulated in KC cell line when exposed to 0.5nM TGF-β1 24 hours. This induction was markedly attenuated in the KS7C cell line. β-actin was used as loading control. Shown are representative blots from three independent experiments. The total Smad2/3 and β-actin are the same as those for Figure 3.17 as data was collected from same blot.

3.11 Tetracycline inducible Smad7 overexpression in hPCCs

To delineate the mechanism of pRb hyper phosphorylation by overexpression of Smad7 and to verify if the findings from the mouse model are comparable to the human disease model, we established tetracycline inducible Smad7 (Tet-Smad7 OE) hPCCS (ASPC-1, BXPC-3 and COLO-357) as described in Chapter 2. Primarily, the COLO-357 cell lines were validated for induction of Smad7 mRNA and protein with doxycycline. The sham and Tet Smad7 OE cells were plated in duplicates in TF media. Twelve hours after plating, the media on 1 set of sham and 1 set of Tet-Smad7 OE cells was replaced with TF media containing 2µg/mL final concentration of doxycycline. RNA and protein were collected from each set and analyzed. The Sham cells when treated with doxycycline had no effect on Smad7 expression, indicating that doxycycline by itself does not affect Smad7 expression (Figure 3.28 A and B). There was no difference in Smad7 mRNA or protein expression between Sham cells in TF or treated with doxycycline and in Tet-Smad7 OE cells grown in TF media. This indicates that the promoter for Tet-Smad7 is not leaky. Tet-Smad7 OE COLO-357 cells grown in doxycycline showed ~4.4 fold increase in *Smad7* levels compared to the cells in TF alone or Sham cells grown in TF or doxycycline. When blotted with the Smad7 antibody, there were multiple non-specific

bands in all groups, however a prominent band at ~50 kDa (expected size for Smad7 which is 46kDa) appeared only in the doxycycline treated Tet-Smad7 OE cells. To confirm that the band was Smad7 and to test the efficiency of the Tet promoter, an experiment was performed, where the Tet-Smad7 OE cells were treated with doxycycline for 24 hours, then washed and kept in TF media for 24 hours. Simultaneously, similar experiments were carried out where cells were treated with doxycycline for 24 hours, then washed and grown in TF media for 48 hours (Figure 3.28 C and D). Smad7 mRNA and protein were induced with doxycycline and this was followed by reduction in the mRNA and protein levels when the doxycycline was removed. Thus, stable tetracycline Smad7 inducible COLO-357 were successfully generated and validated.

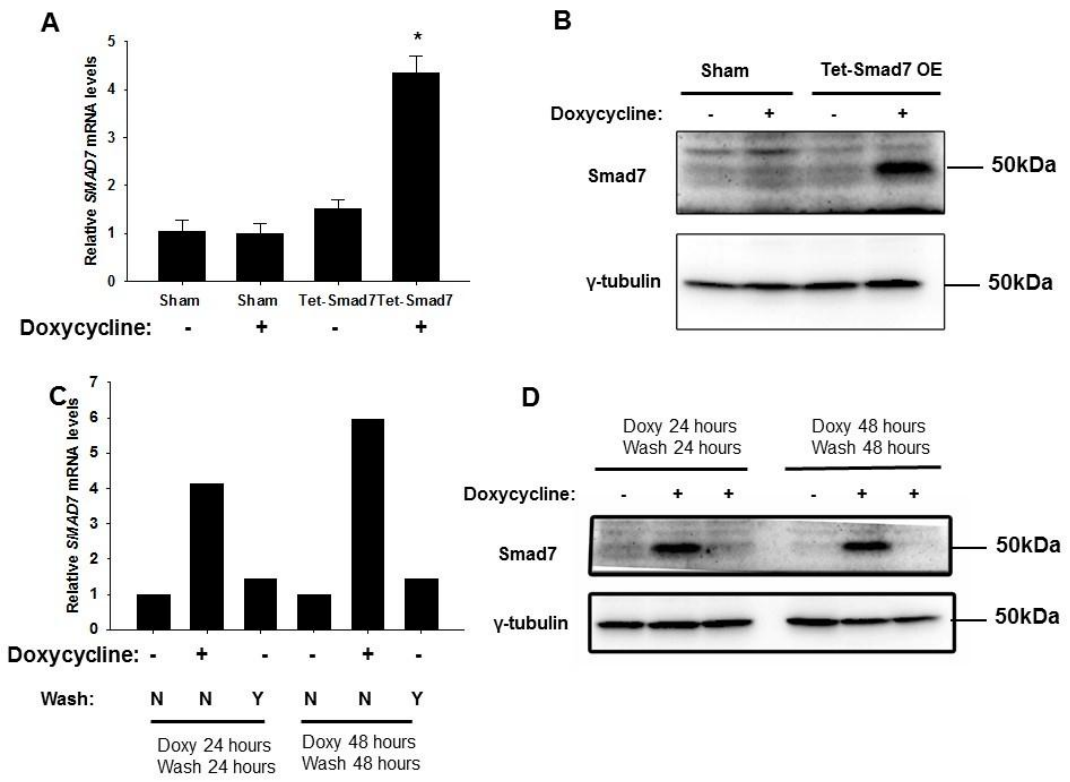

Figure 3.28 Tet-inducible Smad7 OE in COLO-357

(A) Bar graph shows that high expression of *SMAD7* mRNA levels in doxycycline treated COLO-357 cells transduced with Tet-Smad7. Data are represented as mean ± SEM for three individual experiments for each cell line. **(B)** Western blot with anti Smad7 indicating significantly different expression of Smad7 in Tet-Smad7 cells treated with doxycycline compared to TF media or sham cells in TF media or doxycycline**.** γ-tubulin was used as loading control. Shown is representative blot from 3 independent experiments. **(C)** Bar graph showing expression of *SMAD7* mRNA levels in doxycycline treated COLO-357 cells transduced with Tet-Smad7 which were reduced when doxycycline was removed as early as 24 hours. **(D)** Western blot with anti Smad7 indicating upregulation of Smad7 with doxycycline treatment at 24 and 48 hours and reduction in Smad7 levels when doxycycline was removed from the media for 24 or 48 hours. γ-tubulin was used as loading control.

Similar to COLO-357 cells, ASPC-1 (Figure 3.29 A& C) and BXPC-3 (Figure 3.29 B & D) cells were stably transduced with the Tet-Smad7 OE plasmid and validated for expression of Smad7 mRNA and protein levels. Next, the p-pRb in Tet-Smad7 hPCCs, with or without doxycycline and with or without TGF-β1 were analyzed. The data generated for p-pRb status with Smad7 OE and treatment with TGF-β1 was not

conclusive, hence all further experiments were performed with previously generated COLO-357 overexpressing c-Myc tagged Smad7 cells (CS7)[123].

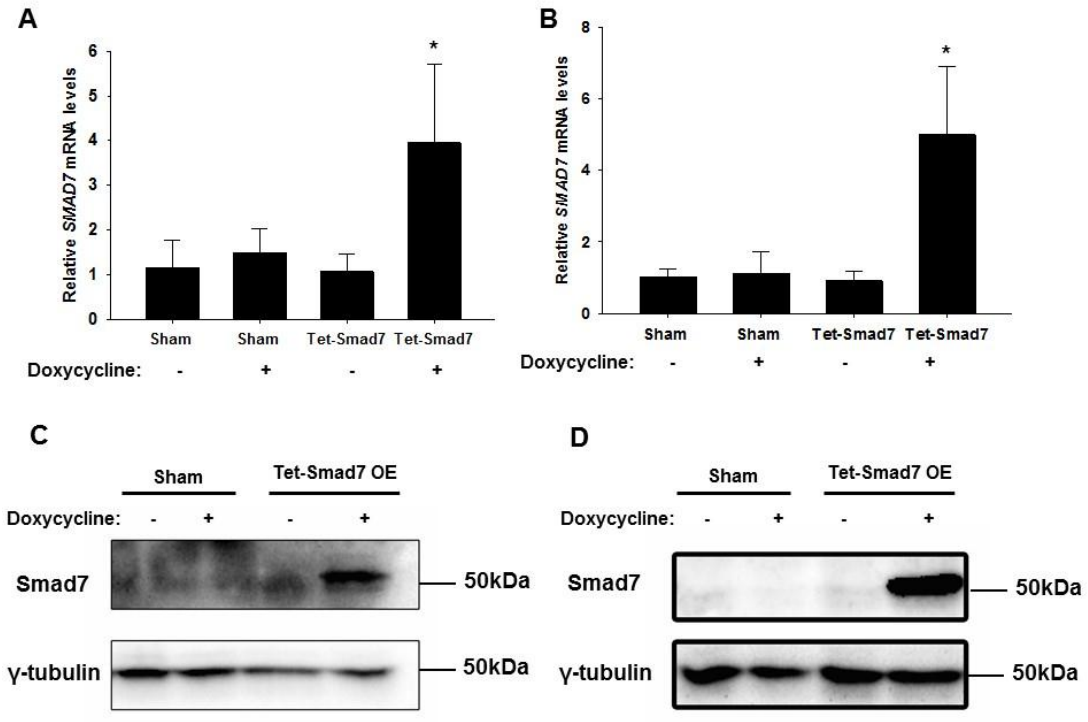

Figure 3.29 Tet- inducible Smad7 OE in ASPC-1 and BXPC-3

(A & B) Bar graph showed high expression of *SMAD7* mRNA levels in doxycycline treated ASPC-1 cells (A) and BXPC-3 cells (B) transduced with Tet-Smad7. Data are represented as mean ± SEM for three individual experiments for each cell line. *p value < 0.05 considered significant. **(C & D)** Western blot with anti Smad7 indicating significantly different expression of Smad7 in ASPC-1 (C) and BXPC-3 (D) cells transduced with Tet-Smad7 cells treated with doxycycline compared to TF media or sham cells in TF media or doxycycline**.** γ-tubulin was used as loading control. Shown are representative blots from 3 independent experiments.

3.12 Overexpression of Smad7 in hPCCs

The c-terminal Myc tagged SMAD7 was overexpressed in a recently derived PDX-cell line, IUSCC-PC1 (IUS7). COLO-357 (CSham) and IUSCC-PC1 (IUSham) transduced with the empty vector were used as controls. The expression of Smad7 was validated in

the cell lines by q-PCR and western blotting. The CS7 cell lines exhibited a 30-fold increase in *SMAD7* mRNA levels compared to CSham cells (Figure 3.30 A). For the protein expression, the lysates were run in duplicates. One set was blotted for Smad7 antibody and the other for c-Myc tag. The bands by western blotting ran at the same molecular weight and showed overexpressed protein at around 50kDa molecular size band which is around the expected size for Smad7 (46KDa is the precise molecular weight). β-actin and Erk-2 were used as loading controls for Smad7 and c-Myc respectively (Figure 3.30 B). The IUS7 cells displayed a 57-fold increase in *Smad7* mRNA compared to the Sham cells (Figure 3.30 C). For the IUS7 cells, only the Smad7 antibody was used to confirm overexpression (Figure 3.30 D).

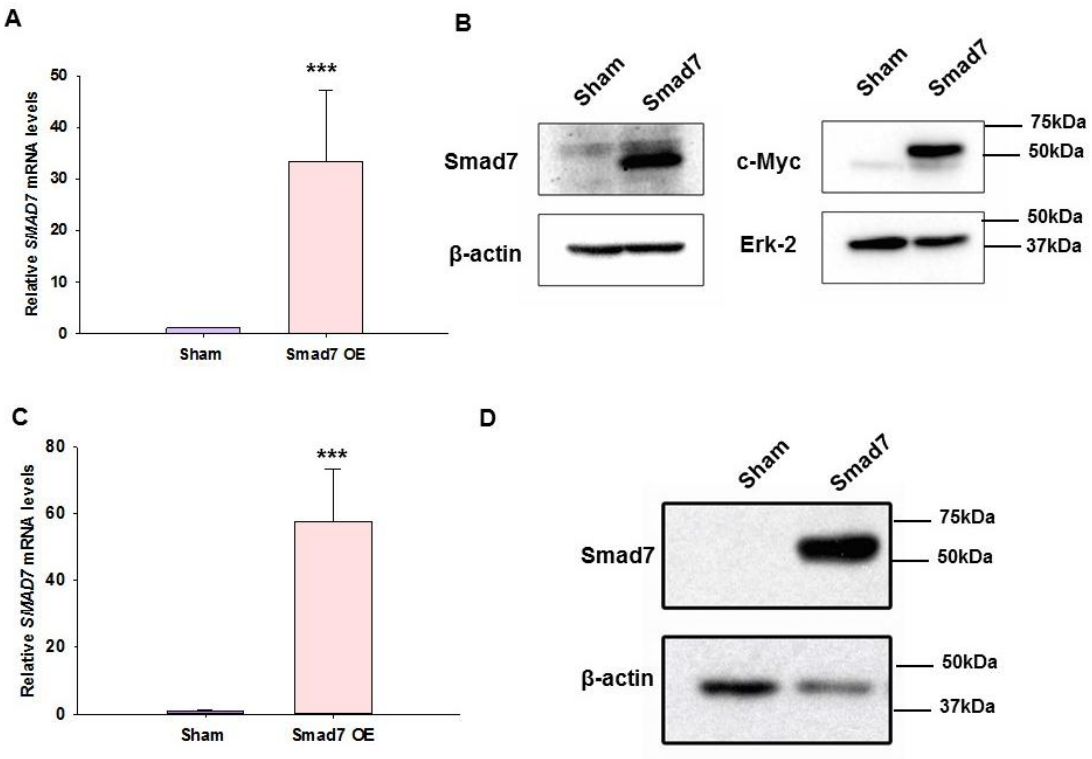

Figure 3.30 Smad7 OE in hPCCs

(A) Bar graph showed high expression of *SMAD7* mRNA levels in CS7 cells (pink) compared to sham cells (purple) ($p<0.0001$). Data are represented as mean ± SEM for three individual experiments for each cell line. **(B)** Western blot with anti-Smad7 and anti-c-Myc indicated significantly different expression of Smad7 or c-Myc in CS7 cells compared to sham. β-actin and Erk-2 were used as loading controls. Shown are representative blots from 3 independent experiments. **(C)** Bar graph showed high expression of *SMAD7* mRNA levels in IUS7 cells (pink) compared to sham cells (purple) ($p<0.0001$). Data are represented as mean ± SEM for three individual experiments for each cell line. **(D)** Western blot with anti-Smad7 indicated significantly different expression of Smad7 in IUS7 cells compared to sham. β-actin was used as loading control. Shown are representative blots from 3 independent experiments.

3.13 Effects of Smad7 overexpression and TGF-β1 on p-pRb, p-Smad2 and p-Smad3

Previously, our lab published that when CS7 cells were treated with 500 pM of TGF-β1 for 24 hours, TGF-β1 mediated phosphorylation of Smad2 and de-phosphorylation of pRb was not attenuated by Smad7 overexpression[123]. To determine if there were changes in p-Smad3 with Smad7 overexpression and TGF-β, we next treated the CSham and CS7 OE cells with 500 pM of TGF-β1 for 24 hours and blotted for phospho- and total Smad2 and Smad3. Total Smad2 and Smad3 levels did not change with Smad7 overexpression or with TGF-β1 treatment. (Figure 3.31). TGF-β1 markedly increased p-Smad2 and p-Smad3 levels in CSham cells.Smad7 overexpression decreased basal levels of p-Smad2 and p-Smad3 levels when compared to Sham cells. Smad7 overexpression did not attenuate p-Smad2 levels with TGF-β1 treatment, however p-Smad3 levels were lowered when compared to sham cells treated with TGF-β1.

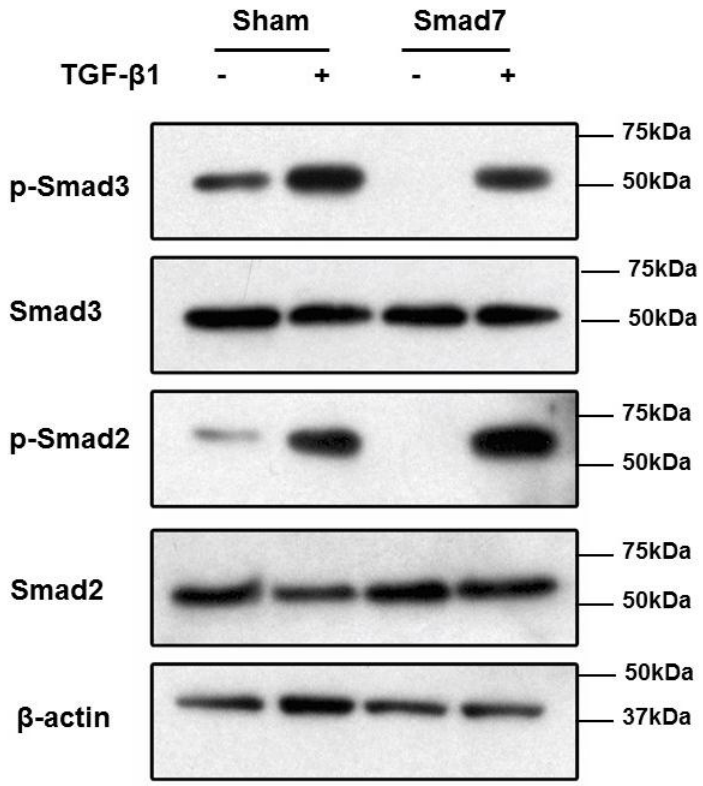

Figure 3.31 Effects of Smad7 overexpression and TGF-β1 on p-Smad2 and p-Smad3

p-Smad2 and p-Smad3 levels were upregulated when Csham cells were treated with 0.5nM TGF-β1 for 24 hours. Smad7 overexpression did not affect p-Smad2 upregulation by TGF-β1, however it decreased p-Smad3 upregulated by TGF-β1. Total Smad2 and Smad3 levels did not change with Smad7 overexpression or TGF-β1 treatment. β-actin was used as loading control. Shown are representative blots from 3 independent experiments.

To quantify phosphorylated Smad2 and 3 levels between the Sham and Smad7 cells treated with TGF-β, we quantified the intensities of the protein bands and normalized the p-Smad2 levels to the total Smad2 levels. The ratio of phosphorylated Smad2 to total Smad2 between the groups was similar, however we found a significant difference in the ratio of the phosphorylated to the total Smad3 proteins (Figure 3.32).

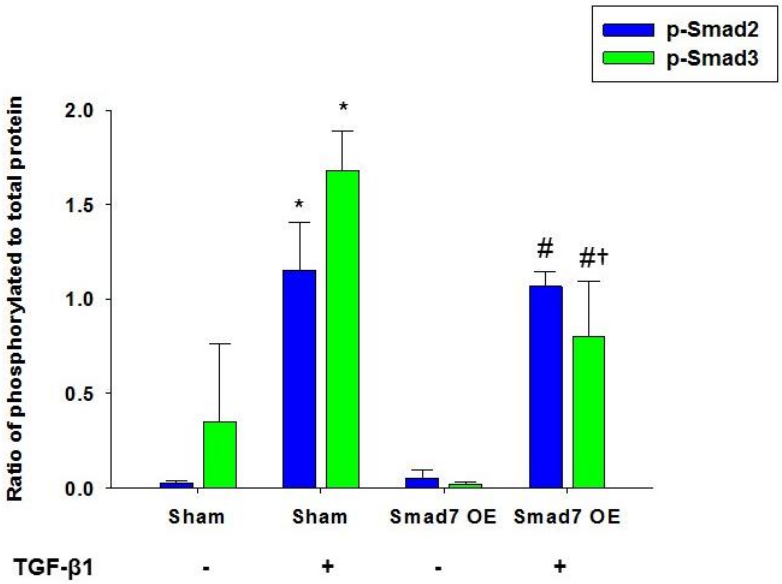

Figure 3.32 p-Smad3 levels decrease significantly with Smad7 overexpression and TGF-β1

The ratio for Smad2 (blue) was significantly different with TGF-β1 treatment in Sham (p=0.005) and Smad7 OE (p=0.0001) compared to SF conditions. There was no significant difference in the ratio between Sham and Smad7 cells in SF condition or those treated with TGF-β1. The ratio for Smad3 (green) was significantly different with TGF-β1 treatement in Sham (p=0.021) and Smad7 OE (p=0.028) compared to SF conditions. There was no significant difference in the ratio between Sham and Smad7 cells in SF condition, however there was a significant difference in the ones treated with TGF-β (p=0.0368). Data are represented as mean ± SEM for three individual experiments for each cell line.(* p<0.05, compared to Sham SF; † p<0.05, compared to Sham + TGF-β, # p<0.05, compared to Smad7 OE SF by 2 tailed student *t* test).

These results corroborate with the *in vivo* findings, where p-Smad2 and p-Smad3 get attenuated differently with Smad7 overexpression. To see if these findings were similar in another hPCC, the IUS7 cells were treated with 500 pM of TGF-β1 for 24 hours and analyzed the phosphorylated and total levels of pRb, Smad2 and Smad3 in these cells. The Sham cells were used as controls. The IUSham cells when treated with TGF-β1 show a marked decrease in p-pRb levels (Figure 3.33 A). There was no difference between the p-pRb levels between the Sham and Smad7 overexpressing cells grown in SF media. The Smad7 OE cells treated with TGF-β1 did not show a decrease in p-pRb

levels when compared to Smad7 OE cells grown in SF media. This data follows a similar trend to the COLO-357 cells. Next we analyzed canonical TGF-β signaling activity by probing for p-Smad2 and p-Smad3. IUSham cells when treated with TGF-β1, showed a marked increase in p-Smad2 (Figure 3.33 B) and pSmad3 (Figure 3.33 C) levels compared to Sham cells grown in SF media. Smad7 OE resulted in a decrease in basal p-Smad2 and p-Smad3 levels when compared to Sham cells. When Smad7 OE cells are treated with TGF-β1, Smad7 attenuated the levels of phosphorylated Smad2 and Smad3 when compared to Sham cells treated with TGF-β1.

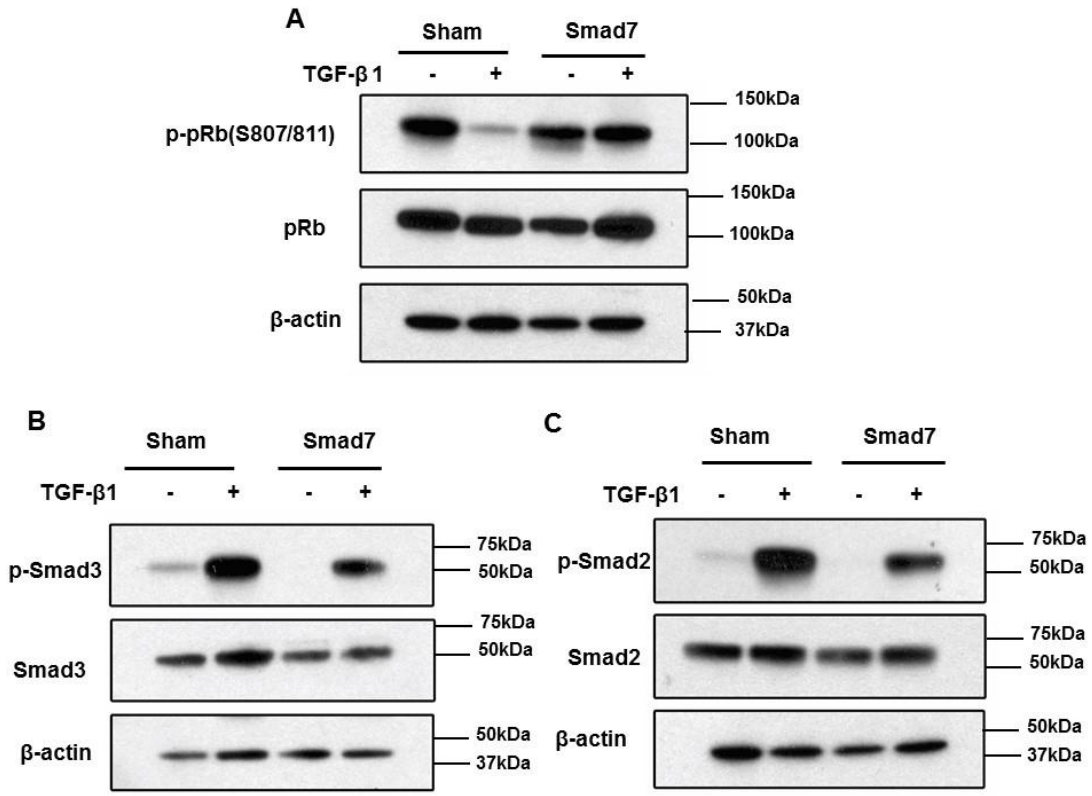

Figure 3.33 Effects of Smad7 overexpression and TGF-β1 on p-pRb, p-Smad2 and p-Smad3 in IUSCC-PC1 cells

IUsham cells treated with 0.5nM TGF-β for 24 hours exhibit a decrease in p-pRb, (A) p-Smad2 (B) and p-Smad3 (C) levels. Smad7 overexpression results in attenuation of TGF-β1 mediated decrease in p-Rb and increase in p-Smad2 and p-Smad3. Total pRb, Smad2 and Smad3 levels did not change with Smad7 overexpression or TGF-β1 treatment. β-actin was used as loading control. Shown are representative blots from 3 independent experiments.

The protein band intensities on the western blots were then quantified for the ratio of levels of the p-Smad2 and p-Smad3 to their respective total proteins. There was a significant difference in the ratios of phosphorylated to total protein for Smad2 and Smad3 in the TGF-β1 treated groups compared to SF for Sham and Smad7 OE (Figure 3.34). There was a decrease in the ratio between Sham and Smad7 OE cells grown in SF conditions or those treated with TGF-β1, however it was not significant. Overall, in

IUSCC-PC1 cells, Smad7 OE attenuated TGF-β signaling and kept pRb hyper phosphorylated.

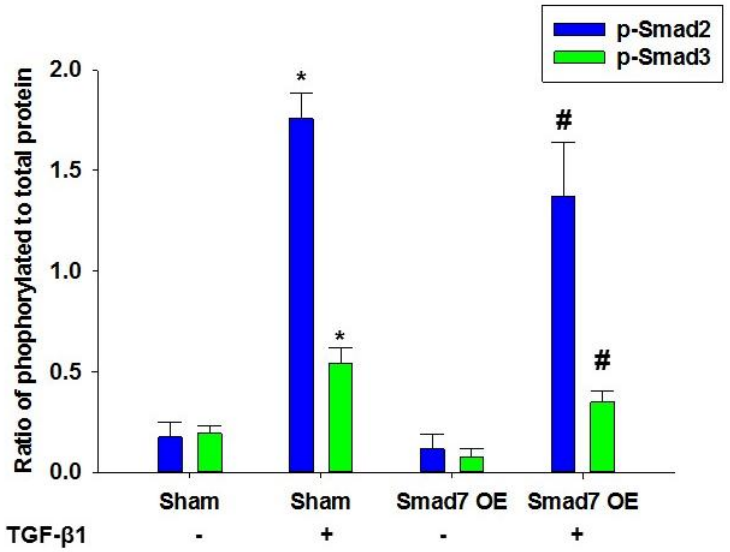

Figure 3.34 p-Smad2 and p-Smad3 levels decreased in IUSCC-PC1 cells overexpressing Smad7 and treated with TGF-β1

Quantification of ratio of p-Smad2 to total Smad2 (blue) and p-Smad3 to total Smad3 protein (green) in IUSCC-PC1 cells overexpressing Smad7 and/or treated with TGF-β. The ratio for Smad2 (blue) was significantly different with TGF-β1 treatment in Sham (p=0.0001) and Smad7 OE (p=0.005) compared to SF conditions. There was no significant difference in the ratio between Sham and Smad7 cells in SF condition or those treated with TGF-β1. The ratio for Smad3 (green) was significantly different with TGF-β1 treatement in Sham (p=0.0058) and Smad7 OE (p=0.0076) compared to SF conditions. There was no significant difference in the ratio between Sham and Smad7 cells in SF condition or those treated with TGF-β1. Data are represented as mean ± SEM for three individual experiments for each cell line.

3.14 Smad7 overexpression and p21

The KS7C mouse model displayed loss of p21 in high grade PanIN lesions. Previous studies from our lab have shown that levels of p21, a TGF-β induced cell cycle inhibitory protein are decreased in hPDAC samples even in the presence of high p-Smad2 or

activated TGF-β signaling [39]. It was also reported that TGF-β stimulates *CDKN1A* (gene encoding p21) promoter, using luciferase reporter assay in COLO-357 cells [121]. In the same study, Smad7 OE attenuated TGF-β mediated activation of *CDKN1A*promoter. Thus the *CDKN1A* mRNA levels in Smad7 overexpressing cells were analyzed next. In COLO-357 (Figure 3.35 A) and IUSCC-PC1 (Figure 3.35 B) Sham cells, TGF-β1 increased expression of *CDKN1A*. When Smad7 was overexpressed in these cells, the *CDKN1A* levels were significantly reduced by 2-folds. When Smad7 over expressing cells are treated with TGF-β1, *CDKN1A* levels were increased when compared to SF conditions, however they were significantly lower than the TGF-β treated Sham cells.

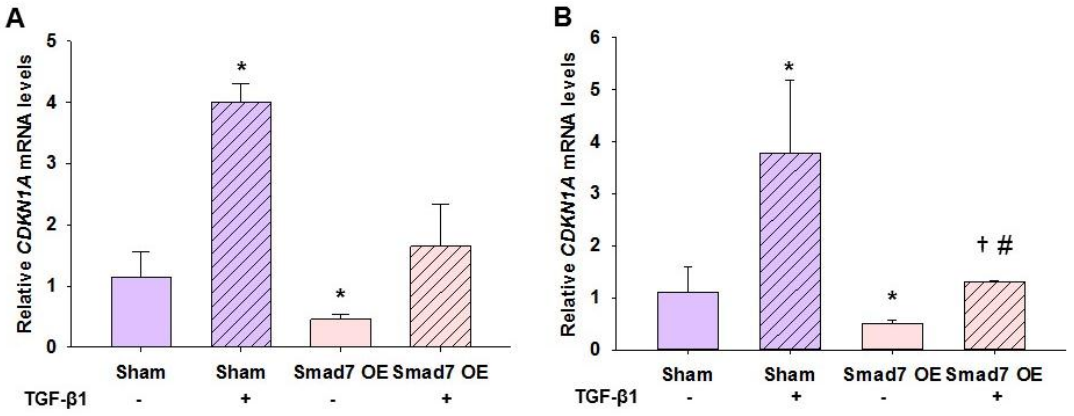

Figure 3.35 Smad7 overexpression and *CDKN1A*

(A and B) TGF-β1 treatment (pattern bar) resulted in significant upregulation of *CDKN1A*mRNA levels in COLO-357 (A) and IUSCC-PC1 (B) Sham cells (purple bars) (p=0.01 for both). Smad7 overexpression (pink bars) resulted in significant decrease of *CDKN1A* mRNA in both cell lines (p=0.04 for both). There was a significant decrease in *CDKN1A* mRNA levels between the Sham and Smad7 OE, TGF-β treated groups for IUSCC-PC1 (p=0.02) (* $p<0.05$, compared to Sham SF; † $p<0.05$, compared to Sham + TGF-β, # $p<0.05$, compared to Smad7 OE SF by 2 tailed student *t* test).

Next, the levels of p21 were analyzed in the CS7 (Figure 3.36A) and IUS7 (Figure 3.36B) cells. The basal levels of p21 were very low in the Sham cells for both the cell types. Upon TGF-β1 treatment, p21 levels increased in the Sham cells. Smad7 overexpressing cells had almost no or lowered p21 compared to Sham cells grown in SF

conditions. When TGF-β1 was added to Smad7 overexpressing cells, in COLO-357 cells, p21 levels were upregulated to the same level as that of Sham, while in the IUSCC-PC1, the upregulation of p21 by TGF-β1 was attenuated.

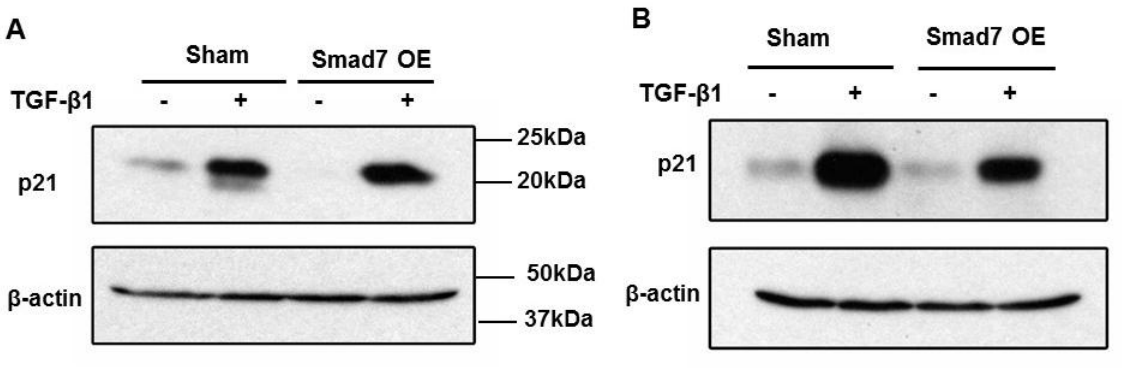

Figure 3.36 Smad7 overexpression and p21

(A and B) Smad7 overexpression decreased p21 levels in COLO-357 (A) and IUS7 (B) cells.TGF-β1 treatment upregulated p21 levels in Sham cells, and this effect was attenuated with Smad7 overexpression in IUS7 cells, but not in CS7 cells. β-actin was used as loading control. Shown are representative blots from 2 independent experiments for A and 3 independent experiments for B.

Since p21 levels regulate p-pRb status, Smad7 maybe attenuating p21 levels, resulting in prevention of dephosphorylation of pRb. These results, along with the*in vivo* data indicate that Smad7 regulates p-Smad2 and p-Smad3 differently in pancreatic cells and in mouse tissues, resulting in attenuation of TGF-β mediated cell growth inhibition (Figure 3.37).

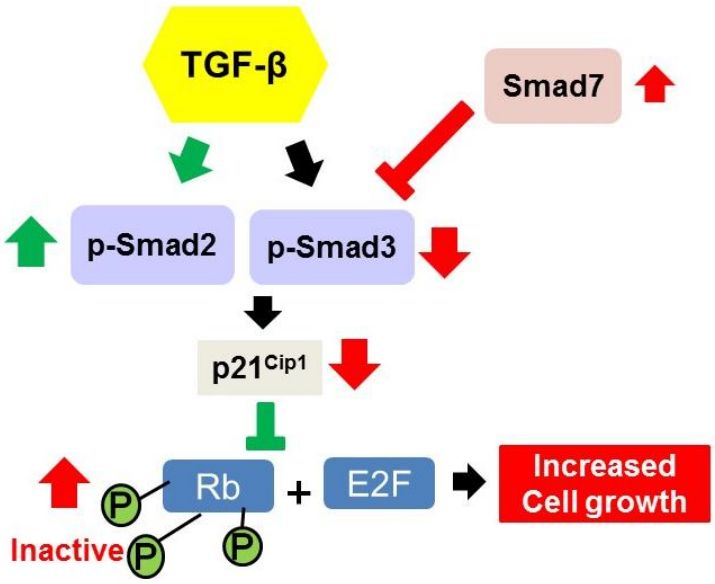

Figure 3.37 Smad7 OE allows activation of p-Smad2 by TGF-β1, however it attenuates p-Smad3 levels, thus decreasing p21 and keeping pRb inactivated

Smad7 OE does not block TGF-β mediated p-Smad2 (depicted by green arrows); however Smad7 OE attenuates p-Smad3 levels, such that it results in downregulation of p21 levels, resulting in accumulation of p-pRb (inactive pRb). The signaling path results in transactivation of E2F, increasing transcription of cyclins and increased cell proliferation.

3.15 Gene Set Enrichment Analysis and validation of Smad3 dependent, TGF-β regulated genes

The tissues from Smad7 overexpressing mouse (KS7C) stained negative for p–Smad3 levels and in the KS7C cell line, upregulation of p-Smad3 levels with TGF-β was attenuated. Therefore, I hypothesized that Smad7 overexpression preferentially attenuates p-Smad3 levels over p-Smad2 levels, resulting in differential regulation of TGF-β regulated genes. Next, to determine the genes that are regulated by TGF-β and are Smad3 dependent. A Smad3 dependent TGF-β gene signature was generated by using the microarray expression data from a previous study conducted in A549 lung epithelial cells [152]. The gene signature was generated by comparing gene expression in A549 cells treated with TGF-β versus SiS3 (specific inhibitor of p-Smad3) combined with TGF-β, with each treatment being for 24 hours. Next, GSEA was carried out for

Smad3 dependent TGF-β gene signature on a ranked list of genes that were differentially regulated in human PDAC tissues and their adjacent normal [156]. The genes that were differentially regulated in PDAC versus control tissues, correlated strongly with the Smad3 dependent, TGF-β gene signature. (Figure 3.38). This work was done by another graduate student in the laboratory at IUSM.

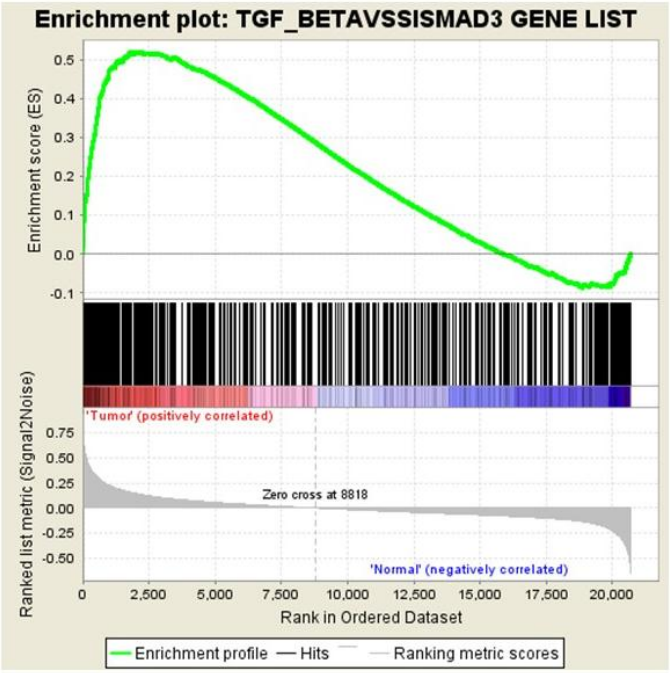

Figure 3.38 Gene Set Enrichment Analysis and validation of Smad3 dependent, TGF-β regulated genes

Gene array from inhibition of Smad3 in lung cancer cells, followed by TGF-β treatment leads to deregulation of TGF-β-mediated genes which are enriched in hPDAC tumors when compared to normal.

Next, the significantly upregulated genes from the Smad3 dependent TGF-β gene signature that were significantly up regulated in PDAC and have been previously shown to play a role in increasing PDAC aggressiveness were chosen for validation. The genes were *GPX2, MUC1, MUC13* and *AGR2*. Their expression was tested in the CS7 and IUS7 cells with or without TGF-β1. In COLO-357 Sham cells, and treated with TGF-β the *MUC1, MUC13* and *AGR2* expression was significantly decreased (Figure 3.39). Smad7

overexpression in the COLO-357 cells in SF conditions increased the levels of *MUC1, MUC13* and *AGR2* significantly. *GPX2* levels were increased with Smad7 overexpression, however the change in mRNA levels were not significant. Next the Sham and Smad7 TGF-β1 treated groups were compared. TGF-β1 lowered the expression of all four genes. *GPX2* was not significantly different in the Sham and Smad7 overexpressing groups, however *MUC1, MUC13* and *AGR2* were significantly elevated in the Smad7 overexpressing cells treated with TGF-β.

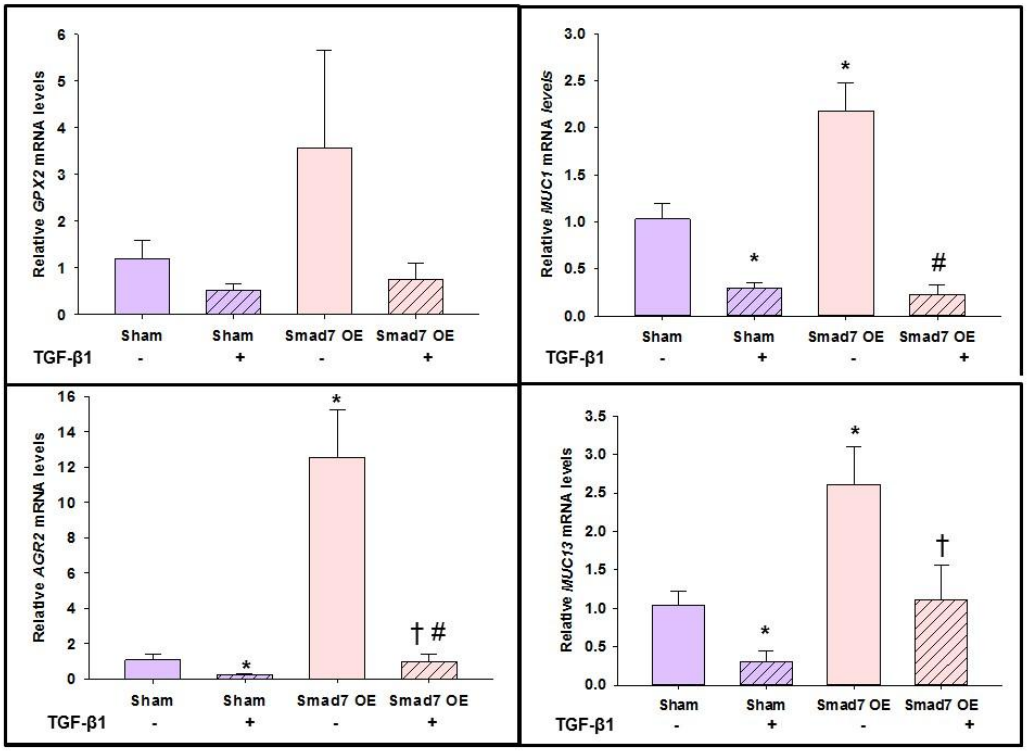

Figure 3.39 Smad7 OE enhances expression of *MUC1, MUC13 and AGR2* in CS7 OE cells

TGF-β1 (pattern) significantly lowered and Smad7 OE (pink) significantly increased *AGR2, MUC1* and *MUC13* levels compared to Sham (purple bars). *MUC13* and *AGR2* levels were significantly different in the TGF-β1 treated Sham and Smad7 OE groups. (* $p<0.05$, compared to Sham SF; † $p<0.05$, compared to Sham + TGF-β1, # $p<0.05$, compared to Smad7 OE SF by 2 tailed student t test).

In the IUSCC-PC1 cells all four genes were significantly decreased with TGF-β treatment when compared to SF in Sham cells (Figure 3.40) and significantly elevated

with Smad7 overexpression when comparing the SF conditions alone. When IUS7 cells were treated with TGF-β1, all four genes were lowered when compared to SF conditions, however their levels were significantly different from TGF-β1treated IUSham cells. These results indicate that Smad7 OE in hPCCs lowers the induction of Smad3 dependent genes in response to treatment with TGF-β1.

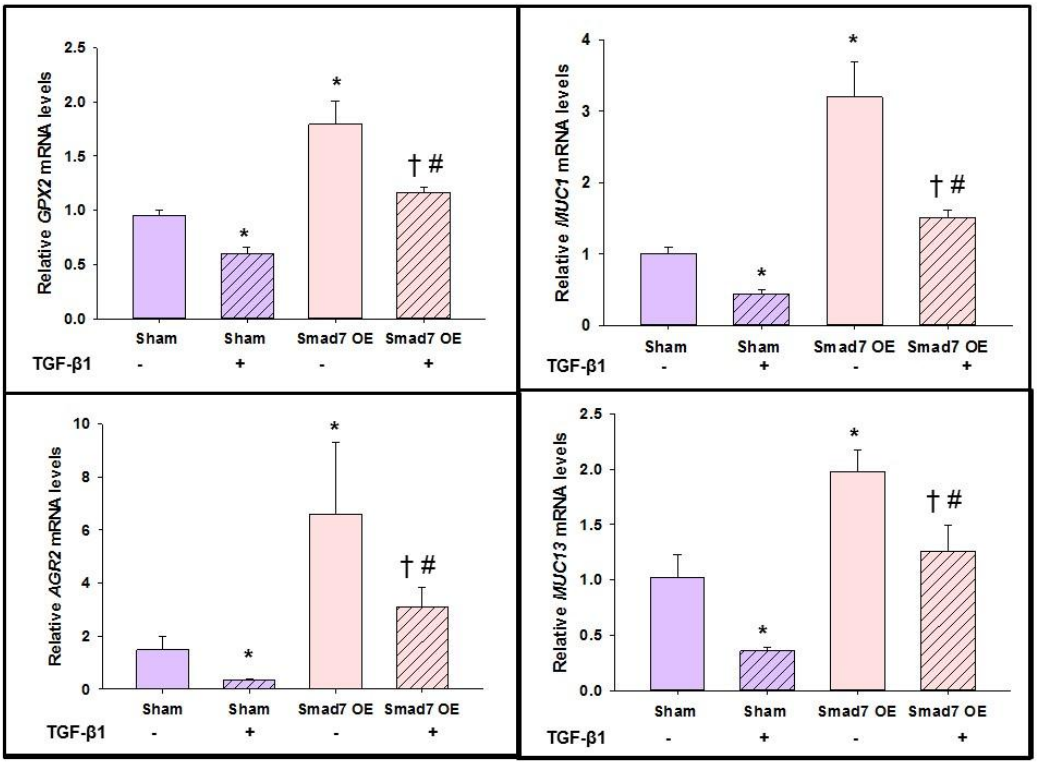

Figure 3.40 Smad7 OE enhances expression of*GPX2*, *MUC1, MUC13* and *AGR2*in IUS7 OE cells

TGF-β1 (pattern) significantly lowers and Smad7 OE (pink) significantly increased*GPX2*, *AGR2, MUC1* and *MUC13* levels compared to Sham (purple bars). *GPX2*, *AGR2, MUC1* and *MUC13*were significantly different in the TGF-β1 treated Sham and Smad7 OE groups. (* $p<0.05$, compared to Sham SF;†$p<0.05$, compared to Sham + TGF-β1, # $p<0.05$, compared to Smad7 OE SF by 2 tailed student *t* test).

3.16 Knockdown of SMAD3 in COLO-357

Based on the results of the GSEA analysis and validation of Smad3 dependent genes in Smad7 overexpressing cells, Smad3 was stably knocked down in COLO-357 (CS3KD) cells to determine if *CDKN1A* and p-pRb levels were regulated directly by Smad3. COLO-357 cells were stably transduced with shRNA against *SMAD3.* These cells were validated for *SMAD3* knockdown by qPCR and western blotting. The *SMAD3* levels were reduced by 50% in the *SMAD3* knockdown cells (Figure 3.41 A) and there was a reduction in the protein levels (Figure 3.41B).

Knockdown of Smad3 in COLO-357 cells resulted in decreased *CDKN1A*levels (Figure 3.41 C) and increased p-pRb when compared to Sham cells (Figure 3.41 D). TGF-β1 mediated upregulation of *CDKN1A* and dephosphorylation of pRb were attenuated when there was loss of Smad3.

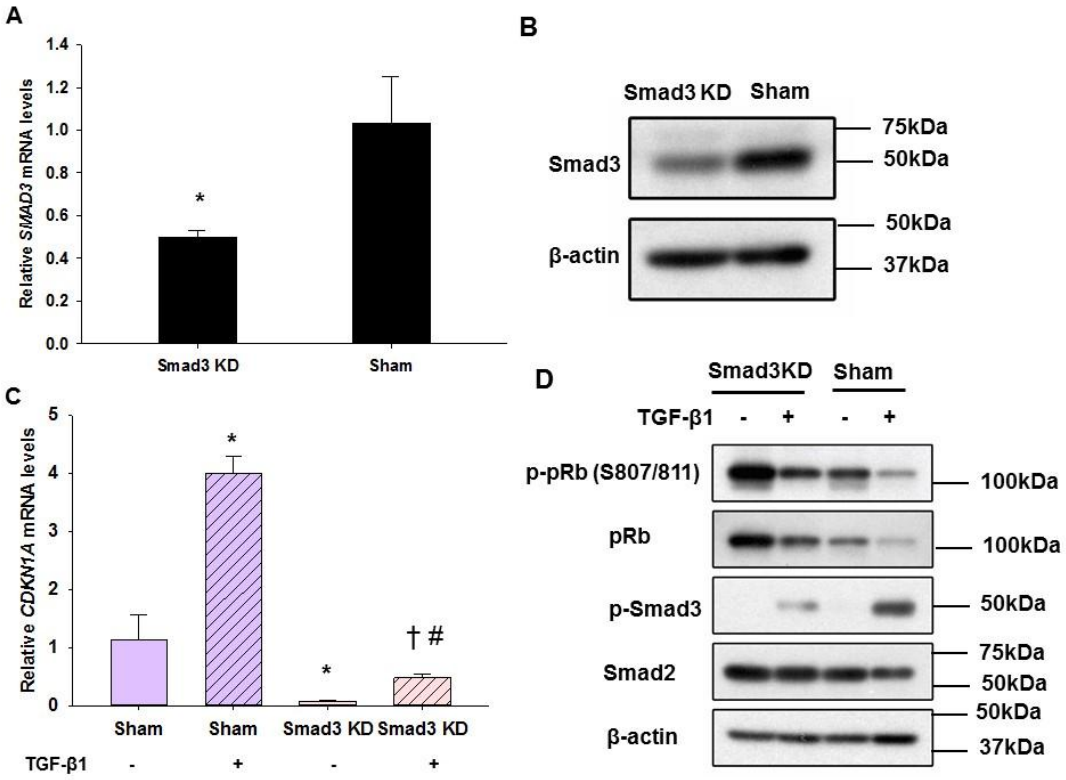

Figure 3.41 Knockdown of Smad3 in COLO-357

(A) There was a 50% reduction in *SMAD3* mRNA levels in CS3 KD cells compared to sham cells (p=0.00045). Data are represented as mean ± SEM for three individual experiments for each cell line. **(B)** Western blot with anti Smad3 indicate decreasedSmad3 levels in the Knockdown cells compared to sham**.** β-actin was used as loading control. Shown are representative blots from 3 independent experiments. **(C)**TGF-β1 treatment (pattern bar) resulted in significant upregulation of *CDKN1A* mRNA levels in COLO-357 Sham (purple bars) and Smad3 KD (pink bars) cells. Smad3 Knockdown resulted in a significant decrease in basal *CDKN1A*mRNA levels and between the sham and Smad3 KD, TGF-β1 treated groups. Data are represented as mean ± SEM for three individual experiments for each cell line.(* p<0.05, compared to Sham SF; † p<0.05, compared to Sham + TGF-β1, # p<0.05, compared to Smad3 KD SF by 2 tailed student *t* test). **(D)** When CS3KD cells were treated with 500nM TGF-β1, p-pRb levels were increased, and p-Smad3 levels were decreased. Total Smad2 levels did not change with Smad3 KD or TGF-β1 treatment. β-actin was used as loading control. Shown are representative blots from 3 independent experiments.

3.17 SMAD3 CRISPR of hPCCS

To confirm the effects observed by *SMAD*3 knockdown, CRIPSR of *SMAD3* in COLO-357 and IUSCC-PC1 cells was carried out. The CRIPSR was performed as described in Chapter 2. The cell clones were validated for loss of Smad3 by western blotting (Figure 3.42). When blotted for total Smad3, the mixed pool of COLO-357 Sham cells and the 2 single clones (D5 and E5) showed presence of Smad3 protein. This band disappeared completely in the Smad3 CRIPSR mixed pool of COLO-357 cells and the 4 single clones D7, E7, F6 and F7. Since there was a faint upper band seen in the SMAD3 CRISPR cells with the Total Smad3 antibody, I stripped the blot and re-probed with Total Smad2/3 antibody. The COLO-357 Sham mixed pool cells and single clones D5 and E5 showed presence of Smad2 and Smad3. The mixed pool from Smad3 CRISPR cells showed no presence of Smad3 and neither did the clones D7, E7, F6 or F7, however they did show presence of Smad2. Sequencing of PCR amplified region around Exon 6 confirmed partial deletion of Exon 6 in the CRIPSR clone F7. Thus the Smad3 CRIPSR was successful in the F7 derived clone of COLO-357 cells.

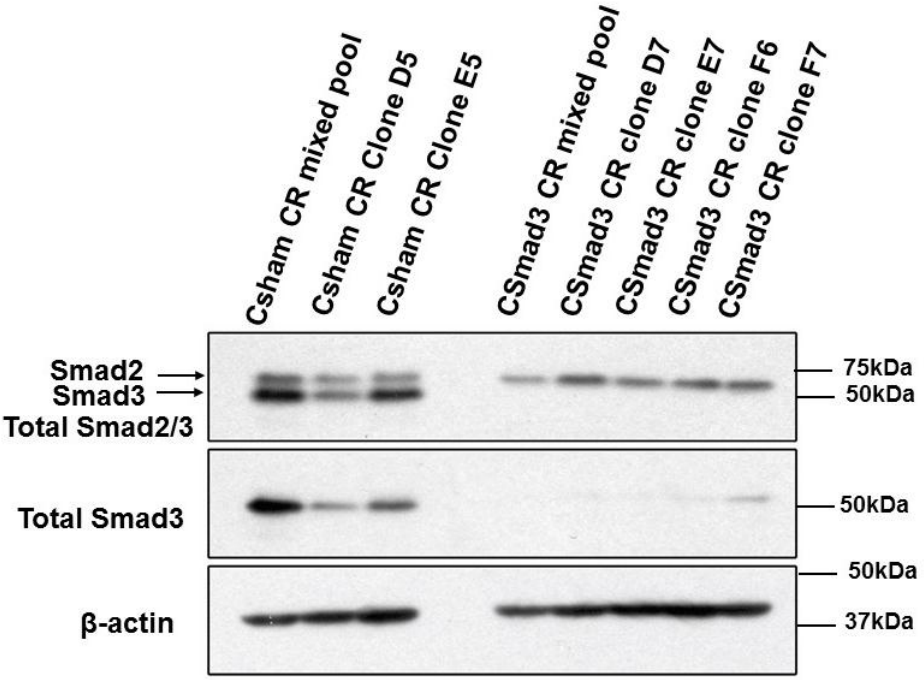

Figure 3.42 Smad3 CRISPR in COLO-357

Western blot with anti-Smad3 indicated complete loss of Smad3 levels in the CRISPR mixed pool, and the 4 clones, D7, E7, F6 and F7 cells compared to sham mixed pool cells and the two clones, D5 and E5 for COLO-357 cells**.** Blotting with Total Smad2/3 antibody showed intact Smad2 band (upper) for all the cells, however the lower band (Smad3) was absent in the mixed CRISPR cells as well as the 4 clones. β- actin was used as loading control. Shown are representative blots from 2 independent experiments.

Similarly western blotting for IUSCC-PC1s (Figure 3.43) was carried out, for mixed population of cells and a single clone for Sham and Smad3 CRISPR cell. The Smad3 protein was successfully CRISPR in IUSCC-PC1s.

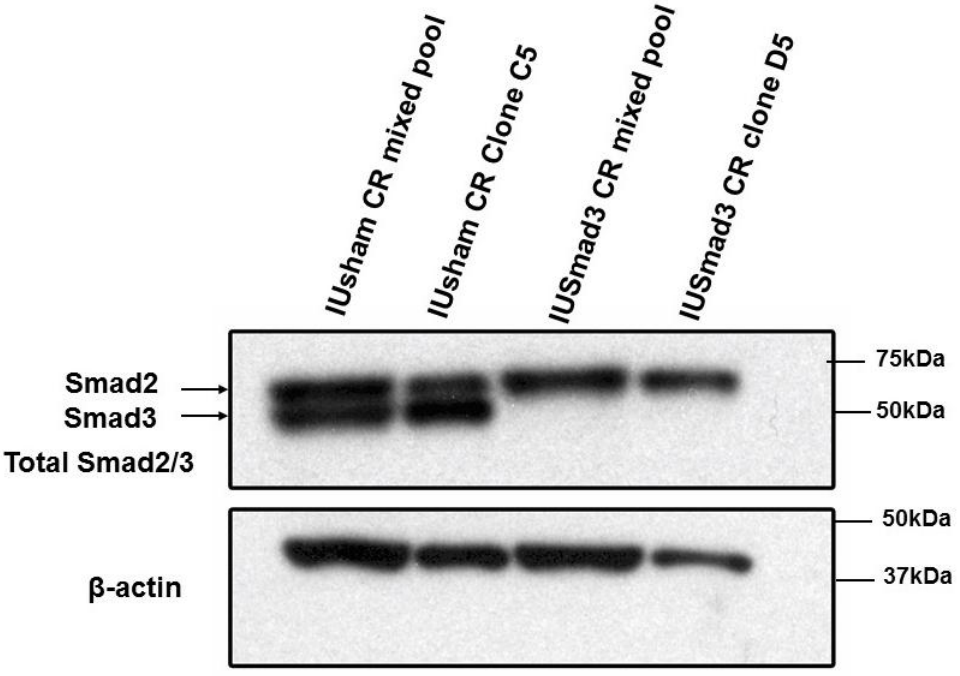

Figure 3.43 Smad3 CRISPR in IUSCC-PC1 cells

Western blot with anti-total Smad2/3 antibody showed intact Smad2 band (upper) for all the samples, however the lower band (Smad3) was absent in the mixed CRISPR cell pool as well as the single cell clone D5. β- actin was used as loading control. This was an initial experiment (n=1).

3.18 AGR2 is upregulated by knockdown of Smad3 and overexpression of Smad7

AGR2 is an ER stress marker that belongs to the protein disulfide isomerases family[163, 164]. AGR2 is upregulated in PDAC and correlates with poor survival [165-168]. AGR2 is suppressed by TGF-β via Smad4 and co-localizes with MUC1 in PanIN lesions [169]. *AGR2* was amongst the top 5 genes in the array of TGF-β regulated genes, dependent on Smad3. Thus, we confirmed the upregulation of *AGR2* levels with Smad3 knockdown (Figure 3.44 A). *AGR2* upregulation with Smad7 overexpression in hPCCS was validated by qPCR (Figure 3.39 and 3.40). Next the effects on AGR2 protein with TGF-β and Smad7 overexpression were analyzed. AGR2 protein levels follows similar patterns as the AGR2 mRNA with TGF-β1 and Smad7, where TGF-β1

lowered AGR2 levels and Smad7 OE increased basal AGR2 levels when compared to Sham in COLO-357 (Figure 3.44 B) and IUSCC-PC1 (Figure 3.44 C) cells. Smad7 overexpressing cells attenuated TGF-β1 mediated suppression of AGR2 in COLO-357 cells. In IUSCC-PC1, the attenuation of AGR2 level was not as prominent as the Sham cells. Taken together, these results indicate that expression of AGR2 levels are suppressed by TGF-β1 as shown previously. Smad3 knockdown increases *AGR2* levels and Smad7 overexpression increases *AGR2* mRNA and protein levels.

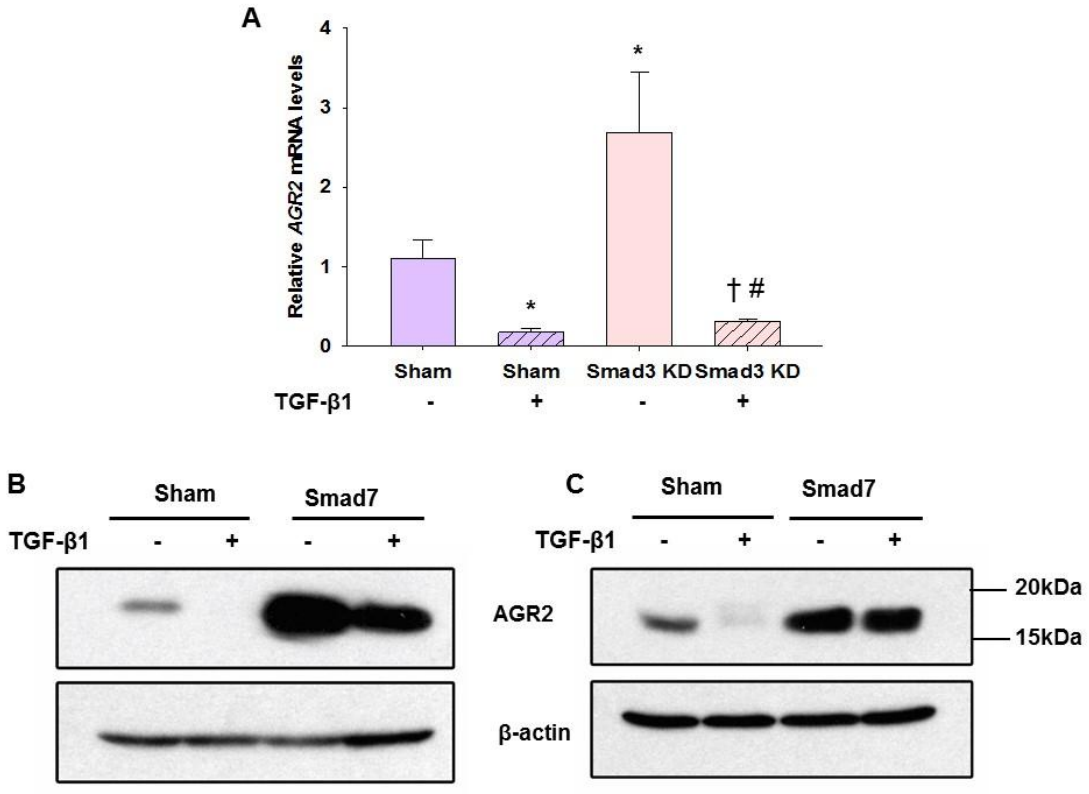

Figure 3.44 AGR2 is upregulated by knockdown of Smad3 and Smad7 OE in hPCCs

(A) Smad3 knockdown in hPCCs increased*AGR2* mRNA levels p<0.001. TGF-β1 (pattern) significantly lowers and Smad3 KD (pink) significantly increased*AGR2* levels compared to Sham (purple bars). *AGR2* levels are significantly different in the TGF-β1 treated Sham and Smad3 KD groups. (* p<0.05, compared to Sham SF; ǂ p<0.05, compared to Sham + TGF-β1, # p<0.05, compared to Smad7 OE SF by 2 tailed student *t* test). **(B-C)** TGF-β1 lowered AGR2 protein levels in COLO-357 (B) and IUSCC-PC1 (C) cells. Smad7 OE significantly increased AGR2 protein levels in both cell lines. Smad7 attenuated TGF-β1 mediated AGR2 suppression. β-actin was used as loading control. Shown are representative blots from 3 independent experiments.

3.19 AGR2 is upregulated in KS7C mice tissues and cell lines

Since Smad7 OE and deletion of Smad3 led to increased *AGR2* expression in hPCCs, I next analyzed *AGR2* expression in the KS7C and KTetS7C cell lines that were derived from the mouse tumors. The KS7C cell line showed a marked increase in *AGR2* levels

when compared to KC (Figure 3.45 A). In the KtetS7C cell lines, doxycycline was added to induce Smad7 overexpression. The KtetS7C cells in TF media were used as controls. Smad7 induction resulted in increased *AGR2* levels in these cells (Figure 3.45 B).

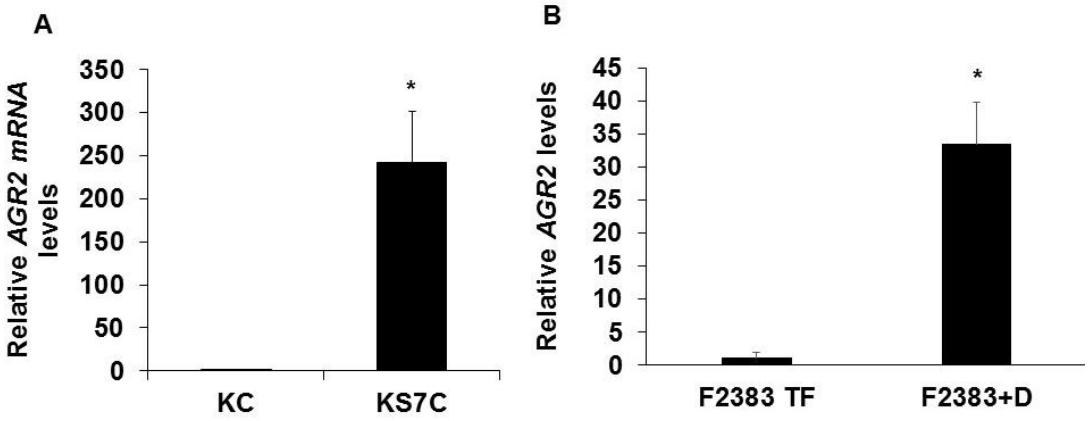

Figure 3.45 AGR2 is upregulated in KS7C and KtetS7C cell lines

(A) *AGR2* levels were significantly higher in KS7C cell lines compared to KC ($p<0.0001$). **(B)***AGR2* levels were significantly higher with induction of *Smad7* in the KtetS7C cell line when treated with doxycycline ($p<0.001$). Data are represented as mean ± SEM for three individual experiments for all qPCR data.

AGR2 was abundant in KS7C mice pancreas when compared to KC mice by IHC (Figure 3.46).

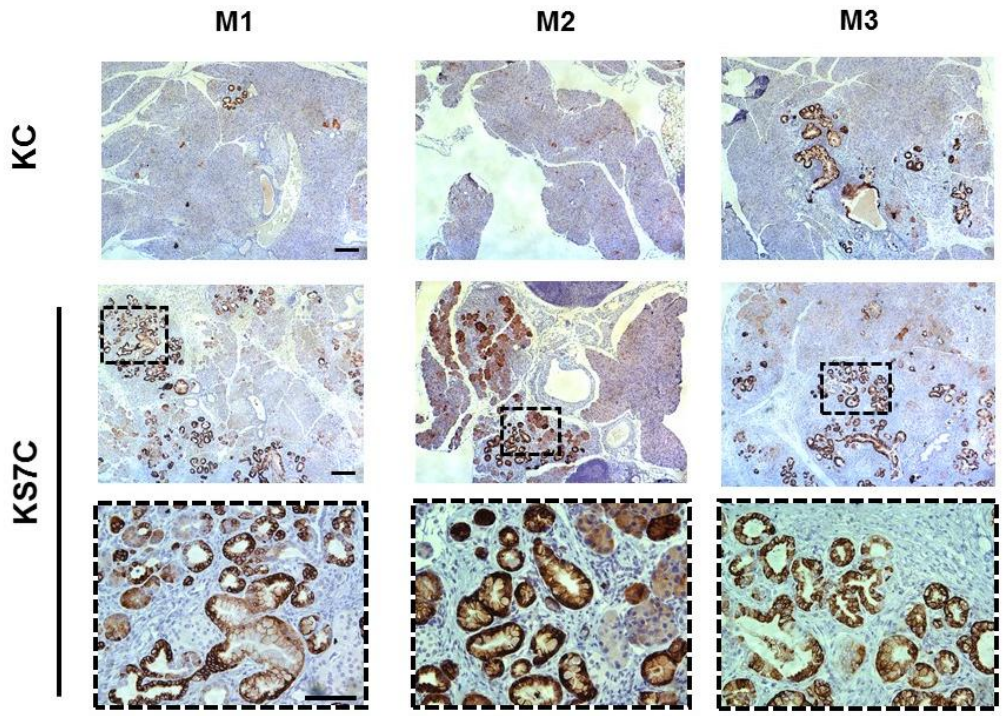

Figure 3.46 AGR2 is upregulated in KS7C mouse tissues

Representative images for AGR2 staining from 3 KC and 3 KS7C mice (M1, M2 and M3) tissues (4X magnification) which showed increased expression of AGR2 in KS7C mice when compared to KC mice. Lower most panel are 20X magnified images of KS7C tissue areas marked in dotted rectangle. Scale bars represent 100µM.

This finding was consistent in the tetracycline inducible Smad7 mouse model (Figure 3.47). Thus Smad7 overexpression *in vitro* increases *AGR2* levels in murine cells and in tissues.

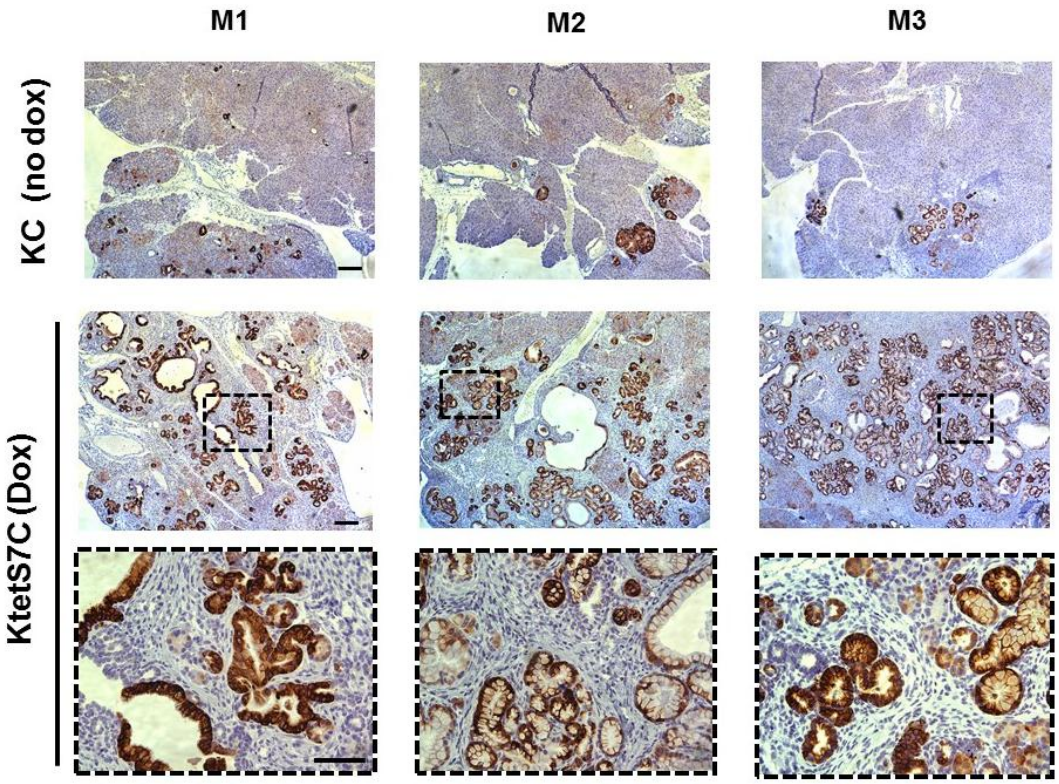

Figure 3.47 AGR2 levels are upregulated in KtetS7C mice pancreatic tissue fed with doxycycline

Representative images for AGR2 staining from 3 KtetS7C with or without Doxycycline (4X magnification). Lower most panel are 20X magnified images of KtetS7C tissue areas marked in dotted rectangle. Scale bars represent 100µM.

3.20 Smad3 and Smad4 suppress AGR2 by directly binding to its promoter and this binding is abolished in presence of Smad7

Smad7 overexpression increased *AGR2* mRNA and protein levels in hPCCs and mouse tissues. To determine if Smad7 directly bound to the *AGR2* promoter to regulate its levels, a ChIP assay with c-Myc tag in hPCCs overexpressing c-Myc tagged Smad7 was carried out. Smad7 did not bind directly to the *AGR2* promoter (Figure 3.48 A). Since knockdown of Smad3 resulted in increased *AGR2* levels, we hypothesized that Smad3

binds to the *AGR2* promoter to repress its activity. ChIP assays with Smad3 and Smad4 demonstrated that the two bound directly to the*AGR2* promoter, and this binding was abolished in the presence of Smad7 overexpression (Figure 3.48 B). Therefore, these results support the hypothesis that *AGR2*levels are directly repressed by Smad3 and Smad4. When Smad7 is overexpressed, the binding of Smads 3 and 4 to the *AGR2* promoter was inhibited or decreased, resulting in increased expression of *AGR2*. ChIP assay analysis with Smad3 and Smad4 binding to *AGR2* promoter were consistent in the IUSCC-PC1 cells (Figure 3.48 C).

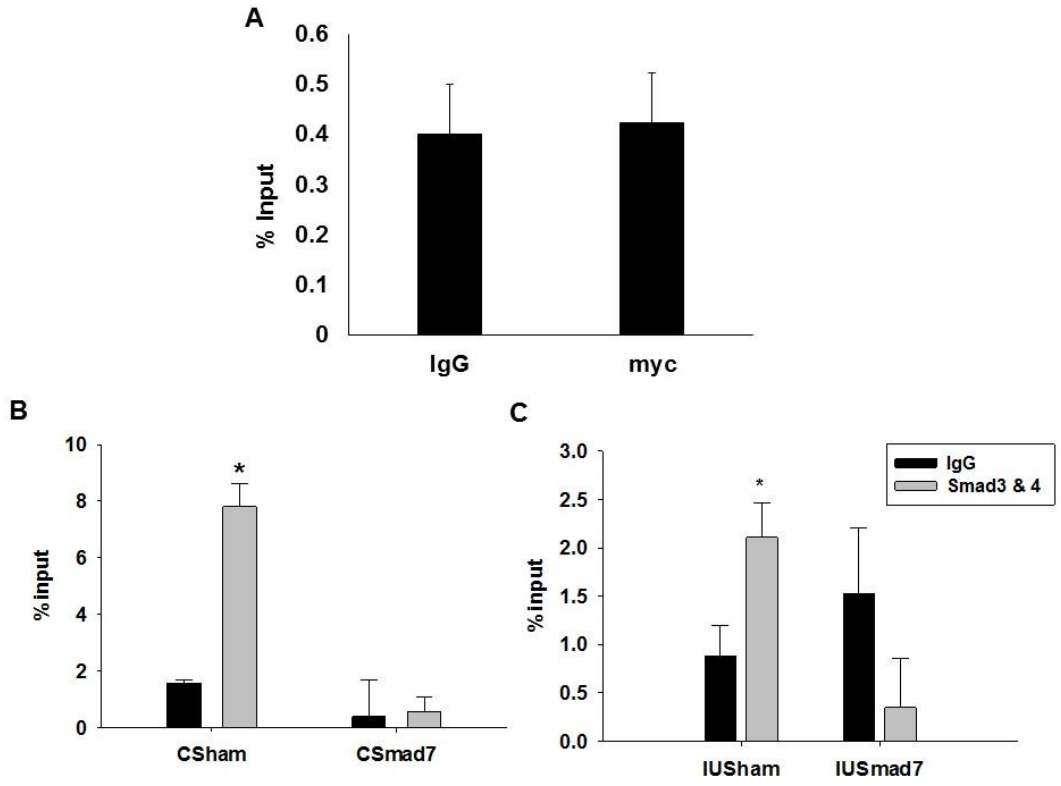

Figure 3.48 Smad3 and Smad4 suppressed AGR2 by directly binding to its promoter and this binding was abolished in presence of Smad7

(A) ChIP - qPCR assays revealed that Smad7 did not bind directly to the *AGR2* promoter. **(B)** ChIP assay in CSham cells revealed that Smad3 and 4 bound to *AGR2* promoter (p=0.023). This binding was abolished with Smad7 overexpression in COLO-357 cells. **(C)** ChIP assay in IUSham cells revealed that Smad3 and 4 bound to *AGR2* promoter (p=0.029). This binding was abolished with Smad7 overexpression in IUSCC-PC1 cells. Data are represented as mean ± SEM for three individual experiments for all qPCR data.

3.21 Smad7 and Pancreatitis

Pancreatitis is an important risk factor associated with pancreatic cancer. TGF-β is an important regulator of inflammation and fibrosis and Smad7 has been shown to inhibit this effect. Furthermore, previous studies have shown that Smad7 overexpression is protective against caerulein-induced chronic pancreatitis [138, 139]. Previous studies have shown that induction of acute pancreatitis in rats administered with caerulein results in upregulation of TGF-βI, II and III [134]. Studies by Wilde et al [135] have shown that an intact TGF-β signaling pathway in required for induction of inflammation by caerulein. Another group [131, 132, 137] showed using transgenic mouse models of dominant negative mutant TβRII, that when subjected to caerulein injections, the mice pancreata displayed amelioration of fibrosis. The Korc lab has previously shown that inducing acute pancreatitis in *Kras* mutant mice results in rapid PDAC progression[112]. Together these prior reports support the hypothesis that in the presence of Smad7, the progression to PDAC will regress in mice with *Kras* mutation after induction of acute pancreatitis. To test this hypothesis, the KS7C mice were injected with Caerulein as described in Chapter 2. KC mice were used as controls. Simultaneously KC and KS7C mice injected with vehicle alone were used as controls for caerulein effects. The mice were injected at 2.5 months of age and then sacrificed 2 months later. The histology of the KC mice exhibited marked acinar cell loss. Instead these tissues were replaced with low and high grade PanIN lesions and stroma. The KS7C mice on the other hand had less tissue remodeling in their pancreas and exhibited only ADMs and low grade PanINs (Figure 3.49 A). The number of KC mice that exhibited PanIN 2, 3 and developed PDACs were significantly more than KS7C mice (Figure 3.49 B). Next, Masson's trichrome staining was performed on the mice tissues to analyze collagen deposition, an indicator of fibrosis. Three mouse pancreata were stained from the vehicle injected group and 4 from the caerulein injected group (Figure 3.49 C). The KS7C control mice displayed lesser collagen deposition than the KC mice in the pancreas, however this difference was not statistically significant (Figure 3.49 D). The KC mice subjected to caerulein exhibited significant increase in collagen deposition when compared to vehicle injected mice. There was no difference in the collagen deposition between the KS7C caerulein injected or control mice. There was a significant decrease in collagen deposition between KC and KS7C mice that had been injected with caerulein. These results indicate that overexpression of Smad7 reduces overall collagen deposition and thus fibrosis when mice are subjected to acute pancreatitis.

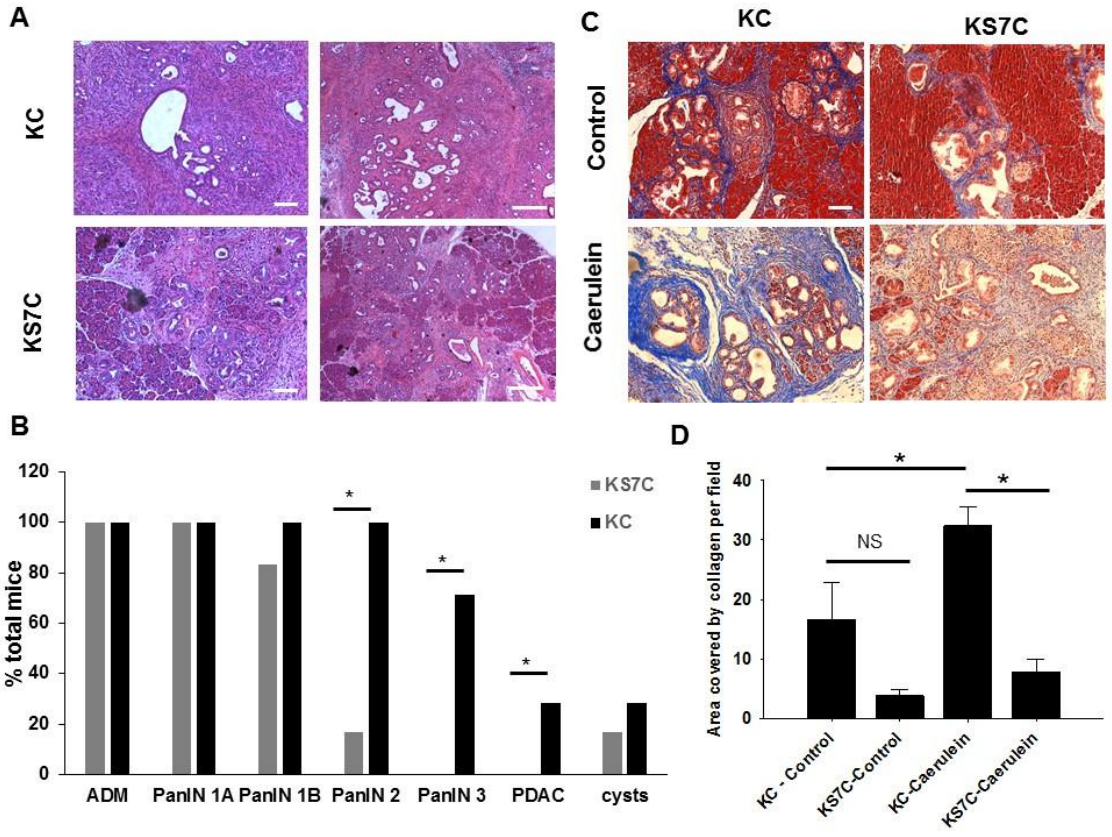

Figure 3.49 **Smad7 and Pancreatitis**

(A) Representative images from KC and KS7C mice showing that KC mice have complete tissue remodeling with cancer. Section from KS7C mouse shows normal tissue, surrounding lowgrade PanINs. Scale bars 100µM. **(B)** Bar graph represents the percent of total KC mice (black) and KS7C mice (gray) injected with caerulein, exhibiting different grades of PanIN. (* $p<0.05$). **(C)** Representative images from KC and KS7C mice showing that KC mice have increased collagen deposition (blue) compared to KS7C mice. Scale bars represent 100µM. **(D)** Quantification of collagen deposited for each group shows that caerulein increased collagen deposition significantly in KC mice. There was a significant decrease in collagen deposition between KC and KS7C mice injected with caerulein. For each group N=3 for KC and N=4 for KS7C were used. From each mice 5 random field were imaged and quantified. Data are represented as mean percent ± SEM of area covered by collagen.

Altogether, the above observations indicate that in case of inflammation or acute pancreatitis, Smad7 may play a protective role by attenuating inflammatory responses and fibrosis deposition, thus resulting in slowing down the PanIN to PDAC progression.

4. Discussion

TGF-β and its isoforms are overexpressed in PDAC and correlate with poor survival [27]. It is surprising that Smad7, which is an inhibitor of TGF-β is also overexpressed in PDAC [120, 121]. Clinical studies in PDAC patients demonstrate that low levels of Smad7 correlate with poor prognosis and increased lymph node metastasis[129]. However, the effects of Smad7 overexpression (Smad7 OE) *in vitro* and *in vivo,* results in abrogation of TGF-β mediated cell growth inhibition and increased tumorigenesis [121-123]. Thus, to delineate the role of Smad7 overexpression in PDAC we created a mouse model specifically overexpressing Smad7 in the pancreas.

4.1 Overexpression of Smad7 functions with oncogenic Kras to accelerate PDAC progression in a transgenic mouse model

We determined that overexpression of Smad7 (Smad7 OE) alone did not affect the histology of the pancreas or induce acinar to ductal metaplasia in either of the mouse models of Smad7 OE (KS7C and KtetS7C). These observations differ from the findings by Kuang et al [130] who indicated that Smad7 OE lead to induction of PanIN-2 in the pancreas of 6 months old mice even in the absence of oncogenic *Kras*. The differences between this earlier Smad7 findings and our findings may be due to differences in the model system, which features *Pdx-1* driven Cre recombinase to target Smad7 expression in the pancreas. By comparison Kuang et al [130] utilized the *Elastase* promoter to drive Smad7 expression in acinar cells. The*Pdx-1* promoter drives expression of Cre in all the three cell types, the ductal, acinar and pre-endocrinal of the pancreas versus the elastase which is specific to the acinar cells [160, 170]. Additionally, the amount of overexpression of Smad7 in the two models described in this thesis when compared to, may be different than that of Kuang et al, resulting in different outcomes. Another study by Smart et al [171] which featured Smad7 OE by *Pdx-1,* revealed abnormalities in the pancreas and foregut development. The physiological function of islets was also disrupted in these mice, with low insulin and high glucagon levels. The KS7C and KtetS7C mouse models described in this thesisexhibited similar levels of *Smad7* expression and showed normal pancreatic histology and expression of glucagon, insulin, and amylase up toat least6 months of age. Therefore we hypothesize that the levels of Smad7 overexpression may differ due to differences in transgene copy number, promoter efficiency or different mouse strains.

When a *Kras* mutation was introduced into the Smad7 overexpressing mice, there was enhanced progression of PanIN lesions to PDAC and a significant decrease in survival. Of importance, these results were reproducedin thetetracycline-induced Smad7 model where induction of Smad7 combined with oncogenic Kras at 1 month, 2 months or 3 months of age, enhanced progression to PDAC. In the earlier study by Kuang et al.[130], effects of Smad7 OE were assessed without combination with another transgene. As described earlier, *Kras* is an important driver oncogene in PDAC. This study for the first time unravels the role of Smad7 in the presence of oncogenic *Kras* using GEMMs of PDAC. The study by Xin Lui et al [172] describes how Smad7 OE in keratinocytes requires oncogenic ras (v-*ras*) to form squamous cell carcinoma, whereas Smad7 OE alone resulted in hyperplasia in this cell type. These findings are in agreement with the findings of Kuang et al and the data for KS7C and KtetS7C mice, where oncogenic *Kras* is important and required for acceleration to the cancerous stage.

The KS7C mice exhibited heterogeneity in the progression of the disease pathology, with a few mice exhibiting accelerated progression to PDAC as early as 7 weeks of age to some exhibiting advanced lesions, but no PDAC. This finding may be due to the differences in efficiency of the promoters driving any of the transgenes. Previous studies [173]have also used fluorescent tracing and determined that when there are multiple transgenes present in a mouse model, the efficiency of recombination for the different transgenes by cre-recombinase in the same cells is different[174, 175]. This may explain why mice from the same litter exhibited differences in the number and aggressiveness of the PanIN lesions. Unfortunately IHC staining with anti-HA or anti-Smad7 was not successful probably due to low expression levels of Smad7 and lack of specific antibodies. These reasons made it difficult to confirm the recombination status and expression of *Smad7* transgene in the mouse tissues. Quantification of *Smad7* mRNA in KS7C mice of the same age, exhibiting differences in pathology was done for a total of 3 mice (Supplementary figure 6.2), which suggests that there may be a correlation between the levels of *Smad7* and number and aggressiveness of the lesions exhibited by mice. In follow up studies, the number and ages of mice would be expanded to confirm this hypothesis.

Another potential reason for the heterogeneity in the number of lesions observed in the mice may be due to the differences in cellular signaling events that occur downstream of Kras and Smad7 resulting in initiation of ADM and progression to PDAC. In the

transgenic mouse models of PDAC, to the best of my knowledge, no studies have been done by sequencing multiple pancreata or tumors to examine the differences among mice with same genotype. Anecdotally researchers agree that there is considerable variations in KPC mice in terms of onset of disease[159]. As PanINs progress to PDAC, the different cells from the same mouse could accumulate different mutations that could then lead to enhanced progression of disease in a subset of cells, while the rest of the pancreas exhibits normal cellular architecture.

4.2 Smad7 promotes PDAC progression by disrupting TGF-β-directed inhibition of cell growth by a signaling pathway involving inactivation of pRb

Inactivation of pRb in combination with induced TGF-β signaling, are important hallmarks in mPDAC and hPDAC [39, 114]. I now demonstrate that pRb is inactivated in a patient derived hPCC with an oncogenic *KRAS* mutation and in the GEMMthat features Smad7 OE and oncogenic Kras. Cells isolated from pancreata of KC mice exhibited cell cycle arrest, as illustrated by decreased p-pRb levels in SF conditions. By comparison, tumor cells derived from the KS7C mice exhibited increased levels of p-pRb in SF conditions which further suggests that Smad7 OE confers a growth advantage to the cells. Treatment of KC cells with TGF-β, lead to a decrease in p-pRb, not readily detectable. Furthermore, when the KS7C cells were treated with TGF-β, the levels of p-pRb decreased when compared with the SF condition; however p-pRb levels were still higher than the KC cell line. These results indicate that Smad7 inactivates pRb, resulting in increased proliferation, in agreement with previously reported findings from the Korc lab. Thus it was shown that Smad7 overexpression in COLO-357 cells results in pRb inactivation [123] and that pRb inactivation allowed TGF-β to be a mitogen as a consequence of the activation of non-canonical signaling pathways, including those featuring ERK, Src, and Smad4-dependent upregulation of Wnt7b, which acts to further increase mitogenesis[39]. Overexpression of Smad7 in COLO-357 cells, did not block TGF-β mediated activation of MAPK, JNK1/2, p38 and AKT2 [123] which are known to increase EMT, migration and invasion of cancer cells. Activation of these proteins by TGF-β in the presence of inactivated pRb leads to increased mitogenesis [39]. Therefore, it will be important to analyze the activation of MAPK, JNK1/2, p38 and AKT2 in the KS7C mouse model to determine if Smad7 allows activation of these pathways by TGF-β *in vivo*. Furthermore, if one or more of these key regulators are activated, it would

be important to determine if inhibition of the non-canonical signaling in combination with Smad7 could decrease PDAC progression in a transgenic mouse model.

To confirm that tumorigenic outcomes by Smad7 OE involve inactivation of pRb, an*Rb1* heterozygous deletion was introduced in KS7C mice ($KR^{+/-}$S7C) and compared to mice that had a *Kras* mutation and homozygous deletion*Rb1* (KRC) in the pancreas. The $KR^{+/-}$S7C mice developed PanINs and PDAC at a similar rate compared to the KRC mice and exhibited increased pRb phosphorylation in their lesions. These observations were also consistent with the KS7C mice. The $KR^{+/-}$S7C mice pancreata also presented with other similarities to the KRC mice pancreata, such as inflammation associated with disease and cystic lesions (seen in N=3) which also suggest that Smad7 OE and heterozygous loss of *Rb1* may have similar downstream implications compared to the homozygous loss of *Rb1*. The presence of p-pRb in the $KR^{+/-}$S7C mice tissues also confirmed that the effects seen in the mice were not because of loss of heterozygosity of *Rb1*, but due to effects of Smad7 OE. These results suggest that Smad7 may exert its effect in PDAC via inactivation of pRb. To further demarcate the events downstream of pRb, it would be interesting to generate additional cell lines from the $KR^{+/-}$S7C mice tumors and investigate the effects ofTGF-β1on proliferation and colony growth in 3D tissue culture.

4.3 Overexpression of Smad7 and effects of TGF-β on Smad2 and Smad3

Smad7 OE did not decrease p-Smad2 levels in the KS7C mice tissues;however, elevated levels of Smad7 did result in decreased levels of p-Smad3. Smad7 OE in hPCCs, it blocked the phosphorylation of both Smad2 and Smad3. with an enhanced effect on levels of p-Smad3 as compared to p-Smad2. However this effect was cell type dependent. For example, Smad7 OE did not attenuate TGF-β1 mediated phosphorylation of Smad2 in COLO-357 cells; however elevated levels of Smad7 did attenuate p-Smad2 levels in IUSCC-PC1 cells, while they lowered levels of p-Smad3 in both cell lines. In both cell lines, enhanced expression of p21 and attenuation of AGR2 by TGF-β1 in presence of elevated Smad7 had different outcomes. The results obtained from the *in vitro* and *in vivo* analysis of Smad7 OE and treatment with TGF-β suggests that Smad7 regulates the function of TGF-β1ina context-dependent manner and some of the possibilities for the differences observed in the results are discussed below.

Previously it was observed that when COS-7 cells (kidney fibroblasts) overexpressing Smad7, were treated with TGF-β1 it led to the localization of Smad7 to the cytoplasm [123]. Smad7 OE also attenuated or blocked translocation of Smad2 and Smad3 from the cytoplasm to the nucleus which is as expected of the canonical TGF-β signaling pathway [64]. However, when Smad7 was overexpressed in COLO-357 cells (PDAC cells), Smad7 failed to translocate to the cytoplasm upon TGF-β signaling activation. Smad2 and Smad3 remained nuclear even when Smad7 was overexpressed and the cells were treated with TGF-β1[123]. The differences observed with Smad7 OE on the canonical TGF-β signaling pathways between the cell lines may be due to factors, such as expression of SMURFS which regulate the shuttling of Smad7 between the nucleus and cytoplasm [77, 78, 176]. In IUSCC-PC1, we did not verify the distribution of Smad7 and its effects on p-Smad2 or p-Smad3 localization to confirm whether it exhibited similar results as COLO-357. These effects of differences in localization are likely due to differences in the levels of p-Smad2 and p-Smad3, thus affecting the actions of TGF-β on gene expression.

Another potential explanation for the differences observed in the results between the two hPCCs may be due to the genetic alterations between each of the cell lines. For example COLO-357 cells do not have a *Kras* mutation, whereas IUSCC-PC1 has a *Kras* mutation. Perhaps oncogenic Kras is driving differential signaling which maybe the primary reason for differences in levels ofp-Smad2, AGR2 and p21 with Smad7 OE and TGF-β treated cells. Thus, it would be interesting to see the outcomes with Smad7 OE and TGF-β treatment when oncogenic *Kras* is introduced into COLO-357 cells to specifically determine the effects of overexpression of Smad7 and *Kras* in this signaling context and PDAC.

A third explanation for the differences in p-Smad2, AGR2 and p21 levels with Smad7 OE and TGF-β in the hPCCs may involve other transcription factors that regulate their expression [163, 177]. The Smad3 complex maybe an important factor, but it may not be the only transcription factor responsible for regulation on these genes. To confirm that effects observed with Smad7 OE are modulated by Smad3, we next knocked down Smad3 in hPCCs and examined the effects on *CDKN1A*, *AGR2* and p-pRb.

4.4 Overexpression of Smad7 decreased p-Smad3 levels, modulating expression of *CDKN1A* and *AGR2*: two potentially important targets that regulate cell cycle and migration

The effects of Smad7 overexpression and knockdown of Smad3 were similar on *CDKN1A* levels and inactivation of pRb *in vitro.* TGF-β increased *CDKN1A* levels in hPCCs, and Smad7 OE resulted in reduced basal transcript levels of *CDKN1A*. Knockdown of Smad3 in COLO-357 also resulted in downregulation of *CDKN1A*, indicating that Smad3 regulates *CDKN1A*levels in hPCCs.We hypothesize that increased cell proliferation seen *in vivo* with elevated levels of Smad7 could be a consequence of decreased levels of p-Smad3. GSEA of genes that change with inhibition of Smad3 using SiS3 and TGF-β[152] indicated that these genes are significantly enriched in hPDAC, implying that deregulation of Smad3 may be vital for progression of hPDAC. Overall, our findings suggest that Smad7 significantly decreases the levels of p-Smad3 and low levels of phosphorylated Smad3, result in PDAC aggressiveness mediated by TGF-β signaling.

Based on our studies and several published reports, the effects of Smad3 on p21 seem to be specific to Smad3. Similar to our findings, studies by Anny et al.[178] in HaCaT cells (immortalized keratinocyte cells)demonstrate that individual knock down of Smad3, led to decreased p21 levels and coincident with enhanced phosphorylation of pRb, were independent of Smad2 and Smad4 knockdown. Furthermore, depletion of Smad3 resulted in increased levels of plasminogen activator inhibitor (PAI-1) as was observed previously in Smad7 overexpressing COLO-357 cells [121]. In another study, keratinocytes from *Smad3* knockout mice, transduced with *V-ras*, resulted in a by-pass of senescence via downregulation of p15 and c-Myc, which culminated in malignancy [179]. Furthermore, this signaling pathway was shown to be Smad3 specific and could not be rescued by overexpression of Smad2 or Smad4. Studies comparing knockdown of Smad3 and Smad2 independently in PANC-1 cell (PDAC cell) indicated that depletion of Smad3, but not of Smad2 resulted in decreased cell growth inhibition by TGF-β [180]. Together these earlier observations and ours indicate that Smad3 is indispensable for regulation of p21 levels in hPCCs and TGF-β1 mediated cell growth inhibition.

In pancreatic cancer cells and tissues inactivation of Smad3 by Smad7OE resulted in decreased expression of *CDKN1A*, increased p-pRb and abrogation of TGF-β mediated cell growth inhibition. Levels of p21 are also lowered by Smad7 OE in KS7C mice.

Decreased p21 levels have been shown to correlate with lower survival in PDAC patients [39, 181]. The PDAC mouse model harboring a heterozygous deletion of *p21* and a *Kras* mutation exhibit increased PanIN lesions compared to the KC mice and havea mean survival of 75 days [181]. Together these earlier observations and our results suggest that downregulation of p21 in PDAC plays a role in disease progression and one of the mechanisms that leads to downregulation of p21 in GEMMs and patients may be through Smad7 OE and subsequent inactivation of p-Smad3.

In hPCCs, the *CDKN1A* and p21 levels were regulated differently at the transcript level versus the protein levels. Smad7 overexpression was associated with low basal *CDKN1A* levels and an attenuated increase in the presence of TGF-β1. At the protein level, p21 levels were enhanced by TGF-β1 to the same extent in both, the Smad7 overexpressing cells and control. This finding suggests that there might be other factors that may play a role in stabilization of *CDKN1A*mRNA transcripts when cells are treated with TGF-β1, thus resulting in upregulated p21 protein levels by TGF-β1 even in the presence of Smad7 OE.In the KS7C transgenic mouse model however, there was loss of p21. Taken together these results indicate that the regulation of p21 protein levels may involve a different mechanism in hPCCs versus in the tissue. It would be important to see if p21 is regulated at transcript levels in KS7C tissues to confirm the effects of Smad7 seen mechanistically in hPCCs.

In contrast to p21 expression with Smad7 OE, *AGR2* expression is markedly increased in our GSEA analysis and has been shown to play a role in PDAC aggressiveness [163, 166, 167, 169, 182]. KC mice with *AGR2* deletion show delayed progression of PanIN [163] indicating its importance in PDAC progression. Our results showed that AGR2 mRNA and protein increased with Smad7 OE and knockdown of Smad3 in hPCCs. This increase in AGR2 expression was also observed in KS7C and KtetS7C mice as compared to KC mice, indicating that another mechanism by which Smad7 OE results in PDAC progression might be via upregulation of AGR2. Previously we have shown that *AGR2* levels are suppressed by Smad4 [169]. ChIP results demonstrated that Smad3 and Smad4 bind to the *AGR2* promoter in hPCC and that Smad7 OE inhibits their binding to the *AGR2* promoter. These findings imply that together Smad3 and Smad4 bind to the *AGR2* promoter and repress its transcription. When overexpressed, Smad7 inhibits the binding of Smad3 and Smad4 to the *AGR2* promoter, resulting in

upregulation of AGR2 mRNA and protein (Figure 4.1). Upregulation of AGR2 in mice that overexpress Smad7 may be explained by the decrease in p-Smad3 levels.

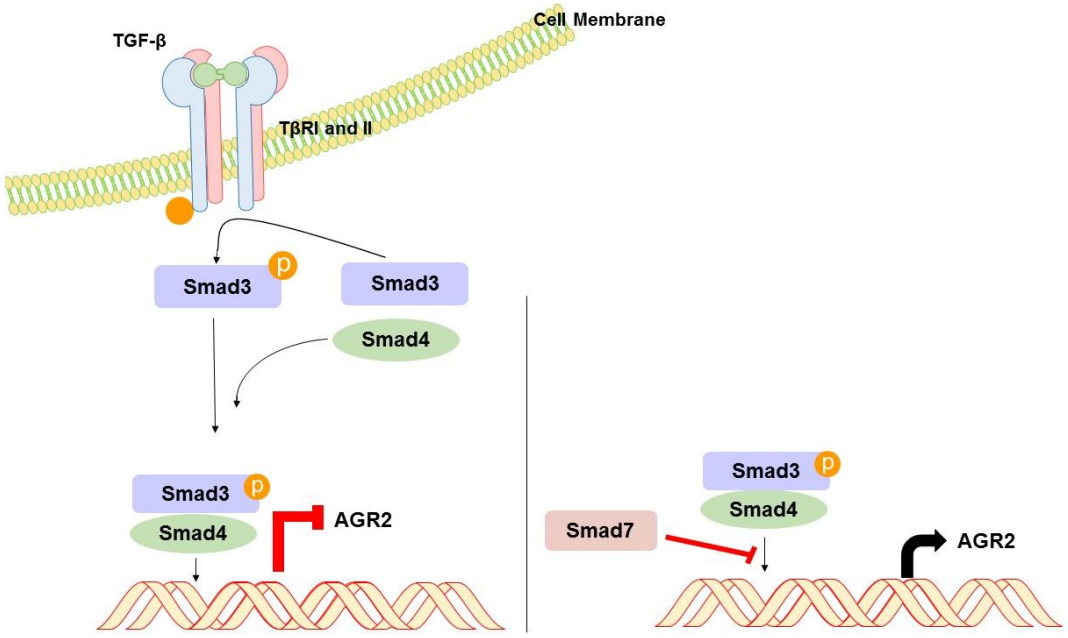

Figure 4.1 Schematic representation of TGF-β mediated *AGR2* expression

TGF-β1 suppresses *AGR2* expression via Smad3 and Smad4. When Smad7 is overexpressed Smad3 and Smad4 do not bind to the *AGR2* promoter, resulting in its upregulation of *AGR2* transcription.

TGF-β1 decreased expression of AGR2 mRNA and protein levels in COLO-357, while Smad7 OE increased the levels of AGR2 mRNA and protein. When Smad7 overexpressing COLO-357 cells were treated with TGF-β1, Smad7 attenuated the TGF-β mediated decrease of AGR2 mRNA and protein. In IUSCC-PC1 cells, Smad7OE attenuated TGF-β1 mediated downregulation of *AGR2*, however the AGR2 protein in IUS7 under SF conditions and following treatment with TGF-β1 were similar. This indicates that other factors likely stabilize the AGR2 protein, thus resulting in blocking the TGF-β1 mediated downregulation of AGR2 when Smad7 is overexpressed in IUSCC-PC1 cell line.

4.5 Smad7 and pancreatitis

Chronic Pancreatitis (CP) is an important risk factor for PDAC [41, 42, 44]. Previous studies have shown that TGF-β signaling is important for induction of inflammation (pancreatitis) by caerulein and the fibrosis associated with it [133-135, 137, 140]. Induction of acute pancreatitis in KC mice results in enhanced PDAC progression [112]. When KS7C mice were injected with caerulein, overexpression of Smad7 resulted in decreased fibrosis and attenuation of PDAC progression when compared with KC mice injected with caerulein. These results are in agreement with previous studies, where attenuation of TGF-β resulted in inhibition of caerulein-induced pancreatitis [135] and decreased fibrosis [137]. Studies by Jing He et al [138] and Xuan Li et al [139] using Smad7 overexpressing and Smad7 null transgenic mice demonstrated that in a model of chronic pancreatitis, Smad7 inhibits the TGF-β mediated inflammatory response and fibrosis, thus preventing damage to the pancreas. Oncogenic Kras plays an important role in prevention of tissue repair after damage caused by pancreatitis [111, 112, 183] (Figure 4.2).

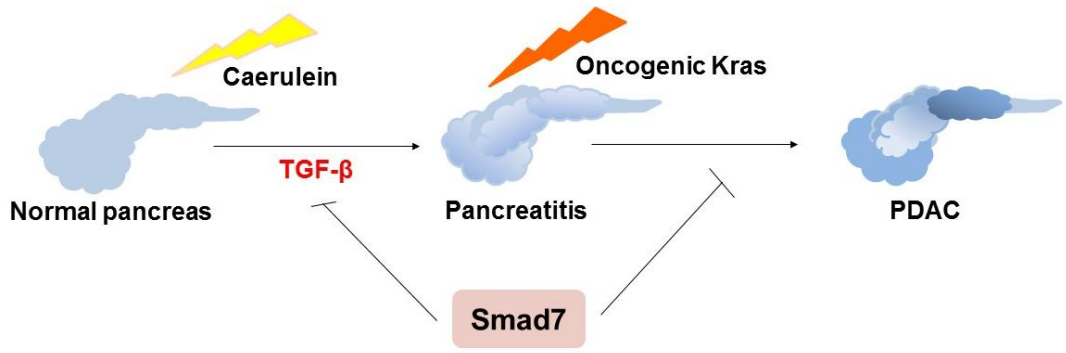

Figure 4.2 Smad7 inhibits tissue damage and fibrosis in chemical induction of pancreatitis

Caerulein induces pancreatitis which results in upregulation of TGF-β followed by increased fibrosis. This effect is blocked by Smad7 OE. Induction of Inflammation in the presence of oncogenic Kras results in accelerated progression to PDAC. However, in the presence of high levels of Smad7, caerulein-induced pancreatitis was associated with attenuated tissue remodeling and lowered deposition of collagen.

In KC mice, PanIN lesions are surrounded by activated stroma[112, 184]. The microenvironment for PDAC has a higher ratio of T regulator cells (Tregs) compared to T effector (Teff) cells, as well as a higher ratio of M2 to M1 macrophages[185]. High Treg ratios suppress the immune system and are associated with lower PDAC patient survival. Therefore we hypothesized that in the presence of Kras mutation, when mice pancreata are subjected to acute pancreatitis, there is infiltration and development of PanIN and stroma that results in an immune suppressive tumor environment. When Smad7 is overexpressed, it may modulate TGF-β mediated responses by inhibiting Treg formation, resulting in an inverted ratio for Treg and Teff, thus reducing the inflammatory response and fibrosis. To test this hypothesis in the future, the pancreata from KC and KS7C mice could be analyzed for infiltration of M1 and M2 macrophages and the Teff and Treg. This can be done using cell surface markers, such as CD4, CD8, and FoxP3 for T cells and CD163, CD120 for macrophages [185, 186].

5. Conclusion and future directions

In conclusion, using mouse models we have now established that Smad7 OE in the presence of oncogenic *Kras* results in increased PDAC aggressiveness as demonstrated by increased number of PanIN lesions. TGF-β is overexpressed in PDAC[27], however its tumor suppressor activity is lost. The tumor promoting role of TGF-β has been well studied, and now we show that Smad7 overexpression *in vivo* blocks TGF-β-mediated cell cycle inhibition. *Smad7* levels were increased in mice with dominant negative*p53*mutation and *Kras* mutation (KPC) (Figure 3.11). Mongersen, an oral *SMAD7* antisense drug, has now finished phase II clinical trials for Crohn's Disease[187]. Smad7 inhibits TGF-β mediated epithelial cell growth inhibition [121-123], thus it would be interesting to test this Mongersen in the well characterized KPC mouse model of PDAC and see if it has any effects treating the progression of tumors and metastatic disease observed in KPC mice.

Smad7 exerts effects on p-Smad3, which acts as a switch for effects exerted by TGF-β downstream of Smad3. Lowered p-Smad3 levels result in upregulation of tumor promoting genes, such as like *AGR2* and suppression of tumor suppressors like *CDKN1A* (Figure 5.1), however the total Smad3 levels do not change. The precise mechanism by which Smad7 lowers p-Smad3 levels has not been uncovered in this thesis work. There are two likely possibilities by which Smad7 could lower p-Smad3 levels. Firstly, by preventing Smad3 phosphorylation by TGβ receptors and secondly by rapidly dephosphorylating p-Smad3, thus preventing its binding with Smad4 and translocation of the complex to the nucleus (Figure 5.2). One of the ways to test this hypothesis would be to perform cell fractionation experiments and determine the distribution of Smad3 in the nucleus and cytoplasm and how the distribution changes with overexpression of Smad7 and/or TGFβ1.

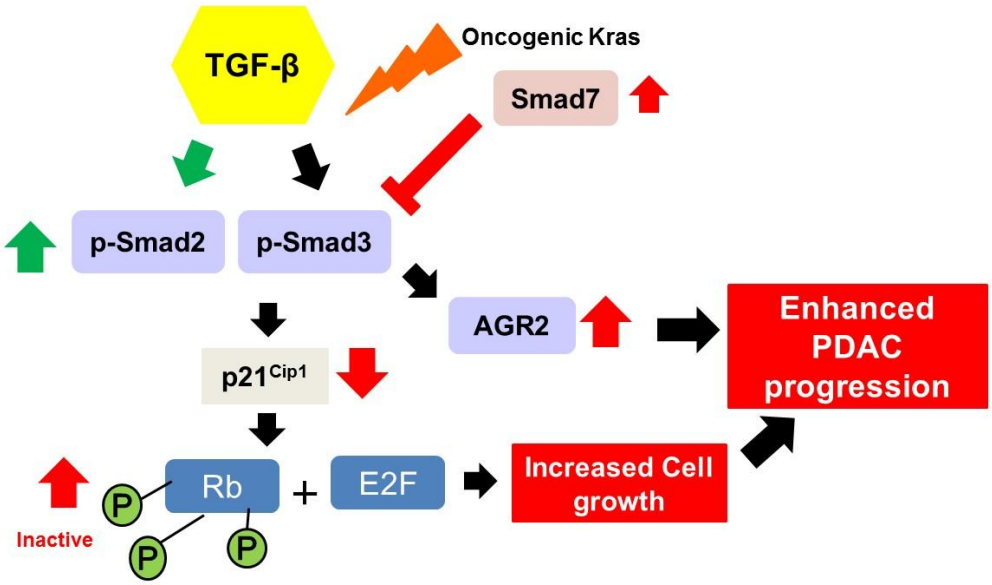

Figure 5.1 Schematic representation summarizing the effects of overexpression of Smad7 and enhanced PDAC progression

Smad7 OE in the presence of oncogenic Kras does not block TGF-β mediated p-Smad2 (depicted by green arrows); however Smad7 OE attenuates p-Smad3 levels, such that it results in downregulation of p21 levels, resulting in accumulation of p-pRb (inactive pRb). The signaling path results in transactivation of E2F, increasing transcription of cyclins and increased cell proliferation. Simultaneously, decreased p-Smad3 causes attenuation of Smad3 mediated repression of AGR2, thus resulting in increased AGR2 levels. Red color indicates pro-tumorigenic effects. Together, these actions lead to enhanced PDAC progression.

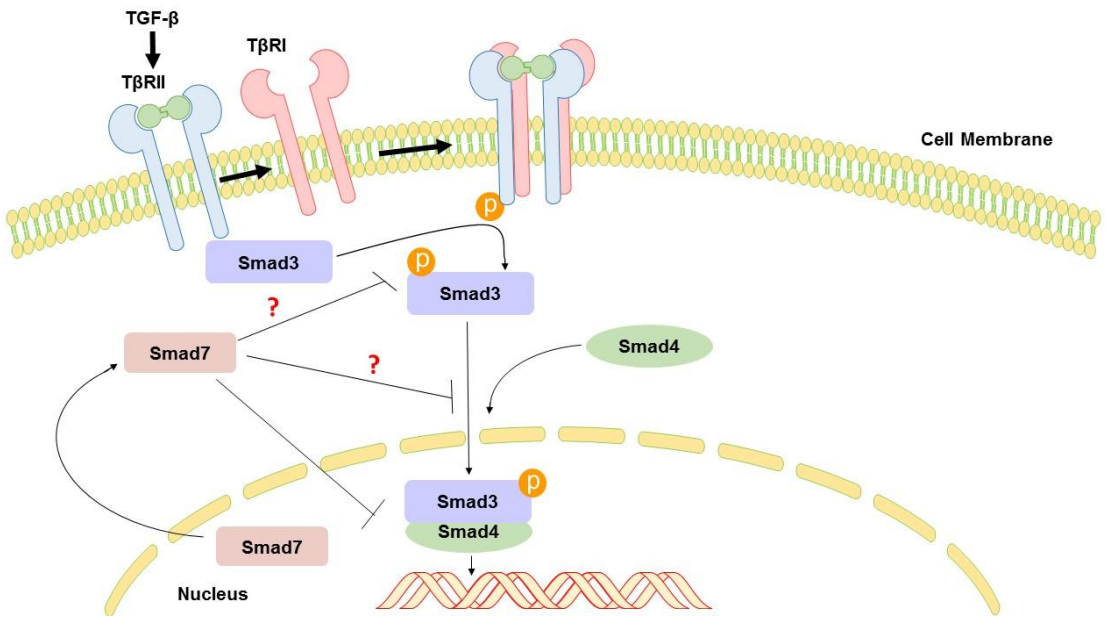

Figure 5.2 Schematic representation of possible ways that Smad7 may lower p-Smad3 levels

Smad7 lowers p-Smad3 levels by either inhibiting phosphorylation of Smad3 by TβRI or by dephosphorylating Smad3 preventing it from binding to Smad4 and translocating to the nucleus.

It would be helpful to confirm that Smad7 mediates its signaling effects via Smad3 and not by Smad2. To test this idea, genetic manipulation of Smad2 via CRISPR or knockdown could be performed in hPCCs and the effects on expression of AGR2 and p21 mRNA and protein analyzed. If the effects are predominantly through Smad3 and not Smad2, then we would expect to observe no changes in levels of p21 or AGR2 with loss of Smad2 in presence of TGF-β. Lastly, high levels of p-Smad2 levels in hPDAC samples have been shown previously as an indicator for activated TGF-β signaling in cancer cells [39]. Thus, it would be important to measure p-Smad3 levels in hPDAC tissues and determine if there is a negative co-relation with elevated Smad7 levels. The effects of overexpressed Smad7 on preferential inhibition of p-Smad3, suggest a switch between the oncogenic and tumor suppressor roles of TGF-β.

Overall, our studies with the transgenic mouse model have provided a deeper understanding into the effects of Smad7 on the TGF-β canonical signaling pathway,

bringing us closer to target Smad7 as therapeutic for PDAC and promote anti-tumorigenic effects of TGF-β.

6. Supplementary information

6.1 *Kras^{G12D}* recombination in mouse tissues

Some of the mice which genotyped positive for *Kras^{G12D}* and *Pdx1-Cre* or *Kras^{G12D}*, *SMAD7* and *Pdx1-Cre*displayed normal histology with intact architecture of the pancreas. To understand the reasons why this may have happened, the *Kras^{G12D}* recombination was examined in these mice. The mice with pathology were used as control. To confirm recombination of *Kras^{G12D}*, primers and protocol were used according to Jackson lab protocol for *Kras^{G12D}* Conditional PCR (Figure 6.1A). T2407, T2491 and T2226 were 12 month KS7C mice which showed no pathology but were positive for all three genes by genotyping. NT, T2146, T2205, T2284, T2331 mice were positive for all 3 transgenes and showed pathology. RNA was isolated from pancreas of these mice and a known positive control (mice with *Kras^{G12D}* and *Pdx1-Cre* transgene) was used. The 500bp product confirmed presence of *LSL-Kras^{G12D}*transgene. The 622 bp product indicated the presence of wildtype (WT) *Kras* allele. The 650bp product confirmed the presence of recombined *LSL-Kras^{G12D}*transgene. The mice T2409 and T2491 showed presence of the *LSL-Kras^{G12D}*transgene however it did not undergo recombination. The *LSL-Kras^{G12D}*transgene in T2226 underwent recombination, but showed very little pathology (Figure 6.1B).

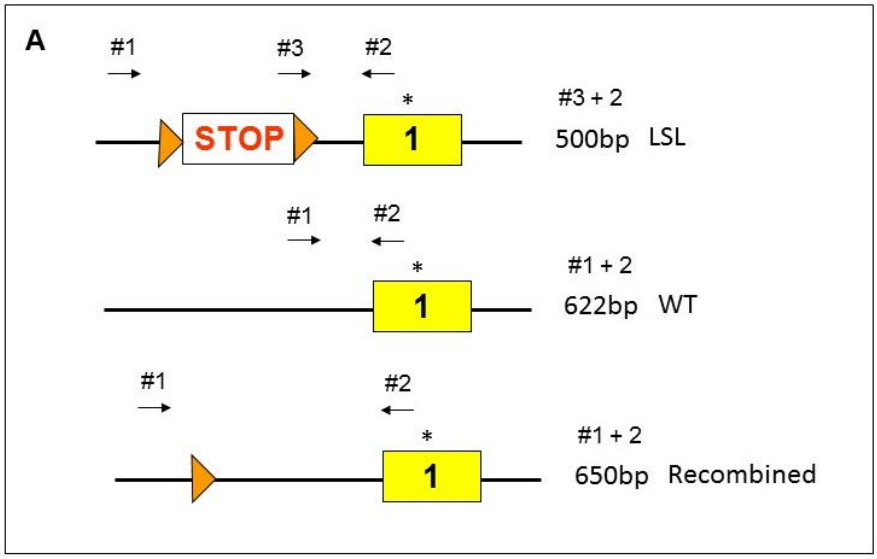

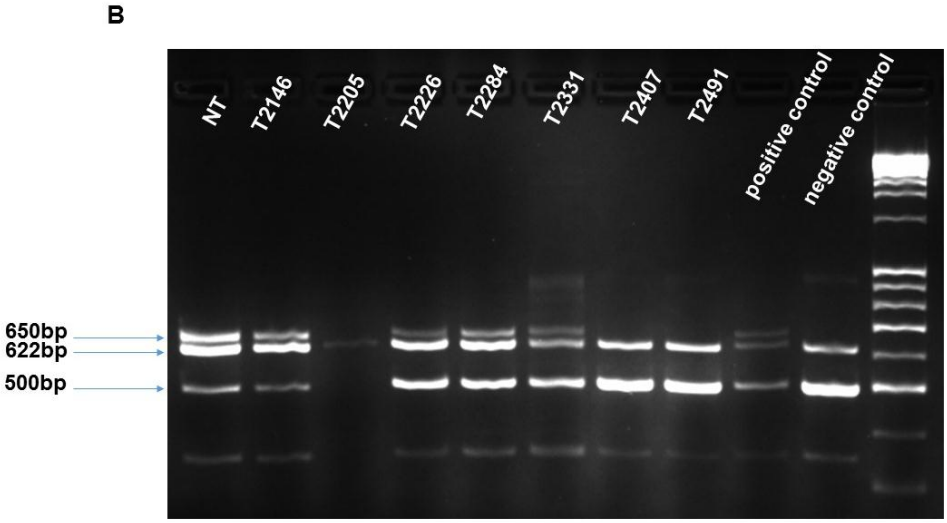

Figure 6.1 PCR detected recombination of *LSL*- Kras^{G12D} transgene

(A) PCR amplification of *LSL*- *Kras*^{G12D} transgene yields a 500bp product with primers #3 and 2. The recombined *LSL*- *Kras*^{G12D} transgene yields a 650bp product and the WT Kras a 622bp with primers #1 and 2. **(B)** PCR amplification of cDNA from mice pancreas showed that the positive control had presence of all three products indicating successful recombination of *LSL*- *Kras*^{G12D} transgene, which was absent in the negative control as expected. Two of the three mice (T2226, T2407 and T2491) showed absence of recombined *LSL*- *Kras*^{G12D} transgene.

We next analyzed the levels of *SMAD7* in these mice and confirmed that T2409, T2491 and T2226 had no overexpression of *SMAD7.* This could explain the less diseased pathology of the mouse. The Kras G12D Conditional PCR was carried out for all mice without pathology and these were then excluded from the analysis (Figure 6.2).

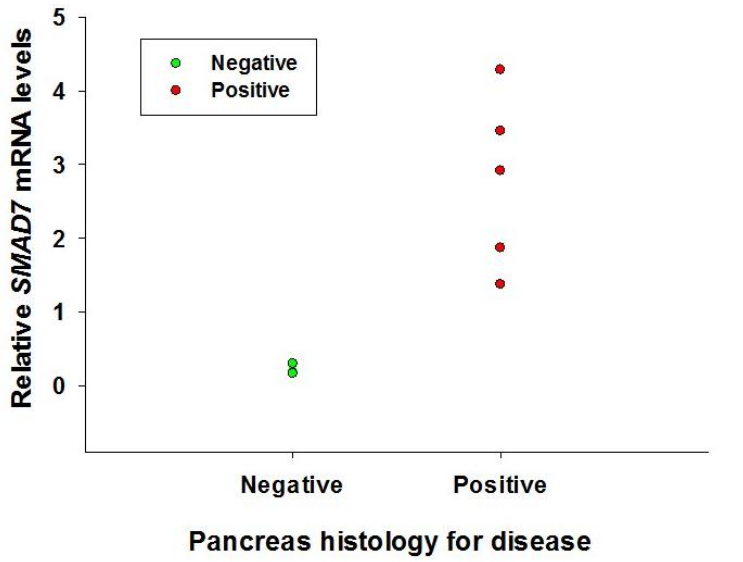

Figure 6.2 Expression of *SMAD7* in KS7C mice with negative and positive pathology

SMAD7 mRNA levels measured by q-PCR were significantly lower in KS7C mice which were negative for pathology (green) when compared to KS7C that exhibited pathology (red) in the pancreas.

6.2 *Rb1* recombination in cell line from KR$^{+/-}$S7C mice and pRb expression.

To confirm that the *Rb1* single allele in the KR$^{+/-}$S7C mice was intact and functioned as expected we first did *Rb1* recombination analysis by PCR. The *Rb1* allele deletion involves deletion of Exon 19 in the *Rb1* gene which results in loss of pRb. One set of PCR primers flank the regions around Exon 19. Therefore when the exon is intact a larger product is formed, as seen in the KC and KS7C cell line, however when there is a deletion the product is smaller in size as seen by the smaller product in KR$^{+/-}$C and KR$^{+/-}$ S7C cell lines. Where upper band indicates presence of intact exon 19 and lower one represents deleted exon 19. The other set of primers are designed to amplify the region flanking the lox p sites around exon 19. In a mouse with homozygous deletion, no

product will be formed, and in a mouse with heterozygous deletion there will be a 235bp product formed as seen in Figure 6.3. Thus by PCR method the $KR^{+/-}$S7C cell line were confirmed to be heterozygous for *Rb1* without loss of heterozygosity.

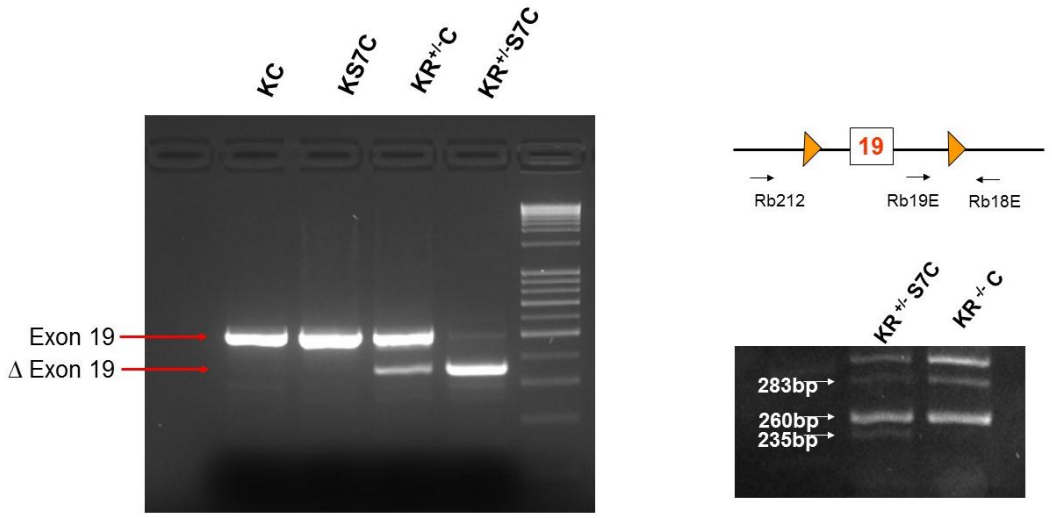

Figure 6.3 PCR detection for *Rb1* deletion

PCR amplification of genomic DNA from cell lines for genotyping of Rb1. **(B)** PCR amplification of cDNA from mice pancreas showed that the positive control for *Rb1* deletion ($KR^{-/-}$C) had presence of the 260bp product indicating loss of exon 19 and absence of 283bp product indicated lack of intact exon 19. The KC and KS7C cell lines were positive only for wild type exon 19, while the KRS7C cell line shows presence of both bands, confirming heterozygosity for *Rb1* transgene.

Next, to confirm expression of pRb in these cell lines the protein from the cells was isolated, separated by gel electrophoresis and blotted with anti-pRb antibody. The Figure 6.4 shows expression of pRb in the KC, KS7C, $KR^{+/-}$C and $KR^{+/-}$S7C cell lines, confirming expression of pRb in all the cell lines.

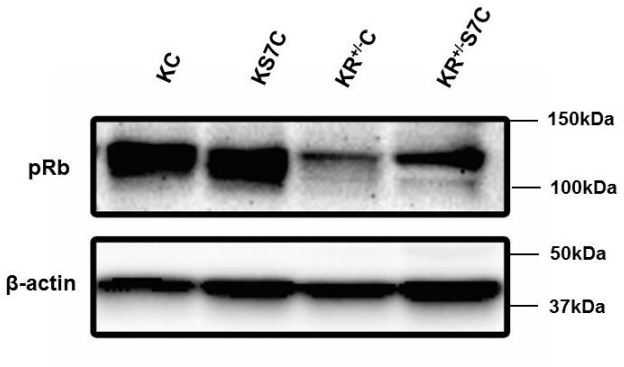

Figure 6.4 pRb expression in tumor derived murine cell lines

Western blot with anti-pRb indicated presence of pRb in KC and KS7C cell lines. In $KR^{+/-}C$ and $KR^{+/-}$ S7C cell lines the pRb levels are present, however reduced when compared to KC and KS7C cell lines. β-actin was used as loading control. Shown are representative blots from 3 independent experiments

6.3 Immunoprecipitation (IP) of Smad7 and PP-1

We hypothesize that Smad7 binds with PP-1, resulting in decreased p-Smad3 levels or increased p-pRb. To test this hypothesis, we carried out an IP with c-Myc tag as described earlier in chapter 2 and probed for PP-1 catalytic subunit. Figure 6.5A shows that c-Myc IP was successful as the IP with Smad7 overexpressing COLO-357 cells shows distinct band with Smad7. Blotting the c-Myc-IP with PP-1 (Figure 6.5B) showed that Smad7 and PP-1 form a complex. The soup after antigen- antibody was also run, which shows that PP-1 remains unbound in the lysate in Sham cells, however in Smad7 overexpressing cells, most of the PP-1 is bound to Smad7 and is removed from soup. This experiment was performed once with Tet-Smad7 COLO-357 and once with COLO-357 constitutively expressing Smad7. The amount of pull down in the tet-Smad7 v/s the constitutive Smad7 cells was different, owing to the differences in amounts of Smad7 levels overexpressed in the two cell lines.

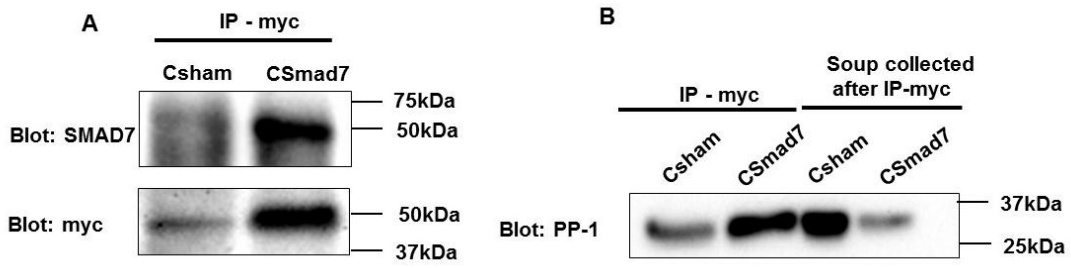

Figure 6.5 Immunoprecipitation of Smad7 and PP-1

(A) Western blot with anti-c-Myc and anti-Smad7 confirm successful pull down of Smad7 in CSmad7 cells when compared to Csham cells. **(B)** Western blot with anti-PP1 after IP with anti-c-Myc antibody showed that PP-1 bound to Smad7 in CSmad7 cells. The soup after antibody-antigen pull down during IP shows removal of PP-1 from soup, thus confirming that Smad7 binds with PP-1.

Supplementary tables

Table 6.1 Expression of TGF-β mediated Smad3 dependent genes.

GENE_SYMBOL	logFC	adj.P.Val
KANK4	-5.54017602666667	2.84849087890363e-14
COL1A1	-5.32464619466667	5.04719187373406e-14
C20orf160	-5.160246489	6.74271845993217e-13
INHBB	5.121086058	6.79969557151773e-13
MARCH4	-5.114444256	9.14565576711578e-13
COL22A1	-4.980302075	9.14565576711578e-13
RGMA	-4.878878008	1.87203254522402e-12
LEFTY2	-4.65730220166667	2.29386822029635e-12
SLN	-4.622404638	2.29386822029635e-12
MAF	-4.518065675	2.6009757215957e-12
AGR2	4.51724214666667	4.55585303438102e-12
KIF26B	-4.512902306	5.09178504704738e-12
BCAS1	4.50237311066667	5.67978803547205e-12
TNFAIP6	-4.39067652066667	6.1101373922509e-12
GSTA5	4.24202532266667	6.5561793754626e-12
CRLF1	-4.22358469133333	7.27660710424072e-12
C15orf48	-4.19772507133333	8.35085946379151e-12
SERPINE1	-4.17044398166667	9.85447674523448e-12
ZBED2	-4.100225975	9.85447674523448e-12
TF	4.097648297	9.85447674523448e-12
SPON2	4.092811869	1.0108347762857e-11
DOCK2	-4.011560016	1.08210995860228e-11
RET	-3.986156827	1.15102574908618e-11
PACSIN1	3.96808003133333	1.37500591525221e-11
SLC26A9	3.96409701533333	1.37500591525221e-11
DACT1	-3.961207129	1.37500591525221e-11
MFAP4	-3.86278868566667	1.38575173564305e-11
OSTBETA	3.85782712966667	1.38575173564305e-11
FRMD6	-3.834923246	1.48703296969347e-11

RASGRP1	-3.77935782033333	1.54534268551438e-11
LOX	-3.764458134	1.54534268551438e-11
LPAR5	-3.752690725	1.54534268551438e-11
RNF43	3.73569102733333	1.55738735339639e-11
RHOV	3.73444811266667	1.96478685590584e-11
KCNJ15	-3.654122303	2.25900563163813e-11
TSPAN2	-3.64085642766667	2.32450694487283e-11
PVRL4	-3.62812431633333	2.39369645196538e-11
PIK3AP1	-3.625712684	3.39734682486697e-11
IGFBP5	-3.61955629733333	3.39734682486697e-11
TMEM88	-3.61029387366667	3.65418115448111e-11
MMP2	-3.57630364866667	3.97941312680258e-11
CGB	-3.55660603533333	4.00328054457391e-11
ACOX2	3.540256309	4.18651844984236e-11
PPP1R14C	-3.509664476	4.18651844984236e-11
MMP10	-3.503883926	4.57221449197131e-11
CACNA1I	-3.49842832833333	4.67058733014329e-11
FGA	3.49056601266667	4.67058733014329e-11
CP	3.473055741	5.7276217485458e-11
GPR68	-3.47182135566667	5.7276217485458e-11
ADAM19	-3.38905993	5.7276217485458e-11
ZNF365	-3.38550174366667	5.7276217485458e-11
COL4A1	-3.37682253433333	5.90260227372096e-11
RABGAP1	-3.33262988133333	6.25856361726711e-11
CYP4F3	3.32903214733333	6.34833514160545e-11
PDGFRA	-3.32548621	6.46892531929595e-11
FGA	3.319606301	6.46892531929595e-11
MGAM	3.319155001	6.46892531929595e-11
PLEK2	-3.30346004033333	6.46892531929595e-11
SPDEF	3.286049889	6.49774223855637e-11
CDH22	-3.28348109333333	6.49774223855637e-11
ANXA13	3.28281844166667	6.49774223855637e-11
TIMP3	-3.27389385666667	7.01577423281714e-11

R3HDML	-3.26170046166667	7.24397423681478e-11
PLXNA4	-3.25648175733333	7.39871165375772e-11
CCKBR	3.24464545233333	7.39871165375772e-11
OCA2	-3.24218035533333	8.98816660795501e-11
HOXD10	-3.23613188066667	8.98816660795501e-11
GPX2	3.23416095266667	9.00302723120275e-11
MUC13	3.22815786433333	9.00302723120275e-11
DDC	3.22488391166667	9.02862112653262e-11
WNT5B	-3.21112774333333	9.27235274006547e-11
FAM176A	-3.20008471466667	9.27235274006547e-11
MAF	-3.17050612066667	9.27235274006547e-11
CEACAM6	3.12224817266667	9.69189069507968e-11
GPR115	-3.11744449233333	9.69189069507968e-11
RAB37	3.10318040866667	9.95278360393052e-11
CEACAM6	3.09271240066667	9.95278360393052e-11
CPN1	3.08449553166667	1.03328929837096e-10
TAGLN	-3.08311384333333	1.05754762372201e-10
EHF	3.08263033233333	1.07668918967227e-10
PLA2G12B	3.08201110233333	1.09161305486453e-10
DOK7	3.06362447433333	1.11497244788063e-10
ESAM	-3.06022688266667	1.11497244788063e-10
HNF4A	-3.05383223133333	1.19425139171075e-10
SLC2A12	-3.04513697166667	1.20038256157082e-10
DDIT4L	3.04132713733333	1.20038256157082e-10
MUC5AC	3.036409741	1.22699269164007e-10
C1orf61	3.033280365	1.22952399750947e-10
MEG3	-3.01421503633333	1.24221289510468e-10
LEFTY1	-2.99423803666667	1.35580405523954e-10
XYLT1	-2.98553106066667	1.37378202010544e-10
FGFBP1	2.98401749066667	1.51733645571491e-10
DIO3OS	2.98180119366667	1.51733645571491e-10
SPARC	-2.980808223	1.5221527501096e-10
HAPLN3	-2.98003480566667	1.52642731975161e-10

SRD5A2	-2.967626532	1.57142844302332e-10
PITPNC1	-2.96087354566667	1.57466318335744e-10
SPOCK1	-2.958050313	1.60240232275399e-10
TSPAN7	2.94515172	1.70308113450606e-10
ITGB6	-2.936949738	1.7508092223996e-10
ARRB1	2.93515087733333	1.7508092223996e-10
GPR115	-2.928546625	1.76671793605682e-10
PEAR1	-2.91052854333333	1.76671793605682e-10
GNG4	-2.90922872966667	1.77028927798015e-10
CXCR5	-2.90590559966667	1.8484060847793e-10
LHX4	2.90095814266667	1.90548924223183e-10
HSD17B6	-2.89935440333333	1.91583205100115e-10
NECAB2	2.89539171633333	1.91883597450794e-10
GDA	2.885120996	1.94534659441361e-10
	-2.88271998833333	1.96204109064969e-10
FRMD6	-2.87794971633333	1.98542683060521e-10
TAGLN	-2.87574675366667	2.03895566832801e-10
GDF15	2.864557706	2.03895566832801e-10
BEAN1	-2.86237500933333	2.03895566832801e-10
TAS2R1	-2.84620907	2.03895566832801e-10
GRID1	-2.84450980766667	2.07265112074973e-10
VSTM4	-2.812245632	2.39557102833663e-10
ABLIM3	-2.81109145966667	2.4579045713269e-10
ITGA11	-2.809999498	2.49073867766127e-10
KIF5A	-2.808656112	2.61900870779965e-10
LOC100422737	2.80541499733333	2.92006189390244e-10
SLC6A15	-2.80398127133333	3.04083385343789e-10
FGFR1	-2.803937723	3.060041055099e-10
PLA2G10	-2.78928590433333	3.060041055099e-10
FAM49A	-2.78786549433333	3.07689026930101e-10
UNC13A	2.78196384866667	3.17390459803398e-10
CILP	-2.78182885666667	3.41281767981122e-10
FLRT3	2.77912489866667	3.53576672802847e-10

KCNJ2	2.77591658733333	3.67090861688633e-10
COL5A1	-2.77439309333333	3.67090861688633e-10
PCDHAC2	2.766785395	3.67090861688633e-10
LAMC2	-2.75384008266667	3.91823287340614e-10
RNF144B	2.747229973	3.91823287340614e-10
SLPI	2.743233727	3.98331608120242e-10
APOH	2.74160214966667	4.00542848211979e-10
DUSP26	-2.74086166166667	4.10136331068445e-10
ANKDD1A	-2.73643878033333	4.10707097053326e-10
C4BPB	-2.715511658	4.1167197878266e-10
CYP4F12	2.71427385066667	4.15752577542488e-10
GREM1	-2.71254406066667	4.1617991229746e-10
STK32A	-2.712324188	4.23065618643514e-10
	2.71201713966667	4.44305004819245e-10
RUNX1	-2.694185281	4.44305004819245e-10
INPP4B	-2.69265385133333	4.50067982499643e-10
IL11	-2.682447109	4.65876158500592e-10
CXCR7	-2.68202600366667	4.84680270139213e-10
FGB	2.67462698633333	5.02818988307645e-10
PRRX2	-2.662409606	5.27349517094414e-10
SPRY1	2.66045673733333	5.27349517094414e-10
PER2	2.658663345	5.33927066200457e-10
FGG	2.65805852466667	5.47787351876291e-10
CSF2RA	2.65603348233333	5.6950766321074e-10
CHRNA9	-2.65436665633333	5.72149449240583e-10
RDH10	2.64646641166667	5.76448317428785e-10
TNFRSF19	-2.64525239633333	5.80630686540941e-10
H19	2.644763341	5.80630686540941e-10
C18orf1	-2.63401407766667	5.80630686540941e-10
PDGFB	-2.633731095	5.80630686540941e-10
ERBB3	2.627118391	5.80630686540941e-10
B3GALT5	2.622160357	5.835999112642e-10
FA2H	2.62198626766667	5.835999112642e-10

SLC6A15	-2.617161204	6.06952567808473e-10
ST6GALNAC1	2.60886208733333	6.29673536290518e-10
OSGIN1	2.60211627133333	6.41298162511837e-10
WSCD1	2.59980512633333	6.47461593240722e-10
C2orf82	-2.59940285666667	6.47461593240722e-10
RASSF5	2.597926025	6.47461593240722e-10
VSTM4	-2.592232725	6.72301118157131e-10
	-2.58801225133333	6.75133182307934e-10
VDR	-2.58174733166667	6.75133182307934e-10
C12orf39	2.576985283	7.11153658860745e-10
METTL7A	2.575040609	7.29701832305406e-10
C4orf26	-2.56708607466667	7.3534972971618e-10
TMC8	2.556858214	7.99979856835872e-10
SLC6A15	-2.55486451566667	8.30351620445139e-10
RNF182	-2.55285095533333	8.56587291700358e-10
C11orf41	-2.55035290733333	8.57100027597445e-10
FGA	2.53976565033333	8.78024346697206e-10
EREG	2.53520150133333	8.98498995305366e-10
MEGF6	-2.52527755866667	8.98498995305366e-10
IFITM1	2.52521053466667	8.98498995305366e-10
CXCL5	2.523821575	9.1116463944049e-10
HEATR7B1	2.51997174033333	9.1116463944049e-10
PODXL	-2.50928030733333	9.25148517229183e-10
LOC728392	-2.501001619	9.35064984984945e-10
CDH19	-2.49870996733333	9.58853346963158e-10
MZB1	2.49718849833333	9.59122769238512e-10
CXCL3	2.489638381	9.63473244197662e-10
AREG	2.48765763333333	9.63473244197662e-10
CYP4F11	2.481679489	9.87254780111171e-10
TRIM2	-2.47522834666667	1.00634246088075e-09
C12orf39	2.47517887133333	1.02347996943516e-09
	-2.46869957033333	1.03305577189801e-09
MDGA1	-2.468556277	1.05502393461600e-09

LOC554207	-2.46349204933333	1.05849446365034e-09
PSG8	-2.46130091466667	1.05849446365034e-09
CUX2	-2.461151047	1.09962174057891e-09
COL4A2	-2.458863404	1.11858806077993e-09
S1PR5	-2.456754384	1.15403159375645e-09
SLPI	2.455525307	1.18693354205281e-09
SDK2	2.45122640566667	1.25685420839799e-09
FAM43A	-2.43990188466667	1.25685420839799e-09
MIA2	2.436696881	1.26766890351534e-09
PCDHB6	-2.42670018333333	1.29038605026081e-09
RBMS3	-2.42607446266667	1.31098575901071e-09
CSDC2	-2.424594503	1.33317185228165e-09
MALL	2.41698248633333	1.33540765926928e-09
SLC23A1	2.40760684833333	1.34842471502303e-09
CDH16	2.40459485966667	1.34842471502303e-09
TPM1	-2.40398745	1.34842471502303e-09
	-2.40318250433333	1.42572043625414e-09
SORCS2	-2.401847606	1.44808456328894e-09
SLC6A13	-2.40097560266667	1.50946882193322e-09
ANGPTL4	-2.398306043	1.55681239677897e-09
COL20A1	-2.396326441	1.58958229583319e-09
CYP4F11	2.39469257466667	1.58958229583319e-09
	-2.38744504966667	1.591342259105e-09
AQP3	2.382515593	1.60101821948855e-09
KITLG	2.37836208066667	1.60101821948855e-09
AQP3	2.37757241666667	1.60308145570487e-09
ABLIM3	-2.37177302733333	1.60308145570487e-09
JUNB	-2.36980492866667	1.62164980206999e-09
KRTAP3-3	-2.36843836666667	1.69091228683358e-09
AKR1C4	2.36366565	1.71038050284611e-09
ST3GAL5	-2.35326817466667	1.74930161263952e-09
LZTS1	-2.35048050866667	1.78276946389002e-09
LOC284344	-2.34806778266667	1.80930182846115e-09

KLHDC8A	-2.34460612933333	1.82274532463624e-09
	-2.343064724	1.82274532463624e-09
CDH4	-2.33877697366667	1.90134199220749e-09
NTF4	-2.33606454166667	1.90134199220749e-09
PLEKHH2	2.33254693533333	1.90134199220749e-09
LCE3D	-2.33223902333333	1.9240750509088e-09
SERPINE2	-2.32504849133333	1.9240750509088e-09
CX3CL1	2.321417867	1.9240750509088e-09
CYP4F8	2.320823902	1.99792851321477e-09
ALDH3A1	2.31988413066667	2.00523583933037e-09
CTGF	-2.31786527866667	2.01032968146957e-09
SDPR	2.315158227	2.01032968146957e-09
SCEL	2.31285539666667	2.03427787595626e-09
	-2.30862598466667	2.05606397189318e-09
FOSB	-2.30822992166667	2.06807879837604e-09
PDGFRB	-2.30630004166667	2.06896280174073e-09
CLDN4	-2.29499024833333	2.13717526685588e-09
C11orf41	-2.29357576	2.19691242479674e-09
CCBE1	-2.28650780233333	2.24537602358374e-09
BAIAP2L2	2.278437052	2.30601901743816e-09
ST3GAL5	-2.27050396033333	2.34343625000227e-09
TIMP2	-2.27023562666667	2.35595149994655e-09
PHLDB1	-2.26940242066667	2.35621050275426e-09
RGS9	-2.26831059233333	2.35621050275426e-09
FGF1	-2.26829292466667	2.37524793719708e-09
C11orf86	-2.26443459866667	2.44283746306066e-09
DMBX1	-2.26393490233333	2.56829918094462e-09
	-2.26304683266667	2.58469187430566e-09
KIAA1644	-2.26095305733333	2.58469187430566e-09
ALOX5AP	-2.25662669233333	2.58744692746726e-09
STK32B	2.25629003066667	2.58744692746726e-09
BAIAP2L2	2.25620095133333	2.59799928421846e-09
ABCA9	2.25521701333333	2.72830993508254e-09

LOC100268168	-2.246207512	2.72830993508254e-09
GPR87	-2.245890878	2.72830993508254e-09
PDE11A	-2.24253727733333	2.74241211143386e-09
CFI	2.2422599	2.78552719224958e-09
MEG3	-2.23479968166667	2.80812027951822e-09
SLC6A13	-2.23221732033333	2.84084404055203e-09
ASGR1	2.23179197966667	2.84084404055203e-09
AGT	2.22802793133333	2.84084404055203e-09
KCTD11	-2.22741181933333	2.89115136319385e-09
ISG20	2.227102416	3.01037353146564e-09
ZNF608	-2.22331367166667	3.0289982683888e-09
ULBP2	-2.221129233	3.05035633291483e-09
GPCPD1	2.21829664266667	3.07247396587874e-09
DCBLD1	-2.21523510666667	3.07247396587874e-09
DOCK2	-2.21265734766667	3.10768639910433e-09
TM4SF5	2.21178327033333	3.12702680775706e-09
CCDC80	-2.207672054	3.24314507942262e-09
FBLN2	-2.204188039	3.24314507942262e-09
P4HA3	-2.202860584	3.29527119141267e-09
DKFZP434L187	-2.200081073	3.37154059089304e-09
PPP1R3B	-2.18274195	3.44870210376699e-09
STON1	-2.17826349533333	3.56411116228045e-09
FOXP1	-2.17381210466667	3.68925732908026e-09
PPFIBP2	2.173715454	3.73175274978242e-09
HOXD11	-2.17047847066667	3.74153150782577e-09
TRIM9	-2.16837250433333	3.8172992061942e-09
CATSPER1	-2.16184338733333	3.83152147701729e-09
SPHK1	-2.161304003	3.83152147701729e-09
COL8A2	-2.15743879866667	3.84211512698188e-09
FAM84B	2.156639381	3.84211512698188e-09
TIAM2	-2.156231962	3.90817064947093e-09
DLC1	-2.150574626	3.97740815527792e-09
AMBP	2.15056776366667	3.98534743515426e-09

IRF6	-2.15024411833333	3.98729433935492e-09
S1PR5	-2.14932332633333	3.98729433935492e-09
LOXL4	-2.14728651133333	3.98729433935492e-09
ARHGEF4	-2.139265882	3.98729433935492e-09
KLHL24	-2.13754898	4.00028390184216e-09
PPEF1	2.13393409833333	4.11224201349874e-09
SYT13	-2.133300233	4.17557015778202e-09
LINC00442	-2.129674873	4.17557015778202e-09
NCF2	-2.12860589866667	4.17557015778202e-09
FAT2	-2.128406925	4.21196926875202e-09
	-2.128321013	4.25288410306147e-09
TSPAN12	-2.12737704366667	4.26313744886623e-09
PER2	2.12672696166667	4.27368121145218e-09
TMEM47	-2.12591439333333	4.33476301599907e-09
KDM6B	-2.12298744066667	4.33476301599907e-09
VAV3	2.12214982733333	4.48571952865436e-09
BMP2	-2.12193545833333	4.50501613328235e-09
DOCK4	-2.12042111833333	4.56668253279705e-09
SLC12A2	2.12019589233333	4.58016495635282e-09
FGF2	-2.11410800833333	4.60385346731381e-09
CSF1R	-2.11262628766667	4.84606548887957e-09
ZNF185	-2.107670664	4.84606548887957e-09
ULBP2	-2.107080287	4.878730256918e-09
GALNT4	2.10294321966667	4.878730256918e-09
TPM1	-2.10237644566667	4.93966897959591e-09
CYR61	-2.098457026	5.06634990486752e-09
DOCK4	-2.09834334566667	5.18876085183078e-09
CDH19	-2.09560512133333	5.30358803360427e-09
PBX2	-2.09311102466667	5.69743746118491e-09
TRIM2	-2.09255436633333	5.81875648862345e-09
PCDH9	-2.09255199133333	6.02716719340535e-09
NAP1L3	-2.08298091266667	6.02716719340535e-09
CLIC3	-2.08087571366667	6.04041609141977e-09

LOC284454	-2.07502423466667	6.04041609141977e-09
SUCNR1	-2.073364187	6.04054201361063e-09
CRX	2.06999574366667	6.055667858568e-09
ANGPT1	2.069200057	6.14780232267227e-09
CSF2RA	2.06669525833333	6.14780232267227e-09
	-2.065058873	6.22818685774777e-09
SH3PXD2A	-2.06397378366667	6.36302087416479e-09
CD38	2.063803941	6.44901494288714e-09
EPHB2	-2.061862565	6.54845730829299e-09
IGFBP7	-2.061457431	6.59059397645952e-09
SOCS1	-2.06082129	6.6129531627351e-09
	-2.05798640833333	6.61650093255221e-09
ANKS4B	2.05771571233333	6.61650093255221e-09
MN1	-2.05577793266667	6.66370370022724e-09
PLCH1	2.0519783	6.72882277583433e-09
GJB1	2.046861021	6.72882277583433e-09
NR0B1	2.04576242066667	6.7536118665952e-09
PGM2L1	-2.04526598266667	6.98242315505514e-09
FAM125B	-2.03545678533333	7.03683646073114e-09
NAV2	-2.03334443	7.53458491636884e-09
NUDT10	-2.03169806366667	7.54711237566917e-09
LTBP2	-2.030301572	7.60757900396455e-09
RSU1	-2.027196525	7.74913537072674e-09
LYPD5	-2.02655324	8.02827646401629e-09
EEPD1	-2.02589919733333	8.02827646401629e-09
AKAP2	-2.02482754066667	8.03564051892139e-09
NOG	-2.02332642666667	8.14890551414452e-09
ARL4D	-2.02242278433333	8.20911189091644e-09
DLC1	-2.02120318266667	8.30353493416263e-09
IRS2	2.018514738	8.30353493416263e-09
	-2.01390258466667	8.30353493416263e-09
FOXP1	-2.010898482	8.51899592347641e-09
PIK3IP1	-2.00985571233333	8.51899592347641e-09

SOX2	2.00946746333333	8.51899592347641e-09
C5	2.00414319633333	8.51978047419849e-09
PMEPA1	-2.00042088833333	8.63331357626569e-09
GADD45B	-1.99728443766667	8.63718494856543e-09
P2RY2	-1.99635450466667	8.65014587498943e-09
FNDC5	-1.99129455566667	8.96337797157933e-09
DCBLD1	-1.98536186933333	8.98176288430392e-09
PHEX	1.985137678	9.19174425190031e-09
LPPR1	1.98410087	9.48195000565818e-09
DBC1	-1.98390415333333	9.48195000565818e-09
METRNL	-1.98323634033333	9.55285380026107e-09
CRCT1	-1.983079314	9.68606319409297e-09
HRASLS2	1.981347329	9.75641927265746e-09
JUN	-1.9808297	9.75641927265746e-09
COL4A1	-1.98011510033333	9.86032891668978e-09
TMEM154	-1.979779236	9.86032891668978e-09
COL4A4	-1.97780010566667	9.86032891668978e-09
PRDM1	-1.97745555733333	9.93669114332822e-09
PLCD4	1.97668795166667	1.00254270101291e-08
FGF1	-1.976273319	1.00489321791097e-08
TANC2	-1.97610125733333	1.00489321791097e-08
TBXAS1	1.97515627033333	1.01587712715293e-08
ECM1	-1.97493128	1.02719090968064e-08
ARL4D	-1.97149577833333	1.03324401211756e-08
PARM1	1.970816724	1.04291674807022e-08
SERPINF1	-1.96686500066667	1.05267031281873e-08
SULF2	-1.96531475	1.06208633626866e-08
DLX2	-1.965185965	1.06208633626866e-08
TMEM74	-1.960919259	1.08282459806788e-08
CYP3A5	1.95856846933333	1.09443416810476e-08
C11orf82	1.95520000466667	1.12369189690582e-08
DNER	-1.95278671733333	1.12369189690582e-08
BMP4	1.950526324	1.14233712052579e-08

GRHL3	1.94918702233333	1.15988441578905e-08
CYP3A7	1.948926135	1.17170380702998e-08
ARHGAP31	-1.945706275	1.177394196216e-08
MDGA1	-1.94518776733333	1.18112417890312e-08
	1.94179176833333	1.18112417890312e-08
GNG4	-1.94145481366667	1.19512015271892e-08
	-1.94134133933333	1.2039350280311e-08
ART5	-1.941246469	1.23762956410169e-08
PARM1	1.94004425	1.24131233244433e-08
CYP2S1	1.93970422533333	1.24188125117281e-08
CFH	1.939460217	1.24696411575066e-08
REPS2	-1.93825275566667	1.25410046075436e-08
AUTS2	-1.93391505566667	1.25410046075436e-08
SLCO4A1	1.928310812	1.26263773687695e-08
PHACTR3	-1.926725331	1.26263773687695e-08
RPL27A	-1.92405867266667	1.27101834168891e-08
P4HA3	-1.920629197	1.3380197871846e-08
SCNN1A	1.91909842633333	1.3380197871846e-08
ULBP2	-1.909348229	1.36189767396195e-08
DFNB31	-1.907965705	1.3799664542618e-08
GRTP1	1.90502491566667	1.40681543139269e-08
HOOK1	1.90408278033333	1.41005526245476e-08
P2RY1	1.90401910366667	1.41623639484827e-08
DOK4	1.903931883	1.444163725824e-08
CHRNA3	-1.90153547033333	1.4737274126139e-08
	1.89818077966667	1.475693208059e-08
LCN2	1.89747008	1.48265257770586e-08
FAM175A	-1.89012904033333	1.50547889317623e-08
DZIP1L	-1.886059315	1.51333691332137e-08
C19orf28	-1.88212480866667	1.52435451720019e-08
SGCA	-1.88064506666667	1.52435451720019e-08
FAM71F1	-1.88046670133333	1.52877397064632e-08
FHOD3	-1.88027572133333	1.5315651253694e-08

LIMK2	-1.87929828166667	1.54883019646399e-08
PDZRN4	-1.87795955033333	1.55372890682786e-08
RAI14	-1.87532656066667	1.59812987118297e-08
PLAT	-1.87463525866667	1.60780605232411e-08
KCNMA1	-1.87230069433333	1.61578213718312e-08
AFAP1L2	-1.864118655	1.63020311719093e-08
NUAK1	-1.859515338	1.64721271521487e-08
CYR61	-1.85778368966667	1.64812759475383e-08
QPCT	-1.85753683866667	1.64812759475383e-08
FAM26F	-1.85537057033333	1.65559592879683e-08
HLF	1.85463560966667	1.65584809980791e-08
NGEF	-1.85296104833333	1.65882674737179e-08
KITLG	1.85242253066667	1.65882674737179e-08
KCNN1	-1.85157268133333	1.68746270143757e-08
NRP2	-1.85139867766667	1.69007049656579e-08
GAL	-1.84965868833333	1.69410672259206e-08
RIIAD1	-1.849597445	1.7031775137804e-08
TC2N	1.84641133	1.70402903194994e-08
	-1.83890693633333	1.72618344434678e-08
TGFBR1	-1.833301297	1.74893648327903e-08
AHR	1.82853791033333	1.80746695067806e-08
UNC13A	1.82839606433333	1.80810836468384e-08
TPM1	-1.82827049933333	1.81798032530666e-08
RSU1	-1.82819752566667	1.83951717499812e-08
GPR124	-1.82584426333333	1.86421501509308e-08
SERPINI1	1.82364100733333	1.86421501509308e-08
PPP1R3B	-1.822534814	1.86838614792398e-08
TPPP3	1.82240850466667	1.87089505536187e-08
PRR5L	-1.82186309266667	1.88447032051267e-08
TGFBR3	1.82163617633333	1.88447032051267e-08
TFEB	-1.820695071	1.90909409165011e-08
ITLN1	-1.82019243166667	1.90909409165011e-08
HSPB1	-1.817002997	1.92510788741627e-08

SLC23A3	-1.81618206866667	1.99332092902725e-08
TGFB2	-1.815530589	1.99332092902725e-08
CYR61	-1.81549355933333	1.99332092902725e-08
DOCK3	-1.813201383	2.04023038197314e-08
MMP1	-1.81132674833333	2.09425247698406e-08
CYP1B1	1.81002711533333	2.10427808234417e-08
CAMKK1	-1.80320690533333	2.10807653927956e-08
FOXO1	-1.80231788766667	2.10807653927956e-08
SOX2	1.79797877933333	2.21283953921846e-08
MYOCD	-1.79699795233333	2.21910965926187e-08
DUSP13	1.79666832266667	2.24839794304184e-08
PAG1	-1.79586049133333	2.33424617668907e-08
PTPRR	-1.794957862	2.35897597648384e-08
KCNK5	1.79414714566667	2.36714687443788e-08
CHST11	-1.793392445	2.37629713518075e-08
WNT6	1.792515482	2.37629713518075e-08
HOXB2	1.792163418	2.3990683737266e-08
DBP	1.79037419866667	2.47649325866954e-08
SIM2	-1.78811768466667	2.58649445791988e-08
PMEPA1	-1.78513078033333	2.60233224022183e-08
KCNF1	1.78492156666667	2.62279216724012e-08
RNASE4	1.783939846	2.62661908358731e-08
MICALL2	-1.783721875	2.6512423857241e-08
TSHZ3	-1.78269672766667	2.66243209962905e-08
PPFIBP2	1.78258313633333	2.70121549732771e-08
GPR56	-1.77709104666667	2.77389601678576e-08
TJP2	1.77690998166667	2.77763119542007e-08
GPR37	1.775402612	2.86905908701962e-08
TTLL6	1.77374187166667	2.87828770529278e-08
ZFP36	-1.77235061	2.96161656979086e-08
FRMD5	-1.77079392433333	2.98271028741209e-08
LRP11	-1.76973386066667	3.04901046371787e-08
LIMD1	1.76910462233333	3.04901046371787e-08

	-1.76716951633333	3.05798383183145e-08
NPC2	-1.76548669066667	3.07901409274839e-08
EREG	1.76131685766667	3.09066674088366e-08
	1.7592898	3.14797227416817e-08
NEXN	-1.75711600133333	3.18427825915377e-08
BIN2	1.75668188933333	3.19285171635484e-08
DCBLD1	-1.75360932533333	3.21272116938462e-08
CXCL2	1.75123171533333	3.26645828254085e-08
LTBP3	-1.74831469566667	3.27425389418319e-08
FBXO32	-1.745779005	3.36381118560679e-08
CLN8	-1.743215657	3.44908991990242e-08
TMEM92	-1.74022250233333	3.45631930596017e-08
SMOC1	1.73998156966667	3.56922840392838e-08
TPM1	-1.73763077433333	3.59005543111146e-08
MXD1	-1.73755417366667	3.64063601430817e-08
	-1.73718887833333	3.64063601430817e-08
FGFR1	-1.736068039	3.65824420419311e-08
MYL10	-1.733926247	3.69892950925847e-08
VEGFA	-1.73329971866667	3.72448066918484e-08
MFGE8	-1.73166825	3.78393190686829e-08
CXCL5	1.73087312433333	3.83674074956571e-08
MRAS	-1.73045410833333	3.92386194039128e-08
FGFR1	-1.72904579133333	3.99074869645553e-08
CFHR3	1.72722108866667	3.99074869645553e-08
FAM89B	-1.726761759	3.99074869645553e-08
CEACAM1	1.726052349	4.00706935459578e-08
ITLN2	-1.72576066333333	4.00811071080798e-08
SAMD9	-1.721464076	4.05352380584532e-08
PRKCB	1.719383826	4.07981240708699e-08
C14orf37	-1.717152925	4.12303910786588e-08
CA11	1.71579784033333	4.12303910786588e-08
DCBLD1	-1.715103259	4.17473164009985e-08
TOB1	1.714897426	4.17473164009985e-08

LAMC2	-1.71446800433333	4.34051481749874e-08
PTHLH	-1.71252171733333	4.34976858936906e-08
	-1.71111782566667	4.38161391551656e-08
MEI1	-1.71091984333333	4.39254475240426e-08
GSTT2	-1.70833052566667	4.39687064714498e-08
DLX2	-1.70825536566667	4.39687064714498e-08
ARRDC3	-1.70657849066667	4.39908536884725e-08
PLAU	-1.70598289566667	4.42948770320234e-08
TGFB1I1	-1.70345089233333	4.43954372347099e-08
ATP2A3	-1.703008128	4.53921170456258e-08
LHFP	-1.70254225966667	4.57413093626722e-08
HSPB1	-1.70091063533333	4.58539447269548e-08
COL24A1	1.699309435	4.60205616821375e-08
PDLIM7	-1.69769205966667	4.62448892116798e-08
PYGL	-1.69740612433333	4.63519364772636e-08
ALOX5	-1.69678209	4.69889407243582e-08
PDE8B	1.69540614066667	4.73459791109067e-08
NOX1	1.69449353166667	4.75704765434664e-08
LOC154822	1.69379609866667	4.80411287840896e-08
KRT34	-1.69141750533333	4.81152902613959e-08
INHBA	-1.688136123	4.88143713520117e-08
LOXL2	-1.687971043	4.93258871382206e-08
RFTN1	-1.68795722966667	4.9406237753815e-08
RBP4	1.687650074	4.9406237753815e-08
TUFT1	-1.685928769	4.96841014405645e-08
PPL	1.685272733	4.96841014405645e-08
TNS4	-1.684125925	5.00297642209977e-08
SIRPA	-1.68172303166667	5.00297642209977e-08
CEACAM7	1.68023655666667	5.12217801896295e-08
LOC100506686	1.67755093666667	5.12217801896295e-08
MYL9	-1.67253466066667	5.12217801896295e-08
S100P	1.672060605	5.20903684606703e-08
TSPAN13	1.670632026	5.20903684606703e-08

EPAS1	-1.66930304766667	5.20903684606703e-08
HIP1	1.667764504	5.39311307505547e-08
TPCN1	1.666030971	5.43657701732504e-08
PTK7	-1.66598871066667	5.46055946557815e-08
CLN8	-1.664478682	5.48405558195469e-08
VGLL3	-1.66062629066667	5.57537531158815e-08
TGM2	-1.658069952	5.59052158320934e-08
TNS1	-1.656009515	5.63808358460917e-08
RGS22	-1.65402842166667	5.69040332012633e-08
KIRREL	-1.65192638433333	5.69587385275098e-08
PITX2	-1.65187897666667	5.69587385275098e-08
GALNT9	-1.649962068	5.79094400837515e-08
CORO2B	-1.64988353933333	5.82278555029251e-08
MEX3B	-1.649183244	5.84230646233395e-08
ARHGEF18	-1.64810903933333	5.92997815210519e-08
PDK4	1.64804738	5.93258088895007e-08
FRG2	-1.64720651766667	5.93258088895007e-08
COLEC11	1.646325943	6.02535748078826e-08
ELK3	-1.64497439166667	6.11356507306884e-08
IL6R	1.641122582	6.14994975253263e-08
VEGFA	-1.640209952	6.24876256943096e-08
ARSJ	1.639187694	6.26591642905198e-08
ZNF697	-1.63870695233333	6.36334469031511e-08
EFHD1	-1.638155378	6.367750756735e-08
EPAS1	-1.63776255166667	6.38452235664118e-08
TFAP2C	1.636747486	6.43579222476749e-08
CAMK2D	1.636270835	6.43579222476749e-08
CHST11	-1.63550531966667	6.43684812024604e-08
EPB41L4A	1.635119303	6.43739667848702e-08
FLVCR2	1.633975526	6.47711129566811e-08
DACT3	-1.63393665	6.5767005018807e-08
ROPN1L	1.63327286966667	6.58425098910653e-08
C6orf105	-1.63300748933333	6.59238672784856e-08

VSTM4	-1.63268040466667	6.64925624366874e-08
ACTC1	-1.63255105466667	6.71325101048475e-08
CDH1	1.63019116	6.73164971534131e-08
FAM101B	-1.62844234933333	6.74166752262981e-08
TRIM9	-1.62774090633333	6.79253474824084e-08
CITED4	-1.62627023766667	6.79253474824084e-08
GPR162	1.62348108233333	6.98139477213885e-08
ADAMTS9	-1.62152255033333	7.02053912360362e-08
ELMO1	1.62063807	7.02406241562333e-08
GADD45B	-1.617126901	7.04861317883651e-08
ESAM	-1.616247307	7.14574100618808e-08
TCEAL5	-1.61464680033333	7.36701997476997e-08
HOXC8	-1.613806156	7.39805969111132e-08
VAMP1	1.61356024266667	7.43934459135052e-08
TFAP2A	1.61140779366667	7.48648678562606e-08
TFF3	1.611348443	7.52162495089112e-08
DIRAS3	1.61056225833333	7.52162495089112e-08
LIMA1	-1.610009305	7.56629391221337e-08
SLFNL1	-1.608038597	7.75559652870749e-08
GPCPD1	1.60295485933333	7.93671684304787e-08
ELK3	-1.600770511	7.95108590737857e-08
PLEKHN1	-1.59977799266667	8.01188275311216e-08
APAF1	-1.59691136733333	8.02483186710238e-08
SYT11	-1.59613160633333	8.06176335916832e-08
KCNJ6	-1.594205267	8.1186642637849e-08
RAB20	1.59310462233333	8.13072863473181e-08
WDR66	-1.59110949466667	8.14768548977296e-08
C10orf140	-1.59053513766667	8.20220621234539e-08
SLC5A10	-1.5903545	8.25733464697975e-08
HHEX	1.585677926	8.28410654386093e-08
C3orf80	-1.58503840133333	8.32724138755319e-08
RAB26	1.58474048733333	8.32958268192073e-08
ST8SIA4	1.584265721	8.34894711798238e-08

	-1.582128011	8.36156572892196e-08
C20orf196	1.58010445033333	8.36156572892196e-08
ELF3	1.57922070966667	8.38736928492603e-08
DOK4	1.57870208	8.45780780808961e-08
BHLHE40	-1.57509707733333	8.57164806715003e-08
SAMD14	-1.574983808	8.57164806715003e-08
SERPINB9	1.57418264766667	8.63693639447176e-08
QPCT	-1.571186091	8.64104407261404e-08
AUTS2	-1.57063033566667	8.64652210834065e-08
TM4SF18	1.56974214033333	8.74078025014738e-08
CAMK2D	1.56892650533333	8.76843453935121e-08
FMN1	-1.56485516766667	8.79265809062387e-08
FLRT2	-1.56388159633333	8.87709120063835e-08
HOXB4	1.56243386566667	8.88860073966031e-08
BMP1	-1.56205684	8.99056398226098e-08
ZNF516	-1.55967968433333	8.99056398226098e-08
	-1.55613149733333	8.9949892870986e-08
GCLC	1.55554870933333	9.10029451871216e-08
UACA	-1.55482993133333	9.15021120385151e-08
AHNAK2	-1.55419482133333	9.20509427816119e-08
PPP1R13L	-1.55280512033333	9.24287596190622e-08
DUSP4	1.55245977966667	9.25527148269484e-08
NDST1	-1.55226305133333	9.25527148269484e-08
HIP1	1.54871687533333	9.32589589123038e-08
KCNN4	-1.54810215133333	9.3411020034236e-08
NUAK2	-1.54550886433333	9.34538854580698e-08
BIN1	1.54243934066667	9.3994395598392e-08
BAAT	-1.541295066	9.4645590561058e-08
RAG1	-1.53797784433333	9.52392894689532e-08
TRPM6	-1.536396397	9.59006033866002e-08
TP53I3	-1.53479700166667	9.66955162510512e-08
OPN3	1.532929163	9.67260563003703e-08
MIAT	-1.53277812933333	9.72004690944417e-08

BMPR2	-1.529804144	9.73169921539424e-08
CA2	1.52950755366667	9.76947914550474e-08
ZFYVE28	1.52907456533333	9.82101151245152e-08
TPCN1	1.528478257	9.97211062605636e-08
	-1.52814802366667	1.0020945846639e-07
BEX4	-1.52780939533333	1.00589086517531e-07
GPR56	-1.52731063033333	1.00794370616842e-07
DPEP1	1.526998676	1.01367604529957e-07
MIAT	-1.52611077533333	1.01922402768794e-07
IRX5	1.52593945	1.01922402768794e-07
HILPDA	1.52483412733333	1.01974933112542e-07
COL5A2	-1.52442350533333	1.02517967030522e-07
NRG4	1.52258819866667	1.03941197584243e-07
GATS	1.52254719666667	1.0496613059863e-07
ANG	1.52030746266667	1.06128476134938e-07
MRAS	-1.51717090933333	1.06259411418441e-07
SYT12	-1.51395916233333	1.06259411418441e-07
NR1D2	-1.512984615	1.06581166879353e-07
SDC4	-1.51153262133333	1.06865774268377e-07
SAMD9	-1.51007159866667	1.07949256356466e-07
C21orf63	1.50997547666667	1.08099819027445e-07
TCEAL3	-1.50992212033333	1.09594256396153e-07
KIAA0182	1.50375718566667	1.10434483144447e-07
LFNG	-1.50355014466667	1.10728477188644e-07
ARMCX2	-1.50354038233333	1.11403233273328e-07
PACSIN1	1.50164961166667	1.13118559181904e-07
TNR	-1.50156597366667	1.15276080336234e-07

Table 6.2 Expression of TGF-β mediated Smad3 dependent genes in normal versus PDAC tumors.

Symbol	logFC_normalvPDAC	adj.P.Val_normvalvPDAC	logFC_TGFBCtrlvTGFBSISMAD3
LAMC2	2.638714758	7.15E-15	-2.753840083
AHNAK2	1.862427906	8.84E-15	-1.554194821
FBXO32	1.373784348	3.67E-12	-1.745779005
S100P	1.177982985	4.61E-11	1.672060605
CEACAM6	2.676020543	4.84E-11	3.122248173
KCNN4	0.698837796	5.67E-11	-1.548102151
TNS4	1.324053897	7.13E-11	-1.684125925
SCEL	1.620976035	9.09E-11	2.312855397
ITGA11	1.102795259	1.21E-10	-2.809999498
PDLIM7	0.792141499	3.33E-10	-1.69769206
AGR2	2.022349103	3.76E-10	4.517242147
SLPI	1.687833008	3.76E-10	2.743233727
PLEK2	1.032971634	4.70E-10	-3.30346004
PRR5L	0.659273399	7.62E-10	-1.821863093
PLAU	1.381443313	1.69E-09	-1.705982896
ECM1	0.756255137	2.87E-09	-1.97493128
ZNF185	0.554599712	2.87E-09	-2.107670664

BCAS1	1.09313189	3.54E-09	4.502373111
TGM2	1.238534906	4.00E-09	-1.658069952
BHLHE40	0.834446797	4.83E-09	-1.575097077
RAI14	0.913454379	6.41E-09	-1.875326561
SAMD9	1.250711007	6.58E-09	-1.721464076
PLAT	1.490566633	7.93E-09	-1.874635259
LOXL2	1.038010973	8.07E-09	-1.687971043
HSD17B6	0.834635996	1.17E-08	-2.899354403
CEACAM1	1.140145396	1.47E-08	1.726052349
PVRL4	0.706840539	1.92E-08	-3.628124316
INPP4B	1.093206807	2.24E-08	-2.692653851
SPOCK1	0.721619567	2.24E-08	-2.958050313
FRMD5	0.529038325	2.57E-08	-1.770793924
PARM1	-0.796243106	2.57E-08	1.970816724
FMN1	0.630906131	3.39E-08	-1.564855168
VDR	0.648569588	4.34E-08	-2.581747332
PTPRR	0.941607832	4.46E-08	-1.794957862
C5	-1.17039004	4.55E-08	2.004143196
GREM1	1.470848774	4.67E-08	-2.712544061
IGFBP5	1.447138273	4.83E-08	-3.619556297

INHBA	1.518812046	5.17E-08	-1.688136123
NRP2	0.924357604	5.35E-08	-1.851398678
CHST11	0.7306901	6.08E-08	-1.793392445
COL5A2	1.418450116	1.04E-07	-1.524423505
TFAP2A	0.516178302	1.24E-07	1.611407794
ST6GALNAC1	0.790068419	1.37E-07	2.608862087
ST6GALNAC1	0.78999369	1.41E-07	2.608862087
ADAM19	0.779934481	1.63E-07	-3.38905993
HHEX	-0.69242126	1.88E-07	1.585677926
COL1A1	1.589983519	2.52E-07	-5.324646195
CLDN4	0.591929439	3.47E-07	-2.294990248
SH3PXD2A	0.491748085	5.18E-07	-2.063973784
SERPINI1	-0.859923337	5.63E-07	1.823641007
SULF2	1.069950422	6.25E-07	-1.96531475
GPX2	1.451753819	6.50E-07	3.234160953
FRMD6	0.830707448	9.51E-07	-3.834923246
ZNF365	0.272449595	9.71E-07	-3.385501744
COL5A1	0.731632708	1.10E-06	-2.774393093

KIF26B	0.571986526	1.15E-06	-4.512902306
AHR	0.808778435	1.31E-06	1.82853791
ALOX5AP	0.819059989	1.31E-06	-2.256626692
DCBLD1	0.726552761	1.41E-06	-2.215235107
BMP1	0.503229946	1.45E-06	-1.56205684
PGM2L1	0.752493837	1.88E-06	-2.045265983
MFGE8	0.717092395	1.89E-06	-1.73166825
PPEF1	0.50926607	2.18E-06	2.133934098
DOK4	0.443755012	2.18E-06	1.903931883
GPR87	1.028485416	2.20E-06	-2.245890878
PDK4	-1.373371833	2.31E-06	1.64804738
NRP2	1.077787017	2.79E-06	-1.851398678
PPP1R3B	0.515937544	3.11E-06	-2.18274195
DIRAS3	-0.455027691	3.31E-06	1.610562258
ABLIM3	0.646077395	3.51E-06	-2.81109146
COL4A2	0.693626262	3.68E-06	-2.458863404
SLCO4A1	0.508876441	3.86E-06	1.928310812
TF	-0.661957775	3.88E-06	4.097648297
RAB26	-0.562742927	3.91E-06	1.584740487
OPN3	0.488284657	4.43E-06	1.532929163

TANC2	0.69125832	4.55E-06	-1.976101257
MXD1	0.806420793	4.70E-06	-1.737554174
NRG4	-1.56221159	4.88E-06	1.522588199
B3GALT5	0.787416642	4.92E-06	2.622160357
CXCL5	1.036652749	5.11E-06	2.523821575
FGFR1	-0.563290075	5.23E-06	-2.803937723
C15orf48	0.851246823	5.37E-06	-4.197725071
GATS	-0.536878172	5.77E-06	1.522547197
TMEM88	-0.673378376	5.88E-06	-3.610293874
ARRB1	-0.408728596	6.18E-06	2.935150877
PDGFRB	0.807966905	6.27E-06	-2.306300042
IGFBP7	0.562700168	6.79E-06	-2.061457431
SPARC	1.115853155	6.97E-06	-2.980808223
RNF182	-0.289867302	7.06E-06	-2.552850955
ACOX2	-0.30612535	7.66E-06	3.540256309
PRDM1	0.881028851	8.35E-06	-1.977455557
TUFT1	0.583721626	8.50E-06	-1.685928769
PDE8B	-0.633048043	9.44E-06	1.695406141
PPL	0.498386877	9.52E-06	1.685272733
MICALL2	0.276222936	1.12E-05	-1.783721875

TSPAN7	-0.942579321	1.20E-05	2.94515172
SCNN1A	0.848353302	1.37E-05	1.919098426
LCN2	1.301157545	1.43E-05	1.89747008
ARHGEF18	0.274045069	1.46E-05	-1.648109039
CAMKK1	-0.244857618	1.51E-05	-1.803206905
HILPDA	0.814936842	1.58E-05	1.524834127
METTL7A	-0.643098346	1.66E-05	2.575040609
BMP4	0.481365837	1.74E-05	1.950526324
SLC26A9	0.667944302	1.83E-05	3.964097015
DDC	-0.647526718	2.14E-05	3.224883912
PIK3IP1	0.563708598	2.17E-05	-2.009855712
CP	1.63173183	2.19E-05	3.473055741
HOXB2	0.307422003	2.49E-05	1.792163418
PMEPA1	0.728618312	2.58E-05	-2.000420888
PTK7	0.523494817	2.67E-05	-1.665988711
GSTA5	-0.235668617	2.82E-05	4.242025323
MUC13	1.365925475	3.03E-05	3.228157864
COL4A1	0.730282232	3.91E-05	-3.376822534
AFAP1L2	0.435614933	4.10E-05	-1.864118655

ATP2A3	-0.497214868	4.13E-05	-1.703008128
NUAK1	0.72011331	4.33E-05	-1.859515338
TMEM154	0.56593613	4.87E-05	-1.979779236
MYL9	0.498128263	5.01E-05	-1.672534661
BMPR2	0.548297274	5.25E-05	-1.529804144
XYLT1	0.346416732	5.35E-05	-2.985531061
DPEP1	-0.930168662	5.60E-05	1.526998676
SERPINB9	0.684137339	6.47E-05	1.574182648
FHOD3	0.328892789	6.68E-05	-1.880275721
ALOX5	0.539208754	6.97E-05	-1.69678209
LTBP2	0.549249709	0.000103522	-2.030301572
SPDEF	0.288783808	0.000104772	3.286049889
SIM2	0.279525596	0.000106217	-1.788117685
CYP2S1	0.379490564	0.000144563	1.939704225
MMP2	0.932558908	0.000148334	-3.576303649
NUAK2	-0.382756815	0.000161631	-1.545508864
RFTN1	0.553682027	0.000185334	-1.68795723
LOX	0.95004903	0.000191041	-3.764458134
NCF2	0.697220205	0.000205094	-2.128605899
ELK3	0.554845063	0.000218213	-1.644974392

APOH	-0.704812241	0.0002363	2.74160215
TAS2R1	-0.133767998	0.000254552	-2.84620907
IRF6	0.681927538	0.00026601	-2.150244118
KITLG	0.559299276	0.000270036	2.378362081
FA2H	0.270711868	0.000312491	2.621986268
TAGLN	0.739436423	0.000336684	-3.083113843
HLF	-0.464848851	0.000337291	1.85463561
TGFB1I1	0.230271629	0.000340498	-1.703450892
HIP1	0.38686329	0.000374897	1.667764504
AREG	1.001547601	0.000378632	2.487657633
TGFBR3	-0.557471634	0.000385339	1.821636176
TSHZ3	0.416347175	0.000388172	-1.782696728
TIMP3	0.550649319	0.000392	-3.273893857
C4BPB	0.437964714	0.000403669	-2.715511658
TNFAIP6	1.048675065	0.000428195	-4.390676521
MMP1	1.094245123	0.000452658	-1.811326748
EHF	0.747090293	0.000497861	3.082630332
HAPLN3	0.236638248	0.000661948	-2.980034806
FGFBP1	0.587019891	0.000761854	2.984017491
LIMA1	0.451277966	0.000822742	-1.610009305

AMBP	-0.801298857	0.000836225	2.150567764
KIRREL	0.44918639	0.000904756	-1.651926384
ELMO1	-0.464445647	0.000935111	1.62063807
TNR	-0.201222586	0.000958908	-1.501565974
DACT1	0.348341883	0.000971095	-3.961207129
TRPM6	-0.212309723	0.000973084	-1.536396397
CYP3A5	0.867386978	0.00103882	1.958568469
CYP4F3	0.310734048	0.001040339	3.329032147
ZBED2	0.294506468	0.001270619	-4.100225975
PCDH9	-0.335135395	0.001287402	-2.092551991
LIMK2	0.259861717	0.001378115	-1.879298282
CYP4F12	0.28338208	0.001435476	2.714273851
CFH	0.693140308	0.001625682	1.939460217
AREG	0.693162936	0.001677067	2.487657633
CCKBR	-0.421335222	0.001681073	3.244645452
P2RY1	-0.239280135	0.001718288	1.904019104
TC2N	-0.725634888	0.001760112	1.84641133
TM4SF18	-0.56289415	0.001873779	1.56974214
DUSP26	-0.26381212	0.001905783	-2.740861662
TGFBR1	0.50748759	0.002027592	-1.833301297

BEX4	-0.332725418	0.002110368	-1.527809395
MEG3	-0.409377746	0.002278119	-3.014215036
UACA	0.485077609	0.002410391	-1.554829931
ARRDC3	0.457576126	0.002610096	-1.706578491
HOOK1	-0.642034469	0.002814549	1.90408278
ELF3	0.617512941	0.002994881	1.57922071
SYT11	0.392968803	0.003046216	-1.596131606
EREG	0.585404478	0.003114395	2.535201501
TGFB2	0.650135487	0.003209205	-1.815530589
PYGL	0.567483499	0.003877723	-1.697406124
HSPB1	0.495723393	0.003900552	-1.817002997
GJB1	-0.267295465	0.003915916	2.046861021
ARSJ	0.232173017	0.003947339	1.639187694
GCLC	-0.30298635	0.00419904	1.555548709
TSPAN12	-0.334452472	0.004314602	-2.127377044
ASGR1	-0.205183187	0.004358131	2.23179198
PPP1R13L	0.247333497	0.004442898	-1.55280512
STK32B	-0.18632671	0.004459746	2.256290031
RIIAD1	-0.118414505	0.005000186	-1.849597445
VAV3	-0.257477142	0.00518932	2.122149827

GPCPD1	0.379237014	0.005235482	2.218296643
COLEC11	-0.226975516	0.005256437	1.646325943
CA11	-0.184714824	0.005416679	1.71579784
SLC23A1	-0.199651495	0.005481121	2.407606848
TPM1	0.366559581	0.005600127	-2.40398745
APAF1	0.287496786	0.005601495	-1.596911367
ARHGEF4	-0.215745556	0.005666464	-2.139265882
ROPN1L	-0.185662835	0.005774355	1.63327287
CXCL2	-0.54340524	0.005804707	1.751231715
TFF3	0.479150156	0.006664249	1.611348443
FLVCR2	0.2827053	0.006669499	1.633975526
HRASLS2	0.384607296	0.006730425	1.981347329
VEGFA	0.385459411	0.007006977	-1.733299719
CSF2RA	0.414390116	0.00729303	2.656033482
GALNT9	-0.170665815	0.007299509	-1.649962068
TIMP3	0.434421282	0.008114515	-3.273893857
TBXAS1	0.33313227	0.008519566	1.97515627
GPR68	0.149112027	0.008996534	-3.471821356
MEGF6	0.169605149	0.009474784	-2.525277559
COL4A4	-0.164019572	0.009701733	-1.977800106

TRIM9	-0.174812235	0.009723045	-2.168372504
COL24A1	0.185603487	0.009804752	1.699309435
ANKS4B	0.299613791	0.009874766	2.057715712
TJP2	0.257129574	0.010704573	1.776909982
TMEM92	0.227652681	0.01106979	-1.740222502
TMEM47	0.354955208	0.011495133	-2.125914393
CYP1B1	0.60236247	0.011903708	1.810027115
KCTD11	0.255413271	0.012330674	-2.227411819
FGF1	0.128014067	0.012628227	-2.268292925
FOSB	-0.767734819	0.013093262	-2.308229922
PHACTR3	0.140431563	0.013202524	-1.926725331
TP53I3	0.211476264	0.013606297	-1.534797002
GDA	0.621042941	0.015112439	2.885120996
STK32A	-0.233445612	0.015835331	-2.712324188
TCEAL5	-0.108728946	0.016132055	-1.6146468
SUCNR1	0.173573964	0.016998531	-2.073364187
C14orf37	0.300000898	0.017044936	-1.717152925
LPPR1	-0.194579997	0.017180624	1.98410087
NECAB2	-0.206951858	0.017571132	2.895391716
MMP10	0.391138485	0.019179961	-3.503883926

CRX	-0.14744195	0.020173946	2.069995744
CAMK2D	0.311893324	0.020255864	1.636270835
ERBB3	0.38250676	0.02042191	2.627118391
KDM6B	-0.251947134	0.021547599	-2.122987441
CORO2B	-0.178503365	0.022565104	-1.649883539
ARHGAP31	0.3218602	0.022781959	-1.945706275
SLC12A2	0.387419405	0.022933135	2.120195892
SDPR	-0.22300715	0.023597416	2.315158227
TPPP3	-0.122692223	0.024488604	1.822408505
VAMP1	0.168544225	0.025845602	1.613560243
IL6R	-0.210853406	0.026184057	1.641122582
PIK3AP1	-0.283913324	0.026823639	-3.625712684
RGS9	-0.187027779	0.028323708	-2.268310592
RNF144B	0.261973485	0.028541859	2.747229973
NDST1	-0.172142959	0.028740552	-1.552263051
FAM71F1	-0.117914022	0.029004712	-1.880466701
PTHLH	0.1954058	0.029650409	-1.712521717
PACSIN1	-0.191219083	0.030005537	3.968080031
P4HA3	0.300500447	0.031483439	-2.202860584

TSPAN13	-0.248473242	0.034974069	1.670632026
NOX1	0.214701937	0.03628644	1.694493532
BAAT	-0.202371992	0.039161718	-1.541295066
SERPINE1	0.579197407	0.041267413	-4.170443982
TCEAL3	-0.158374891	0.046257647	-1.50992212
CLIC3	0.223414147	0.046796378	-2.080875714
FLRT3	0.351511789	0.046896843	2.779124899
SYT13	0.33317043	0.04752032	-2.133300233

References

1. N. Volkan Adsay, D.T., and Deniz Altinel., *Solid Tumor Oncology Series.*, in *pancreatic cancer*, S.D.L. Andrew M. Lowy, and and P.A.P.M.D. Anderson, Editors. 2008, Springer. p. 5.
2. Ryan , D.P., T.S. Hong , and N. Bardeesy *Pancreatic Adenocarcinoma.* New England Journal of Medicine, 2014. **371**(11): p. 1039-1049.
3. *Cancer Facts & Figures*. 2017, American Cancer Society.: Atlanta.
4. Siegel, R.L., K.D. Miller, and A. Jemal, *Cancer statistics, 2017.* CA: A Cancer Journal for Clinicians, 2017. **67**(1): p. 7-30.
5. *Cancer Facts & Figures*. 2014, AmericanCancer Society: Atlanta.
6. *Cancer Facts & Figures*. 2015,American Cancer Society: Atlanta.
7. Garrido-Laguna, I. and M. Hidalgo, *Pancreatic cancer: from state-of-the-art treatments to promising novel therapies.* Nat Rev Clin Oncol, 2015. **12**(6): p. 319-334.
8. Hanahan, D. and R.A. Weinberg, *The Hallmarks of Cancer.* Cell. **100**(1): p. 57-70.
9. Hanahan, D. and Robert A. Weinberg, *Hallmarks of Cancer: The Next Generation.* Cell. **144**(5): p. 646-674.
10. Müller, S., et al., *Next-generation sequencing reveals novel differentially regulated mRNAs, lncRNAs, miRNAs, sdRNAs and a piRNA in pancreatic cancer.* Molecular Cancer, 2015. **14**: p. 94.
11. Waddell, N., et al., *Whole genomes redefine the mutational landscape of pancreatic cancer.* Nature, 2015. **518**(7540): p. 495-501.
12. Bailey, P., et al., *Genomic analyses identify molecular subtypes of pancreatic cancer.* Nature, 2016. **531**(7592): p. 47-52.
13. Zeshaan A. Rasheed, W.M., and Anirban Maitra., *Pathology of pancreatic stroma in PDAC*, in *Pancreatic Cancer and Tumor Microenvironment*, M.H. Grippo PJ, Editor. 2012: trivandrum (India).
14. Bailey, J.M. and S.D. Leach, *Signaling pathways mediating epithelial-mesenchymal crosstalk in pancreatic cancer: Hedgehog, Notch and TGFbeta*, in *Pancreatic Cancer and Tumor Microenvironment*, P.J. Grippo and H.G. Munshi, Editors. 2012: Trivandrum (India).
15. Biankin, A.V., et al., *Pancreatic cancer genomes reveal aberrations in axon guidance pathway genes.* Nature, 2012. **491**(7424): p. 399-405.

16. Jones, S., et al., *Core Signaling Pathways in Human Pancreatic Cancers Revealed by Global Genomic Analyses.* Science (New York, N.Y.), 2008. **321**(5897): p. 1801-1806.
17. Witkiewicz, A.K., et al., *Whole-exome sequencing of pancreatic cancer defines genetic diversity and therapeutic targets.* Nature Communications, 2015. **6**: p. 6744.
18. Hahn, S.A., et al., *DPC4, A Candidate Tumor Suppressor Gene at Human Chromosome 18q21.1.* Science, 1996. **271**(5247): p. 350-353.
19. Schutte, M., et al., *DPC4 Gene in Various Tumor Types.* Cancer Research, 1996. **56**(11): p. 2527-2530.
20. Schutte, M., et al., *Abrogation of the Rb/p16 Tumor-suppressive Pathway in Virtually All Pancreatic Carcinomas.* Cancer Research, 1997. **57**(15): p. 3126-3130.
21. Rhim, A.D. and B.Z. Stanger, *Molecular Biology of Pancreatic Ductal Adenocarcinoma Progression: Aberrant Activation of Developmental Pathways.* Progress in molecular biology and translational science, 2010. **97**: p. 41-78.
22. Carr, R.M. and M.E. Fernandez-Zapico, *Pancreatic cancer microenvironment, to target or not to target?* EMBO Molecular Medicine, 2016. **8**(2): p. 80-82.
23. Kleeff, J., et al., *Pancreatic cancer.* Nature Reviews Disease Primers, 2016. **2**: p. 16022.
24. Tosolini, C., C.W. Michalski, and J. Kleeff, *Response evaluation following neoadjuvant treatment of pancreatic cancer patients.* World J Gastrointest Surg, 2013. **5**(2): p. 12-5.
25. Becker, A.E., et al., *Pancreatic ductal adenocarcinoma: Risk factors, screening, and early detection.* World Journal of Gastroenterology : WJG, 2014. **20**(32): p. 11182-11198.
26. Truty, M.J. and R. Urrutia, *Basics of TGF-ß and Pancreatic Cancer.* Pancreatology. **7**(5): p. 423-435.
27. Friess, H., et al., *Enhanced expression of transforming growth factor beta isoforms in pancreatic cancer correlates with decreased survival.* Gastroenterology, 1993. **105**(6): p. 1846-56.
28. Teicher, B.A., *Malignant cells, directors of the malignant process: role of transforming growth factor-beta.* Cancer Metastasis Rev, 2001. **20**.

29. Tian, M., J.R. Neil, and W.P. Schiemann, *Transforming growth factor-β and the hallmarks of cancer.* Cell Signal, 2011. **23**.
30. Lotz, M., E. Ranheim, and T.J. Kipps, *Transforming growth factor beta as endogenous growth inhibitor of chronic lymphocytic leukemia B cells.* J Exp Med, 1994. **179**.
31. Massagué, J., S.W. Blain, and R.S. Lo, *TGF[beta] signaling in growth control, cancer, and heritable disorders.* Cell, 2000. **103**.
32. Kim, S.J., et al., *Molecular mechanisms of inactivation of TGF-beta receptors during carcinogenesis.* Cytokine Growth Factor Rev, 2000. **11**.
33. Bhowmick, N.A., et al., *Transforming growth factor-β1 mediates epithelial to mesenchymal transdifferentiation through a RhoA-dependent mechanism.* Mol Biol Cell, 2001. **12**.
34. Rodriguez, G.C., et al., *Regulation of invasion of epithelial ovarian cancer by transforming growth factor-β.* Gynecol Oncol, 2001. **80**.
35. Neuzillet, C., et al., *Targeting the TGFβ pathway for cancer therapy.* Pharmacology & Therapeutics, 2015. **147**: p. 22-31.
36. Yhun Yhong, S., et al., *Targeting the Transforming Growth Factor-β Signaling in Cancer Therapy.* Biomol Ther (Seoul), 2013. **21**(5): p. 323-331.
37. Flechsig, P., et al., *LY2109761 attenuates radiation-induced pulmonary murine fibrosis via reversal of TGF-β and BMP-associated proinflammatory andproangiogenic signals.* Clin Cancer Res, 2012. **18**.
38. Liu, F., et al., *DUSP1 is a novel target for enhancing pancreatic cancer cell sensitivity to gemcitabine.* PLoS ONE, 2014. **9**(1): p. e84982.
39. Gore, A.J., et al., *Pancreatic cancer–associated retinoblastoma 1 dysfunction enables TGF-β to promote proliferation.* The Journal of Clinical Investigation, 2014. **124**(1): p. 338-352.
40. *Pancreatitis and the Risk of Pancreatic Cancer.* New England Journal of Medicine, 1993. **329**(20): p. 1502-1503.
41. Raimondi, S., et al., *Pancreatic cancer in chronic pancreatitis; aetiology, incidence, and early detection.* Best Practice & Research Clinical Gastroenterology. **24**(3): p. 349-358.
42. Lowenfels , A.B., et al., *Pancreatitis and the Risk of Pancreatic Cancer.* New England Journal of Medicine, 1993. **328**(20): p. 1433-1437.

43. Malka, D., et al., *Risk of pancreatic adenocarcinoma in chronic pancreatitis.* Gut, 2002. **51**(6): p. 849-852.
44. Dhar, P., S. Kalghatgi, and V. Saraf, *Pancreatic Cancer in Chronic Pancreatitis.* Indian Journal of Surgical Oncology, 2015. **6**(1): p. 57-62.
45. al., R.H.H.e., *The Pancreas*, in *Robbins and Cotran PathologicBasis of Disease*, W.S.a.R. Bruliow., Editor. 2010, Saunders Elsevier,.
46. al., W.E.F.e., *Pancreas*, in *Schwartz's Principles of Surgery.*, F.B.e. al., Editor. 2014, McGraw-Hill Education.
47. *The endocrine pancreas*, in *Anatomy & Physiology*. Openstax.
48. Gorelick., C.R.M.a.F.S., *Pancreatic and Salivary Glands*, in *Medical Physiology*, W.F.B.a.E.L. Boulpaep, Editor. 2009, Saunders Elsevier.
49. *cross section of pancreas*.
50. Fu, H., et al., *TGF-beta promotes invasion and metastasis of gastric cancer cells by increasing fascin1 expression via ERK and JNK signal pathways.* Acta Biochim Biophys Sin (Shanghai), 2009. **41**.
51. Lamouille, S. and R. Derynck, *Cell size and invasion in TGF-β-induced epithelial to mesenchymal transition is regulated by activation of the mTOR pathway.* J Cell Biol, 2007. **178**.
52. Taipale, J., et al., *Latent transforming growth factorbeta 1 associates to fibroblast extracellular matrix via latent TGF-beta binding protein.* J Cell Biol, 1994. **124**.
53. Lebman, D.A. and J.S. Edmiston, *The role of TGF-beta in growth, differentiation, and maturation of B lymphocytes.* Microbes Infect, 1999. **1**.
54. Robertson, I.B., et al., *Latent TGF-β-binding proteins.* Matrix biology : journal of the International Society for Matrix Biology, 2015. **47**: p. 44-53.
55. Shi, Y. and J. Massagué, *Mechanisms of TGF-β Signaling from Cell Membrane to the Nucleus.* Cell. **113**(6): p. 685-700.
56. Tsukazaki, T., et al., *SARA, a FYVE Domain Protein that Recruits Smad2 to the TGF[beta] Receptor.* Cell, 1998. **95**.
57. Nakao, A., et al., *TGF-beta receptor-mediated signalling through Smad2, Smad3 and Smad4.* The EMBO Journal, 1997. **16**(17): p. 5353-5362.
58. Pouponnot, C., L. Jayaraman, and J. Massagué, *Physical and Functional Interaction of SMADs and p300/CBP.* J Biol Chem, 1998. **273**.
59. Usui, T., et al., *Extracellular matrix production regulation by TGF-beta in corneal endothelial cells.* Invest Ophthalmol Vis Sci, 1998. **39**(11): p. 1981-9.

60. Hocevar, B.A. and P.H. Howe, *Analysis of TGF-beta-mediated synthesis of extracellular matrix components.* Methods Mol Biol, 2000. **142**: p. 55-65.
61. Moustakas, A., et al., *Mechanisms of TGF-beta signaling in regulation of cell growth and differentiation.* Immunol Lett, 2002. **82**(1-2): p. 85-91.
62. Nakao, A., et al., *Identification of Smad7, a TGF[beta]-inducible antagonist of TGF-[beta] signalling.* Nature, 1997. **389**(6651): p. 631-635.
63. Moustakas, A., S. Souchelnytskyi, and C.-H. Heldin, *Smad regulation in TGF-β signal transduction.* Journal of Cell Science, 2001. **114**(24): p. 4359-4369.
64. Yan, X. and Y.G. Chen, *Smad7: not only a regulator, but also a cross-talk mediator of TGF-beta signalling.* Biochem J, 2011. **434**(1): p. 1-10.
65. Mochizuki, T., et al., *Roles for the MH2 Domain of Smad7 in the Specific Inhibition of Transforming Growth Factor-β Superfamily Signaling.* Journal of Biological Chemistry, 2004. **279**(30): p. 31568-31574.
66. Zhang, S., et al., *Smad7 Antagonizes Transforming Growth Factor β Signaling in the Nucleus by Interfering with Functional Smad-DNA Complex Formation.* Molecular and Cellular Biology, 2007. **27**(12): p. 4488-4499.
67. Hanyu, A., et al., *The N domain of Smad7 is essential for specific inhibition of transforming growth factor-β signaling.* The Journal of Cell Biology, 2001. **155**(6): p. 1017-1028.
68. Hariharan, R. and M.R. Pillai, *Structure–function relationship of inhibitory Smads: Structural flexibility contributes to functional divergence.* Proteins: Structure, Function, and Bioinformatics, 2008. **71**(4): p. 1853-1862.
69. Sudol, M., *WW Domains in the Heart of Smad Regulation.* Structure, 2012. **20**(10): p. 1619-1620.
70. Aragón, E., et al., *Structural basis for the versatile interactions of Smad7 with regulator WW domains in TGF-β pathways.* Structure (London, England : 1993), 2012. **20**(10): p. 1726-1736.
71. Itoh, S., et al., *Transforming Growth Factor β1 Induces Nuclear Export of Inhibitory Smad7.* Journal of Biological Chemistry, 1998. **273**(44): p. 29195-29201.
72. Shi, W., et al., *GADD34-PP1c recruited by Smad7 dephosphorylates TGFbeta type I receptor.* J Cell Biol, 2004. **164**: p. 291 - 300.

73. Valdimarsdottir, G., et al., *Smad7 and protein phosphatase 1alpha are critical determinants in the duration of TGF-beta/ALK1 signaling in endothelial cells.* BMC Cell Biol, 2006. **7**: p. 16.
74. Yan, X., et al., *Smad7 Protein Interacts with Receptor-regulated Smads (R-Smads) to Inhibit Transforming Growth Factor-β (TGF-β)/Smad Signaling.* Journal of Biological Chemistry, 2016. **291**(1): p. 382-392.
75. Yan, X., et al., *Smad7 Interacts with R-Smads to Inhibit TGF-beta/Smad Signaling.* Journal of Biological Chemistry, 2015.
76. Kuratomi, G., et al., *NEDD4-2 (neural precursor cell expressed, developmentally down-regulated 4-2) negatively regulates TGF-beta (transforming growth factor-beta) signalling by inducing ubiquitin-mediated degradation of Smad2 and TGF-beta type I receptor.* Biochem J, 2005. **386**(Pt 3): p. 461-70.
77. Ebisawa, T., et al., *Smurf1 interacts with transforming growth factor-beta type I receptor through Smad7 and induces receptor degradation.* J Biol Chem, 2001. **276**: p. 12477 - 80.
78. Kavsak, P., et al., *Smad7 binds to Smurf2 to form an E3 ubiquitin ligase that targets the TGF beta receptor for degradation.* Mol Cell, 2000. **6**: p. 1365 - 75.
79. Emori, T., K. Kitamura, and K. Okazaki, *Nuclear Smad7 Overexpressed in Mesenchymal Cells Acts as a Transcriptional Corepressor by Interacting with HDAC-1 and E2F to Regulate Cell Cycle.* Biology Open, 2012. **1**(3): p. 247-260.
80. Morgan, D.O., *Principles of CDK regulation.* Nature, 1995. **374**(6518): p. 131-134.
81. Satyanarayana, A. and P. Kaldis, *Mammalian cell-cycle regulation: several Cdks, numerous cyclins and diverse compensatory mechanisms.* Oncogene, 2009. **28**(33): p. 2925-2939.
82. Bartek, J., J. Bartkova, and J. Lukas, *The Retinoblastoma Protein Pathway in Cell Cycle Control and Cancer.* Experimental Cell Research, 1997. **237**(1): p. 1-6.
83. Giacinti, C. and A. Giordano, *RB and cell cycle progression.* Oncogene, 2003. **25**(38): p. 5220-5227.
84. Chellappan, S.P., et al., *The E2F transcription factor is a cellular target for the RB protein.* Cell, 1991. **65**(6): p. 1053-61.
85. Narasimha, A.M., et al., *Cyclin D activates the Rb tumor suppressor by mono-phosphorylation.* eLife, 2014. **3**: p. e02872.

86. Rubin, S.M., *Deciphering the Rb phosphorylation code.* Trends in biochemical sciences, 2013. **38**(1): p. 12-19.
87. Adams, P.D., et al., *Retinoblastoma Protein Contains a C-terminal Motif That Targets It for Phosphorylation by Cyclin-cdk Complexes.* Molecular and Cellular Biology, 1999. **19**(2): p. 1068-1080.
88. Almasan, A., et al., *Deficiency of retinoblastoma protein leads to inappropriate S-phase entry, activation of E2F-responsive genes, and apoptosis.* Proceedings of the National Academy of Sciences, 1995. **92**(12): p. 5436-5440.
89. Iavarone, A. and J. Massague, *E2F and histone deacetylase mediate transforming growth factor beta repression of cdc25A during keratinocyte cell cycle arrest.* Mol Cell Biol, 1999. **19**.
90. Adams, P.D., et al., *Identification of a cyclin-cdk2 recognition motif present in substrates and p21-like cyclin-dependent kinase inhibitors.* Molecular and Cellular Biology, 1996. **16**(12): p. 6623-33.
91. Lim, S. and P. Kaldis, *Cdks, cyclins and CKIs: roles beyond cell cycle regulation.* Development, 2013. **140**(15): p. 3079-3093.
92. Romagosa, C., et al., *p16Ink4a overexpression in cancer: a tumor suppressor gene associated with senescence and high-grade tumors.* Oncogene, 2011. **30**(18): p. 2087-2097.
93. Jiang, H., H.S. Chou, and L. Zhu, *Requirement of Cyclin E-Cdk2 Inhibition in p16(INK4a)-Mediated Growth Suppression.* Molecular and Cellular Biology, 1998. **18**(9): p. 5284-5290.
94. Krimpenfort, P., et al., *p15Ink4b is a critical tumour suppressor in the absence of p16Ink4a.* Nature, 2007. **448**(7156): p. 943-946.
95. Ozenne, P., et al., *The ARF tumor suppressor: Structure, functions and status in cancer.* International Journal of Cancer, 2010. **127**(10): p. 2239-2247.
96. Solomon, D.A., et al., *Identification of p18(INK4c) as a Tumor Suppressor Gene in Glioblastoma Multiforme.* Cancer research, 2008. **68**(8): p. 2564-2569.
97. Dimri, G.P., et al., *Inhibition of E2F activity by the cyclin-dependent protein kinase inhibitor p21 in cells expressing or lacking a functional retinoblastoma protein.* Molecular and Cellular Biology, 1996. **16**(6): p. 2987-97.
98. Arooz, T., et al., *On the Concentrations of Cyclins and Cyclin-Dependent Kinases in Extracts of Cultured Human Cells.* Biochemistry, 2000. **39**(31): p. 9494-9501.

99. Xiong, Y., et al., *p21 is a universal inhibitor of cyclin kinases.* Nature, 1993. **366**(6456): p. 701-704.
100. Nakayama, K., et al., *Mice Lacking p27^{Kip1} Display Increased Body Size, Multiple Organ Hyperplasia, Retinal Dysplasia, and Pituitary Tumors.* Cell. **85**(5): p. 707-720.
101. Lee, M.H., I. Reynisdóttir, and J. Massagué, *Cloning of p57KIP2, a cyclin-dependent kinase inhibitor with unique domain structure and tissue distribution.* Genes & Development, 1995. **9**(6): p. 639-649.
102. Datto, M.B., et al., *Transforming growth factor beta induces the cyclin-dependent kinase inhibitor p21 through a p53-independent mechanism.* Proc Natl Acad Sci USA, 1995. **92**.
103. Pietenpol, J.A., et al., *Transforming growth factor beta 1 suppression of c-myc gene transcription: role in inhibition of keratinocyte proliferation.* Proceedings of the National Academy of Sciences of the United States of America, 1990. **87**(10): p. 3758-3762.
104. Feng, X.-H., et al., *Direct Interaction of c-Myc with Smad2 and Smad3 to Inhibit TGF-β-Mediated Induction of the CDK Inhibitor p15^{Ink4B}.* Molecular Cell. **9**(1): p. 133-143.
105. Shuno, Y., et al., *Id1/Id3 Knockdown Inhibits Metastatic Potential of Pancreatic Cancer.* Journal of Surgical Research. **161**(1): p. 76-82.
106. Cox, A.D., et al., *Drugging the undruggable RAS: Mission Possible?* Nat Rev Drug Discov, 2014. **13**(11): p. 828-851.
107. Liu, J., Ji, S., Liang, C., Qin, Y., Jin, K., Liang, D., Xu, W., Shi, S., Zhang, B., Liu, L., Liu, C., Xu, J., Ni, Q., Yu, X, *Critical role of oncogenic KRAS in pancreatic cancer.* Molecular Medicine Reports, 2016. **13**(6): p. 4943-4949.
108. Rishi, A., et al., *Pathological and Molecular Evaluation of Pancreatic Neoplasms.* Seminars in oncology, 2015. **42**(1): p. 28-39.
109. Hingorani, S.R., et al., *Preinvasive and invasive ductal pancreatic cancer and its early detection in the mouse.* Cancer Cell. **4**(6): p. 437-450.
110. Morris, J.P., S.C. Wang, and M. Hebrok, *KRAS, Hedgehog, Wnt and the twisted developmental biology of pancreatic ductal adenocarcinoma.* Nat Rev Cancer, 2010. **10**(10): p. 683-695.

111. Collins, M.A., et al., *Oncogenic Kras is required for both the initiation and maintenance of pancreatic cancer in mice.* The Journal of Clinical Investigation, 2012. **122**(2): p. 639-653.
112. Carrière, C., et al., *Acute pancreatitis markedly accelerates pancreatic cancer progression in mice expressing oncogenic Kras.* Biochemical and biophysical research communications, 2009. **382**(3): p. 561-565.
113. Aguirre, A.J., et al., *Activated Kras and Ink4a/Arf deficiency cooperate to produce metastatic pancreatic ductal adenocarcinoma.* Genes & Development, 2003. **17**(24): p. 3112-3126.
114. Carrière, C., et al., *Deletion of Rb Accelerates Pancreatic Carcinogenesis by Oncogenic Kras and Impairs Senescence in Premalignant Lesions.* Gastroenterology, 2011. **141**(3): p. 1091-1101.
115. Bardeesy, N., et al., *Smad4 is dispensable for normal pancreas development yet critical in progression and tumor biology of pancreas cancer.* Genes & Development, 2006. **20**(22): p. 3130-3146.
116. Guerra, C. and M. Barbacid, *Genetically engineered mouse models of pancreatic adenocarcinoma.* Molecular Oncology, 2013. **7**(2): p. 232-247.
117. Hingorani, S.R., et al., *Trp53^{R172H} and Kras^{G12D} cooperate to promote chromosomal instability and widely metastatic pancreatic ductal adenocarcinoma in mice.* Cancer Cell. **7**(5): p. 469-483.
118. Korc, M., *Aberrant Transforming Growth Factor-β Signaling in Human Pancreatic Cancer: Translational Implications*, in *Transforming Growth Factor-β in Cancer Therapy, Volume II: Cancer Treatment and Therapy*, S.B. Jakowlew, Editor. 2008, Humana Press: Totowa, NJ. p. 523-535.
119. Rowland-Goldsmith, M.A., et al., *Soluble Type II Transforming Growth Factor-β (TGF-β) Receptor Inhibits TGF-β Signaling in COLO-357 Pancreatic Cancer Cells in Vitro and Attenuates Tumor Formation.* Clinical Cancer Research, 2001. **7**(9): p. 2931-2940.
120. Singh, P., et al., *A study of Smad4, Smad6 and Smad7 in Surgically Resected Samples of Pancreatic Ductal Adenocarcinoma and Their Correlation with Clinicopathological Parameters and Patient Survival.* BMC Research Notes, 2011. **4**: p. 560-560.

121. J Kleeff, T.I., H Maruyama, H Friess, P Truong, M W Büchler, D Falb, and M Korc, *The TGF- signaling inhibitor Smad7 enhances tumorigenicity in pancreatic cancer.* Oncogene, 1999. **18**(39): p. 5363-5372.
122. Arnold, N.B., et al., *Thioredoxin Is Downstream of Smad7 in a Pathway That Promotes Growth and Suppresses Cisplatin-Induced Apoptosis in Pancreatic Cancer.* Cancer Res, 2004. **64**(10): p. 3599-3606.
123. Boyer Arnold, N. and M. Korc, *Smad7 Abrogates Transforming Growth Factor-β1-mediated Growth Inhibition in COLO-357 Cells through Functional Inactivation of the Retinoblastoma Protein.* Journal of Biological Chemistry, 2005. **280**(23): p. 21858-21866.
124. Ekman, M., et al., *APC and Smad7 link TGFβ type I receptors to the microtubule system to promote cell migration.* Molecular Biology of the Cell, 2012. **23**(11): p. 2109-2121.
125. Edlund, S., et al., *Interaction between Smad7 and β-Catenin: Importance for Transforming Growth Factor β-Induced Apoptosis.* Molecular and Cellular Biology, 2005. **25**(4): p. 1475-1488.
126. Stolfi, C., et al., *The dual role of Smad7 in the control of cancer growth and metastasis.* Int J Mol Sci, 2013. **14**(12): p. 23774-90.
127. Xia, H., L.L. Ooi, and K.M. Hui, *MicroRNA-216a/217-induced epithelial-mesenchymal transition targets PTEN and SMAD7 to promote drug resistance and recurrence of liver cancer.* Hepatology, 2013. **58**(2): p. 629-41.
128. Landström, M., et al., *Smad7 mediates apoptosis induced by transforming growth factor β in prostatic carcinoma cells.* Current Biology. **10**(9): p. 535-538.
129. Wang, P., et al., *Low-Level Expression of Smad7 Correlates with Lymph Node Metastasis and Poor Prognosis in Patients with Pancreatic Cancer.* Annals of Surgical Oncology, 2009. **16**(4): p. 826-835.
130. Chenzhong Kuang, Y.X., Xubao Liu, Teresa M. Stringfield, Shaobo Zhang, Zhenzhen Wang, and Yan Chen, *In vivo disruption of TGF-β signaling by Smad7 leads to premalignant ductal lesions in the pancreas.* PNAS, 2006. **103**(6): p. 1858-1863.
131. Hyun, J.J. and H.S. Lee, *Experimental Models of Pancreatitis.* Clinical Endoscopy, 2014. **47**(3): p. 212-216.

132. Hue Su, K., C. Cuthbertson, and C. Christophi, *Review of experimental animal models of acute pancreatitis.* HPB : The Official Journal of the International Hepato Pancreato Biliary Association, 2006. **8**(4): p. 264-286.
133. Friess, H., et al., *Enhanced expression of TGF-betas and their receptors in human acute pancreatitis.* Annals of Surgery, 1998. **227**(1): p. 95-104.
134. Riesle, E., et al., *Increased expression of transforming growth factor beta s after acute oedematous pancreatitis in rats suggests a role in pancreatic repair.* Gut, 1997. **40**(1): p. 73-79.
135. Wildi, S., et al., *Suppression of transforming growth factor β signalling aborts caerulein induced pancreatitis and eliminates restricted stimulation at high caerulein concentrations.* Gut, 2007. **56**(5): p. 685-692.
136. Nagashio, Y., et al., *Inhibition of transforming growth factor [beta] decreases pancreatic fibrosis and protects the pancreas against chronic injury in mice.* Lab Invest, 2004. **84**(12): p. 1610-1618.
137. JEAN–LUC VAN LAETHEM, P.R., ANNE RE´SIBOIS, and JACQUES DEVIE`RE, *Transforming Growth Factor b Promotes Development ofFibrosis After Repeated Courses of Acute Pancreatitisin Mice.* Gasteroentrology, 1996. **110**: p. 7.
138. He, J., et al., *Protection of cerulein-induced pancreatic fibrosis by pancreas-specific expression of Smad7.* Biochimica et Biophysica Acta (BBA) - Molecular Basis of Disease, 2009. **1792**(1): p. 56-60.
139. Li, X., et al., *Cerulein-induced pancreatic fibrosis is modulated by Smad7, the major negative regulator of transforming growth factor-β signaling.* Biochimica et Biophysica Acta (BBA) - Molecular Basis of Disease, 2016. **1862**(9): p. 1839-1846.
140. Bai, H., et al., *The effect of sulindac, a non-steroidal anti-inflammatory drug, attenuates inflammation and fibrosis in a mouse model of chronic pancreatitis.* BMC Gastroenterology, 2012. **12**: p. 115-115.
141. Srinivas, S., et al., *Cre reporter strains produced by targeted insertion of EYFP and ECFP into the ROSA26 locus.* BMC Dev Biol, 2001. **1**: p. 4.
142. Soriano, P., *Generalized lacZ expression with the ROSA26 Cre reporter strain.* Nat Genet, 1999. **21**(1): p. 70-71.

143. Tang, S., et al., *Trigenic neural crest-restricted Smad7 over-expression results in congenital craniofacial and cardiovascular defects.* Dev Biol, 2010. **344**(1): p. 233-47.
144. Chang, S.-C., P.M. Brannon, and M. Korc, *Effects of Dietary Manganese Deficiency on Rat Pancreatic Amylase mRNA Levels.* The Journal of Nutrition, 1990. **120**(10): p. 1228-1234.
145. McGookin, R., *RNA Extraction by the Guanidine Thiocyanate Procedure*, in *Nucleic Acids*, J.M. Walker, Editor. 1984, Humana Press: Totowa, NJ. p. 113-116.
146. Rio, D.C., et al., *Purification of RNA Using TRIzol (TRI Reagent).* Cold Spring Harbor Protocols, 2010. **2010**(6): p. pdb.prot5439.
147. *H&E protocol*. Available from: http://www.ihcworld.com/_protocols/special_stains/h&e_ellis.htm.
148. Gore, J., et al., *TCGA data and patient-derived orthotopic xenografts highlight pancreatic cancer-associated angiogenesis.* Oncotarget, 2015. **6**(10): p. 7504-7521.
149. Ran, F.A., et al., *Genome engineering using the CRISPR-Cas9 system.* Nat. Protocols, 2013. **8**(11): p. 2281-2308.
150. Neupane, D. and M. Korc, *14-3-3σ Modulates Pancreatic Cancer Cell Survival and Invasiveness.* Clinical cancer research : an official journal of the American Association for Cancer Research, 2008. **14**(23): p. 7614-7623.
151. Sempere, L.F., J.R. Gunn, and M. Korc, *A novel 3-dimensional culture system uncovers growth stimulatory actions by TGFβ in pancreatic cancer cells.* Cancer Biology & Therapy, 2011. **12**(3): p. 198-207.
152. Zhang, Y., et al., *High Throughput Determination of TGFβ1/SMAD3 Targets in A549 Lung Epithelial Cells.* PLOS ONE, 2011. **6**(5): p. e20319.
153. Gentleman, R.C., et al., *Bioconductor: open software development for computational biology and bioinformatics.* Genome Biology, 2004. **5**(10): p. R80-R80.
154. Reimers, M. and V.J. Carey, *[8] Bioconductor: An Open Source Framework for Bioinformatics and Computational Biology*, in *Methods in Enzymology*. 2006, Academic Press. p. 119-134.
155. The Gene Ontology, C., et al., *Gene Ontology: tool for the unification of biology.* Nature genetics, 2000. **25**(1): p. 25-29.

156. Yang, S., et al., *A Novel MIF Signaling Pathway Drives the Malignant Character of Pancreatic Cancer by Targeting NR3C2.* Cancer Research, 2016. **76**(13): p. 3838-3850.
157. Subramanian, A., et al., *Gene set enrichment analysis: A knowledge-based approach for interpreting genome-wide expression profiles.* Proceedings of the National Academy of Sciences, 2005. **102**(43): p. 15545-15550.
158. Kleeff, J., et al., *Smad6 suppresses TGF-beta-induced growth inhibition in COLO-357 pancreatic cancer cells and is overexpressed in pancreatic cancer.* Biochem Biophys Res Commun, 1999. **255**(2): p. 268-73.
159. Qiu, W. and G.H. Su, *Challenges and advances in mouse modeling for human pancreatic tumorigenesis and metastasis.* Cancer metastasis reviews, 2013. **32**(0): p. 10.1007/s10555-012-9408-2.
160. Hingorani, S.R., et al., *Preinvasive and invasive ductal pancreatic cancer and its early detection in the mouse.* Cancer Cell, 2003. **4**(6): p. 437-50.
161. Agbunag, C. and D. Bar-Sagi, *Oncogenic K-ras Drives Cell Cycle Progression and Phenotypic Conversion of Primary Pancreatic Duct Epithelial Cells.* Cancer Research, 2004. **64**(16): p. 5659-5663.
162. Sagara, H., et al., *Activation of TGF-β/Smad2 signaling is associated with airway remodeling in asthma.* Journal of Allergy and Clinical Immunology. **110**(2): p. 249-254.
163. Dumartin, L., et al., *ER stress protein AGR2 precedes and is involved in the regulation of pancreatic cancer initiation.* Oncogene, 2016.
164. Brychtova, V., B. Vojtesek, and R. Hrstka, *Anterior gradient 2: a novel player in tumor cell biology.* Cancer Lett, 2011. **304**.
165. Dumartin, L., et al., *AGR2 Is a Novel Surface Antigen That Promotes the Dissemination of Pancreatic Cancer Cells through Regulation of Cathepsins B and D.* Cancer research, 2011. **71**(22): p. 7091-7102.
166. Mizuuchi, Y., et al., *Anterior gradient 2 downregulation in a subset of pancreatic ductal adenocarcinoma is a prognostic factor indicative of epithelial-mesenchymal transition.* Lab Invest, 2015. **95**(2): p. 193-206.
167. Marc-Oliver Riener, C.P., Josefine Gerhardt, Robert Grützmann, Florian R. Fritzsche, Marcus Bahra, Wilko Weichert and Glen Kristiansen, *Prognostic significance of AGR2 in pancreatic ductal adenocarcinoma.* HISTOLOGY AND HISTOPATHOLOGY, 2009. **24**: p. 1121-1128.

168. Makawita, S., et al., *Validation of four candidate pancreatic cancer serological biomarkers that improve the performance of CA19.9.* BMC Cancer, 2013. **13**: p. 404-404.
169. Norris, A.M., et al., *AGR2 is a SMAD4-suppressible gene that modulates MUC1 levels and promotes the initiation and progression of pancreatic intraepithelial neoplasia.* Oncogene, 2013. **32**(33): p. 3867-3876.
170. Burlison, J.S., et al., *Pdx-1 and Ptf1a concurrently determine fate specification of pancreatic multipotent progenitor cells.* Developmental biology, 2008. **316**(1): p. 74-86.
171. Smart, N.G., et al., *Conditional Expression of Smad7 in Pancreatic β Cells Disrupts TGF-β Signaling and Induces Reversible Diabetes Mellitus.* PLOS Biology, 2006. **4**(2): p. e39.
172. Liu, X., et al., *Smad7 but not Smad6 Cooperates with Oncogenic ras to Cause Malignant Conversion in a Mouse Model for Squamous Cell Carcinoma.* Cancer Research, 2003. **63**(22): p. 7760-7768.
173. Snyder, C.S., et al., *A dual color, genetically engineered mouse model for multi-spectral imaging of the pancreatic microenvironment.* Pancreas, 2013. **42**(6): p. 952-958.
174. Gu, G., J. Dubauskaite, and D.A. Melton, *Direct evidence for the pancreatic lineage: NGN3+ cells are islet progenitors and are distinct from duct progenitors.* Development, 2002. **129**(10): p. 2447-2457.
175. Maureen Gannon, Pedro-Luis Herrera, and C.V.E. Wright, *Mosaic Cre-mediated recombination in pancreas using the pdx-1 enhancer/promoter.* Genesis, 2000. **24**: p. 143–144.
176. Asano, Y., et al., *Impaired Smad7-Smurf–mediated negative regulation of TGF-β signaling in scleroderma fibroblasts.* Journal of Clinical Investigation, 2004. **113**(2): p. 253-264.
177. Ouellet, S., et al., *Transcriptional regulation of the cyclin-dependent kinase inhibitor 1A (p21) gene by NFI in proliferating human cells.* Nucleic Acids Research, 2006. **34**(22): p. 6472-6487.
178. Kretschmer, A., et al., *Differential regulation of TGF-[beta] signaling through Smad2, Smad3 and Smad4.* Oncogene, 2003. **22**(43): p. 6748-6763.

179. Vijayachandra, K., J. Lee, and A.B. Glick, *Smad3 Regulates Senescence and Malignant Conversion in a Mouse Multistage Skin Carcinogenesis Model.* Cancer Research, 2003. **63**(13): p. 3447-3452.
180. Ungefroren, H., et al., *Differential roles of Smad2 and Smad3 in the regulation of TGF-β1-mediated growth inhibition and cell migration in pancreatic ductal adenocarcinoma cells: control by Rac1.* Molecular Cancer, 2011. **10**(1): p. 67.
181. Morton, J.P., et al., *LKB1 Haploinsufficiency Cooperates With Kras to Promote Pancreatic Cancer Through Suppression of p21-Dependent Growth Arrest.* Gastroenterology, 2010. **139**(2): p. 586-597.e6.
182. Dumartin, L., et al., *AGR2 is a novel surface antigen that promotes the dissemination of pancreatic cancer cells through regulation of cathepsins B and D.* Cancer Res, 2011. **71**.
183. Guerra, C., et al., *Pancreatitis-induced Inflammation Contributes to Pancreatic Cancer by Inhibiting Oncogene-Induced Senescence.* Cancer cell, 2011. **19**(6): p. 728-739.
184. Rhim, Andrew D., et al., *Stromal Elements Act to Restrain, Rather Than Support, Pancreatic Ductal Adenocarcinoma.* Cancer Cell. **25**(6): p. 735-747.
185. Hwang, H.K., et al., *Prognostic impact of the tumor-infiltrating regulatory T-cell (Foxp3(+))/activated cytotoxic T lymphocyte (granzyme B(+)) ratio on resected left-sided pancreatic cancer.* Oncology Letters, 2016. **12**(6): p. 4477-4484.
186. Özdemir, Berna C., et al., *Depletion of Carcinoma-Associated Fibroblasts and Fibrosis Induces Immunosuppression and Accelerates Pancreas Cancer with Reduced Survival.* Cancer Cell. **25**(6): p. 719-734.
187. Monteleone, G., et al., *Mongersen, an Oral SMAD7 Antisense Oligonucleotide, and Crohn's Disease.* New England Journal of Medicine, 2015. **372**(12): p. 1104-1113.

Curriculum Vitae

Sudha Satish Savant

EDUCATION

- **Ph.D., Molecular Biology and Biochemistry,** Indiana University Indianapolis, IN, September 2017
- M.Sc. Biological Sciences, Narsee Monjee Institute of Management Studies, Mumbai, India, 2010
- B.Sc. Life Sciences and Biochemistry, University of Mumbai, India, 2007
- Advanced Diploma in Biotechnology, University of Mumbai, India, 2007
- Degree of Science Honors in Life Sciences, University of Mumbai, 2006

SKILL HIGHLIGHTS

- Tissue Culture: Use of aseptic isolation, growth and maintenance of murine and human cells in 2D and 3D.
- Molecular Biology: RNA, DNA and protein isolation from cells and tissues, PCR amplification, gene cloning, CRISPR gene editing technology, luciferase reporter assays, immunoblotting, chromatin and protein immunoprecipitations, ELISA.
- Animal studies: Handling and breeding of transgenic mice, collection of tissues from mice, preparation and staining of pathological slides, immunohistochemistry.

PUBLICATIONS

1. **Savant, S**., Noris, A., Conteh, A., *Korc, M. Elucidating the role of Smad7 in Pancreatic cancer progression through *in vivo* studies. *Manuscript in preparation.*
2. **Savant, S**., Arnold, N., Conteh, A., *Korc, M. Regulation and characterization of a novel TGF-β-inducible long non-coding RNA. *Manuscript in preparation.*
3. Nguyen, H.V., Gore, J., Zhong, X., **Savant, S**., Deitz-McElyea, S., Schmidt, C.M., House, M., *Korc, M., *MicroRNA Expression in a Readily Accessible Common Hepatic Artery Lymph Node Predicts Time to Pancreatic Cancer Recurrence Postresection.* Journal of Gastrointestinal Surgery, 2016. PMID 27456015.
4. Dey, S., **Savant, S**., Teske, B., Hatzoglou, M., Calchoven, C., *Wek, R., *Transcriptional Repression of ATF4 Gene by CCAAT/Enhancer-binding Protein β (C/EBPβ) Differentially Regulates Integrated Stress Response.* Journal of Biological

Chemistry, 2012. **287**(26): p. 21936-21949. PMC3381154.

5. *Shalia, K., **Savant, S**., Haldankar, V.,Nandu, T., Pawar, P., Diwekar, S., Shah., V., Bhatt, P., *Study of C-Reactive Protein and Myocardial Infarction in the Indian Population.* Indian Journal of Clinical Biochemistry, 2012. **27**(1): p. 74-82. PMC3286588.

6. *Bhoir, S., Gaikwad, P., Parab, L., Shringarpure, R., **Savant, S**., Verma, P., *RP-HPLC Method Development and Validation for the Simultaneous Estimation of Satranidazole and Ofloxacin in Pharmaceutical Dosage Form.* Journal of Chromatographic Science, 2011. **49**(1): p. 84-87. doi: 10.1093/chrsci/49.1.84.

*Corresponding author.

RESEARCH AND PROFESSIONAL EXPERIENCE

Indiana University School of Medicine **05/2012 – Present**

Department of Biochemistry and Molecular Biology

Doctoral Candidate, Murray Korc, M.D. Laboratory

- Designed experiments, collected and analyzed data for **transgenic mouse model** overexpressing Smad7 along with mutated Kras conditionally in pancreas.
- Designed and performed experiments to characterize a **novel gene**, regulated by TGF-β in pancreatic cancer. In this project we performed biological assays to show that the gene is a **longnon-coding RNA (LncRNA)** and its over-expression in pancreatic cancer cell lines results in their increased proliferation and migration.
- Performed RNA isolation and analysis of miRNA expression in lymph node tissues from pancreatic cancer patients (Refer publication 3).
- Designed and executed CRISPR genome editing methodology in laboratory.
- Served as Lead for the Biochemistry Data Club.
- Active participant in Cancer Biology Journal Club.

Indiana University School of Medicine **09/2011 – 12/2011**

Department of Biochemistry and Molecular Biology

Ph.D. Rotation Project, Ron Wek, Ph.D. Laboratory

- Performed experiments to demonstrate transcriptional regulation of ATF4 gene by CCAAT/Enhancer-binding Protein β (C/EBPβ) under stress.

This project demonstrates how ATF4, the key player of the Integrated stress response, is transcriptionaly reguated under U.V stress. We identified C/EBPβ as the protein repressing ATF4 transcription and identified the region to which it binds. The study was done in MEF cells, using q RT PCR, western blots, luciferase assays and ChIP- Seq to test the various aims. (refer publication 4)

Abhinav College, Mumbai, India **02/2011 – 05/2011**

Department of Microbiology

Microbiology Lecturer

School of Science, N.M.I.M.S University **07/2007 – 12/2010**

Graduate Student

- Thesis project: Designed, performed experiments and published findings on association of Single Nucleotide Polymorphism (SNP) in C- reactive protein (CRP) with its serum levels in patients with myocardial infarction in the Indian population. (Refer publication 5)
- Chemistry Course Project: Developed a method for Reverse Phase HPLC for estimation and validation of Satranidazole and Ofloxacin simultaneously in a pharmaceutical dosage form. This was a short term project which involved development of a new method for accurate, precise and rapid detection of the two drug components. (Refer publication 6.)

Reliance Life Sciences, Mumbai, India **02/2008 – 05/2009**

Research Coordinator

- Recorded and managed patient data and monitored SOPs at a clinical trial site.
- Reported to ethics committee for protocol amendments and deviations.
- Co-ordinated with doctor in charge at site and research team at R&D.

IPCA Pharmaceuticals, Mumbai, India **05/2008 – 07/2008**

Full time intern

- Formulation: converted active compound into pharmaceutical dosage form
- Quality Control: maintained the quality of the product and even the working up to the international standards via GLP
- Bioequivalence: investigated and compared expected in vivo biological equivalence of two proprietary preparations of a drug

Kishinchand Chellaram College, Mumbai University **06/2004 – 05/2007**

Undergraduate Student

- Trainee, Bhartiya Vidya Bhavan's Swami Prakashananda Ayurveda Research Centre in April – May 2005. Research Project on medicinal use of plant *Lawsonia inermis* and its active components.
- Prepared a project thesis accepted for the B.Sc Honour's program by the Kishinchand Chellaram College, University of Mumbai entitled, *"Standardization of Cell Suspension of Melanocytes and Keratinocytes",* 2005 - 2006. Inthis project the concentration of the trypsin which gave maximum number of single cells was determined. The results of this research are a step towards the cure of pigmentary disorder like leukoderma, which is considered as a social stigma in the Indian society.
- Submitted the project entitled "*Decolourisation of dyes by Fungi*" as a requirement for the advanced diploma in Biotechnology, 2006 -2007. In this project the effect of three fungi; Aspergillus, Rhizopus and the Penicillium genus was checked for decolorization on the dyes Congo red, Eosin and Crystal violet.

PRESENTATIONS

- Oral presentation entitled “Elucidating the role of Smad7 in Pancreatic cancer progression through in vivo studies” at Sigma Xi Graduate Student Research Competition, October, 2016 at IUPUI, Indianapolis, USA.
- Presented poster entitled “A novel selenoprotein-like gene induced by TGF-β” at IUPUI research day and Cancer Research Day, April 2015 at IUPUI, Indianapolis, USA.
- Presented a poster on “Study on +1444C>T and -717A>G polymorphisms of human C – reactive protein gene associated with Myocardial Infarction in the Indian population” at The Eighth Asia – Pacific Bioinformatics Conference from January 18 – 21, 2010 at IISC, Banglore, India.
- Presented a poster on “RP – HPLC Method Development and Validation for the Simultaneous Estimation of Ofloxacin and Satranidazole in Pharmaceutical Dosage Form” at the 21st International Ion Chromatography Symposium from September 21 – 24, 2009 at Dublin, Ireland.
- Oral presentation titled, *“Standardization of Cell Suspension of Melanocytes and Keratinocytes,”* at the Research Scholar’s Meet (RSM – JIGYASA), 2008 Kishinchand Chellaram College, Mumbai, India.

VOLUNTEER

Indiana University School of Medicine **05/2012 – 2017**

Officer and member for Scientific Toasters, CC **05/2015 – 2017**

International Graduate Mentoring **05/2013 – 2015**

Graduate Student Mentor **05/2012 – 2017**

IBMG Ambassador **05/2013 – 2017**

Science Central **03/2016**

STEM Communication Fellow

Hoosier Science and Engineering Fair Judge **04/2013**

School of Science, N.M.I.M.S University **2009 – 2010**